


Università degli Studi di Cagliari

PHD DEGREE

Civil Engineering and Architecture

Cycle XXXIII

TITLE OF THE PHD THESIS

Hydrological changes on water resources

(Influenza dei cambiamenti idrologici sulla risorsa idrica)

Scientific Disciplinary Sector(s)

ICAR/02

PhD Student: Dario Ruggiu

Supervisors: Francesco Viola

Andreas Langousis

Final exam. Academic Year 2019 – 2020
Thesis defence: February 2021 Session

La presente tesi è stata prodotta durante la frequenza del corso di dottorato in Ingegneria Civile e Architettura dell'Università degli Studi di Cagliari, XXXIII ciclo, con il supporto di una borsa di studio finanziata con le risorse del P.O.R. Sardegna F.S.E. 2014-2020 - Asse III "Istruzione e Formazione" - Obiettivo Tematico 10, Priorità d'investimento 10ii), Obiettivo Specifico 10.5, Azione dell'accordo di Partenariato 10.5.12

Dario Ruggiu gratefully acknowledges Sardinian Regional Government for the financial support of her/his PhD scholarship (P.O.R. Sardegna F.S.E. - Operational Programme of the Autonomous Region of Sardinia, European Social Fund 2014-2020 - Axis III Education and training, Thematic goal 10, Investment Priority 10ii), Specific goal 10.5.

Abstract

Water is one of the essential elements for the nature and human being. The development of good practise of managing water resources are necessary to maintain sufficient availability and to support socio-economic activities and preserve natural ecosystems. For these reasons, it is fundamental to improve the knowledge of cause-effect relations that drives hydrological cycle, which determines water availability.

Climate and land use (LU) are two of the main drivers of the water cycle and indeed, the knowledge of their influence on hydrology is a fundamental research question. Of course, the future water availability is strictly related to future climatic and LU scenarios and then a critical role is assumed by the prediction and assessment of these two.

A climate and LU change impact study will be developed to investigate the near-future water availability in the Mediterranean area. In detail, on the basis of the state of art and the actual knowledge, the main objective of this dissertation is to estimate the probability density function (*pdf*) of annual surface runoff Q in transient climate and LU conditions in the island of Sardinia (Italy).

The study case has been selected due to the ongoing important process of climate change, overexploitation and degradation of natural resources affecting the entire island (see e.g. ISPRA, ENEA and CIRCE studies).

These analyses might have a strategic importance for stakeholders and government agencies that are interested in the management of water resources due to the well-known issue of water availability in the Mediterranean area. The knowledge of the near-future impact of climate and LU change could be useful to establish regional guidelines and good practices to avoid the ongoing reduction of water resources in Sardinia.

After a detailed review of the existing methodologies for describing and detecting climate and LU change and their influence in hydrological processes, a methodology based on the Budyko's theory that aims at assessing near future Q *pdf* in a closed form has been adopted. Five parameters are requested, referring to mean and standard deviation of annual rainfall P and annual potential evapotranspiration PET and Fu's parameter ω. Sets of these parameters will be assessed to define different climatic and LU scenarios for the near future. EUROCORDEX and Land Use CORINE projects will be used to represent climate and LU in the present and in the near future.

Results showed that in the near future Q will decrease due to the reduction of P and the increase of PET. The variability of Q will decrease due the reduction of variability of P. Finally, it has been observed that in Sardinia the main driver in the change of Q *pdf* will be climate change, while the LU plays a secondary role.

Table of contents

List of figures

List of tables

Introduction

Climate and land use (LU) influence in the water partitioning processes is one of the hot topics in the hydrological community. Budyko's framework proved to be an efficient and powerful tool to demonstrate and predict the contribution of climate and LU in mean annual runoff change. Despite a lot of studies focused on the impact of climate and LU change in long-term hydrological processes by Budyko's framework, there is a lack of studies that focus on both the near future effects of climate and LU change for a regional case. Furthermore, previous studies adopted Budyko's theory just in the assessment of mean value of annual surface runoff Q without digging in the impact of climate and LU on the probability density function (*pdf*). Given these premises, this thesis is an attempt to describe and predict the influence of climate and LU change on the Q *pdf* in the island of Sardinia (Italy). To deal with this research purpose, an approach based on the theory of Budyko (1974) and the equation of Fu (1981) was adopted to define Q *pdf* under transient climate and LU in arid and ungauged watersheds. In detail, the methodology refers to Caracciolo et al. (2017) that, starting from the linearization of Fu's equation by a first order Taylor expansion, provided a closed-form of Q *pdf*. Annual surface runoff distribution is fully determined once five parameters are known: mean and standard deviation of annual rainfall P and potential evapotranspiration PET and Fu's parameter

ω, which accounts for basin characteristic.

Near future and baseline climatic parameters (namely mean and standard deviation of P and PET) will be assessed by climate modelling (CM) outputs respectively from EUROCORDEX project and Sardinian Hydrological Service. Given systematic errors of CM outputs, bias correction (BC) procedures will be used to produce unbiased climatic scenarios. ω will be defined for near future LU scenarios, using proper relations between this parameter and LU properties.

Before proceeding with near future Q *pdf* evaluation, two propaedeutic studies are necessary: first, the verification of normality assumption of P and PET and second the statement of functional relations between ω and LU properties.

Goodness-of-fit metrics for normality assumption will be used to conclude on gaussian distribution assumption of P and PET, which is a necessary hypothesis for using the Q *pdf* in closed form as given by Caracciolo et al. (2017). A non-parametric procedure based on marginal statistics of daily and intra-annual rainfall will be created to dig into the convergence of P to normal shape. Moving from central limit theorem, normality assumption for PET will be discussed and argued as well.

Then, due to the critical role of ω in Budyko's framework and in the characterization of LU influence in water partitioning processes, the thesis will dig into the linkage between this parameter and LU properties, defining a procedure for the assessment of ω and highlighting how water partitioning processes is deeply connected to watershed characteristics.

The next Chapters are structured as follows:

- Chapter 1 illustrates the most important studies that deal with climate and land use effects in hydrology, also approached with Budyko's theory;
- Chapter 2 presents the methods, models and datasets adopted to predict near future *pdfs* of Q by Budyko's framework. In Section 2.1, general methods of Caracciolo et al. (2017)'s approach for the assessment of Q *pdf* are reported. Section 2.2 describes the methods adopted to conclude on normality assumption of P and PET. Goodness-of-fit metrics and a non-parametric normality test for P will be introduced. In Section 2.3, methods, dataset and models used to unravel the linkage between ω and LU properties will be reported. Finally, in Section 2.4 BC methods adopted to create unbiased climatic scenarios and the conceptualization behind LU scenarios will be detailed;
- Chapter 3 reports the preliminary and the key results of this thesis. First, in Sections 3.1 and 3.2, the evidences and results about the hypothesis of normality assumption of P and PET are stated. Section 3.3 discusses the results of the linkage between ω and LU basin properties and introduces the regression equations for the assessment of ω. In Section 3.4.1, BC performances in correcting CM outputs are discussed and given BC CM outputs, reliable 14 climatic scenarios and the associated parameters are presented. Similarly, ten near future LU scenarios and the related ω for Sardinia are reported (Section 3.4.2). Given four combinations of climate and LU scenarios, in Section 3.5,

the final evidences, namely near future Q *pdf* of Sardinia, have been showed and discussed;

- Finally, Chapter 4 presents conclusions and further work purposes.

1. State of art

Climate and land use affect incisively the mechanism of runoff production with different contributions (Piao et al., 2007; Li et al., 2009; Tomer and Schilling, 2009) and they influence each other as well in a complex framework (Bonan, 2008) that today does not allow us to fully understand all the relations (Green et al., 2011). The climate drives hydrological processes within watersheds and in general water budget in different ways: rainfall is the main input into the water cycle and the first contributor to runoff, temperature and solar radiation regulate the evapotranspiration and snowmelt processes. Alteration of climate and land use proprieties induces a change in the hydrological behaviour, then it is crucial to understand, interpret and predict future evolution of these two elements.

1.1. Climate change and hydrology

Most authors linked the climate change to anthropogenic activities, resumable in the increasing rate of greenhouse gas emission (Cox et al., 2000; Nijssen et al., 2001; Kalnay and Cai, 2003; Ramanathan and Carmichael, 2008; Ramanathan and Feng, 2009; Solomon et al., 2009; Montzka et al., 2011; IPCC, 2014). The Earth's temperature has increased by approximately 0.6 °C over the last century, with a raising rate much greater than any other during the last 1000 years, and an increase in extreme precipitation events has been observed (Alexander et al., 2006; Trenberth et al., 2007; IPCC, 2014). All available temperature datasets agree with a positive rate of increase of land surface temperature (Hansen et al., 2001; Smith and Reynolds, 2005; Brohan et al., 2006). Trenberth et al. (2007) highlighted that there is also a clear statistical increase in the numbers of warm nights and a reduction in the numbers of cold nights for 70-75% of the analysed land regions. Regarding precipitation, from 10°N to 30°N an increasing trend has been observed from 1950 to 1960, followed by a reduction after about 1970 which has been particularly detected in 10°N-10°S area too. Climate became significantly wetter in the eastern regions of North and South America, northern Europe, and northern and central Asia. On the other hand, precipitation decreased in the Sahel, the Mediterranean, southern Africa and parts of southern Asia. Despite the reduction of total precipitation amount of some regions, extreme events increased globally. After 1970, droughts raised and became more common, probably due to the increased high temperatures and heat waves. An interesting study of Frich et al. (2002) identified ten climatic extreme

indicators based on daily maximum and minimum temperature series and daily totals of precipitation, calculated from several national climate databases, that together reach global coverage. In 1946-1999 Frich et al. (2002) detected significant and robust change in global climate and in extremes. Regarding temperature, indicators highlighted an increase in warm summer nights, a decrease in the number of frost days and a decrease in intra-annual extreme temperature range. An evidence of general globe warming is given by the systematic increase in the 90th percentile of daily minimum temperatures. The frequency of heavy precipitation events increased in some regions of the world, as drought frequency in other areas.

An analogous study was conducted by Moberg et al. (2006) for Europe. They analysed a century-long daily temperature and precipitation in Europe and calculated a set of climatic indices which refer to daily temperature and extreme precipitation properties for the period 1901-2000. The results of this study showed that in 1946-1999 period is evident a pronounced trend of daily temperature and extreme precipitation. The warming of 1946-1999 period is associated with a raise in high temperature rather than a decrease in low temperature frequency. Moderate and very wet days indices (75% and 95% percentile of daily precipitation empirical distribution) showed a positive trend and outlined that in the wet regions a change in extreme precipitation relative to total amount is more evident than in dry regions.

It is important to predict possible future hydroclimatic forcings because water availability is strictly related to them. In the past years, huge efforts have been done using climate modelling at global scale for simulating the historical rainfall and temperature

(historical scenarios, HS) and predicting the possible climate evolutions under different hypotheses, referred as representative climatic pathways (RCPs). Global circulation models (GCMs) are mathematical models that physically depict the processes in the atmospheric circulation, ocean, cryosphere and land surface system and are the most powerful instruments to predict climate evolution. GCMs represent the climate using a three-dimensional grid that covers all the globe. The horizontal resolution ranges between 250 and 600 km, while the vertical dimension is represented by 10-20 vertical layers in the atmosphere, up to 30 layers in the oceans. For more details about climatic modelling see Mechoso and Arakawa (2015). RCPs are associated to the rate of emission of the anthropogenic gases, atmospheric concentrations, air pollutant emissions, land use and socio-economic scenarios. RCPs include four scenarios: a more stringent scenario (RCP 2.6), two intermediate scenario (RCP 4.5 and RCP 6.0) and the most pessimistic scenario (RCP 8.5). Historical simulations (HS) represent the past timeseries of climatic variables and they are useful in the assessment of the performance of GCM.

For impact assessment studies and hydrological applications, the native resolution scale of GCM is too coarse (Grotch and MacCracken, 1991; Fowler et al., 2007) and fine-resolution data is required for the assessment of reliable water balance components.

Two main groups of downscaling techniques are available to adapt GCM outputs to hydrological purposes: 1) statistical downscaling, which employs statistical relationships that relate regional and local climatic variables and 2) dynamical downscaling, which refers to regional climatic modelling (RCMs) that uses GCMs output as forcings (Giorgi, 1990; Wilby et al., 1998; Schmidli et al., 2006; Tang et al., 2016).

Several comparisons between performances of statistical and dynamical downscaling in reproducing observed climatic properties have been conducted all over limited regions (Mearns et al., 1999; Murphy, 1999; Wood et al., 2004; Boé et al., 2007; Schmidli et al., 2007). Regarding dynamical downscaling approach, different efforts have been made to test the performances of different combinations of GCM and RCMs models within intercomparison experiments like ENSEMBLES (Hewitt and Griggs, 2004), PRUDENCE (Christensen et al., 2007), CORDEX (Giorgi et al., 2009) and CMIP5 (Taylor et al., 2012).

The outputs of the combination of GCM-RCM (hereafter called as climatic models, CM) exhibit considerable bias. Error sources are generated by faulty CM parametrization and partial knowledge of physical and thermodynamic processes (Teutschbein and Seibert, 2012; Stevens and Bony, 2013; Mehrotra and Sharma, 2019), initial and boundary conditions and RCP selected scenario, calibration period, poor or missing land use and topographic data, but mostly by the different combination of GCM and RCM (Mamalakis et al., 2017). The hydrology research community produced many studies that focus on CM outputs to obtain correct forcings for their hydrologic modelling experiments. For the island of Sardinia (Italy), Mascaro et al. (2018) analysed the EUROCORDEX project datasets, whereas the combination of GCM and RCM produced different climatological outputs to test their performances. The analysis highlighted that the capacity of identifying local climatological patterns is limited and that there is a good correlation between observed and simulated climatology means, but the spatial variability is largely overestimated. Furthermore, the results showed that the majority of the models correctly

reproduced the phase of the annual cycle, underestimating the amplitude. Focusing on Sardinia, it is evident a statistically decreasing trend in annual precipitation time series. Similarly, Deidda et al. (2013) focused on detecting the best GCM-RCM couple, using the ENSEMBLE RCM project data, in order to provide good forcings to the hydrological modelling at river level scale, over the Mediterranean area. Mamalakis et al. (2017) also corrected the outputs of different GCM/RCM cascade from the ENSEMBLES project referring to Sardinia by parametric and nonparametric distribution mapping techniques and a parametric approach for the simultaneous bias correction and rainfall downscaling.

Then, given inherent systematic errors, CM rainfall and temperature outputs require a further correction before being used in the hydrologic modelling in order to make them more realistic in predicting future climatic scenarios (Teutschbein and Seibert, 2012).

Given the condition of transient climate observed in the present and assumed for the future, hydrological community adopted climate modelling outputs and tried to quantify the effects in the water resources due to climate change.

Middelkoop et al. (2001) carried on a study about the effect of climate change in Rhine basin, adopting for the several subcatchments a set of different conceptual and physically-based models. The climate change scenarios were based on two GCM models (Hadley centre's high-resolution 11-layer atmospheric GCM and the Canadian CCC model), and were rescaled by MAGICC model, a simple energy bucket model, providing mean monthly temperature, precipitation, wind speed, radiation datasets at a grid resolution 0.5°x0.5° longitude/latitude until 2100. All models agree in the results, indicating high winter discharge due to intensified snow-melt and increased winter precipitation. Another

outcome is the reduction of summer runoff caused by reduced winter snow storage and an increase in evapotranspiration. Considering 165 basins and 12 different climate modelling simulations of the XX and XXI century, Milly et al. (2005) tried to predict the mean and standard deviation of the annual streamflow all over the world. The comparison with the observable data shown that model overestimates the mean values in Africa, in the northeastern South America and in the northeastern America; on the other hand, the models underestimated runoff in the north low latitude Americas and in the southern South America. Referring to the 1900-1970, all climate models agrees to the increase mean runoff in the high latitudes of North America and Eurasia (10–40% by 2050) in the La Plata basin of South America, in eastern equatorial Africa and in some major islands of the equatorial eastern Pacific Ocean, opposite to the decreasing runoff southern Europe, the Middle East, mid-latitude western North America, and southern Africa. Elsner et al. (2010) studied the effect of climate change in a snow-dominated region, the Pacific Northwest area in the USA. They detected future hydrologic trends until 2080 by the climatic modelling output of the IPCC AR4 under different RCP scenarios and the VIC (Liang et al., 1994) and DVSHM (Wigmosta et al., 1994) hydrologic models at daily scale. In the Washington State the increase in the winter precipitation will induce the increasing of the annual runoff from 2020 (+2%) up to +4.2-4.7% in 2080. Soil moisture as well as the liquid content of the snowpack shown a decreasing trend: the first one, compared to the historical mean distribution, will be in the 35th and 43th percentile in 2020 and in 32th and 35th percentile in 2080, while the second one will reduce from 28-30% to 56-70% (2020-2080). Using the same VIC at the daily resolution for Colorado

River, Christensen et al. (2004) tested four climatic scenario due to different greenhouse gas emission of the U.S. Department of Energy/National Center for Atmospheric Research Parallel Climate Model (PCM). Three climatic scenarios are based on "business as usual" (BAU) scenario emission (1995-2098), while the last one refers to the greenhouse gas concentration of the 1995 (50 years long) and to remain constant in the time.

For St. Lawrence tributaries (Quebec, Canada), Boyer et al. (2010) studied the impact of rainfall and temperature changes in the winter and spring seasons. The hydrological model adopted was HSAMI model, a lumped rainfall-runoff model, while three GCM (HadCM3, CSIRO-Mk2 and ECHAM4) and two greenhouse gas emissions scenarios (A2 and B2) were used with a correction by perturbation factor calculated from historical data (1961-1990). Despite the differences due to GCM used, the common results are the increase in winter discharges and a decrease in spring discharges. The effect of longitude has been emphasized and govern the timing of occurrence of maximum peak discharge and the duration of the period affected by marked changes in the temporal distribution of discharge. Another outcome is the shift in advance by 22–34 day, depending on latitude.

An important study of Hagemann et al. (2013) aimed to investigate climate change impact on available water resources. The novelty of this work was represented by the use of multiple global climate and eight hydrological models at global scale. Firstly, Hagemann et al. (2013) stated that in these kinds of experiments the uncertainties arise from different sources (hydrological models, climate models, bias correction of climate models), but supported the idea that is the only possible way to approach hydrological

impact assessments. Runoff and evapotranspiration changed in the future following the projected changes of bias-corrected GCM precipitation. In 2071-2100, runoff decreased following the ensemble mean change of precipitation, over the eastern part of Australia, southern parts of Africa and the US, the north-eastern part of South America, the southern part of Europe, and a large part of the Middle East. The same pattern has been followed by evapotranspiration. The spread in the projected changes is originated by from the considered climatic model and scenario for both runoff and evapotranspiration.

Similarly, for Europe Roudier et al. (2016) studied the effects of climate change, using three hydrological models, namely Lisflood, E-Hype and VIC, and five GCM/RCM combinations and three RCP scenarios. After a preliminary bias-correction of climate modelling outputs (precipitation, maximum, minimum and average temperature, dew point temperature, shortwave and longwave downward radiations) by quantile mapping technique, hydrological models have been run with a resolution of 0.5°x0.5° over Europe. The results are centred on the impact that a +2°C warming generate on meteorological variables and extreme floods. One effect is the increase of floods magnitude significantly in most parts of Europe, referring to 10 and 100 years return period, even where the annual rainfall is expected to decrease. The hydrological models agreed with the fact that in large areas of Italy, France, Spain, Greece, the Balkans, Ireland and the UK, drought magnitude and duration will increase. Generally, according to this study, Europe will be affected by an intensification of the hydrological cycle.

Using VIC model coupled with coupled with glacier melting and glacier evolution schemes, Zhao et al. (2019) studied the impacts of climate change in the Tibet Plateau

system. They selected 5 GCM outputs of rainfall, temperature and wind speed from the Coupled Model Intercomparison, that have been downscaled by DC-V method, a statistical approach that corrects the climate modelling outputs against the observed mean and variance climate. The results showed that precipitation and temperature will increase in Tibet Plateu system, determining a reduction of glacier area greater than 50%. Annual runoff will increase significantly due to increase of precipitation, despite the annual hydrograph will remain substantially unchanged.

The climate change effect in the Mediterranean area has been studied in a recent study of Nerantzaki and Nikolaidis (2020) which focuses on focusing on the frequency, duration and intensity of their drought events. The basin system under study, Koiliaris River Basin and Keritis River Basin is deeply affected by three karst springs, which provide the higher contributors of water for the region of Chania (Greece). Five combination of GCM and RCM have been selected from EUROCORDEX project (Jacob et al., 2014), considering RCP 2.6 and RCP 8.5 scenarios that have been corrected by quantile mapping methodology. These ones represented the forcing of Karst-SWAT model which runs on daily time step. The study highlighted that intense change in surface runoff appears in 2059, when a decrease in annual rainfall leads a decrease in the mean annual karst flow. The frequency of future drought increases and decreases respectively in karst springs with lower and higher water retention time. This leads to an increase in the frequency of low flows, more marked in the dry months.

1.2. Land use change and hydrology

The land use rules water and energy fluxes exchange between soil, vegetation and atmosphere (Breuer et al., 2009) and it is considered one of the main drivers of hydrological changes (Milly et al., 2008; Zhang et al., 2011). Then, it is important to investigate the anthropic modification of land use mainly due to human activities (deforestation/afforestation, urbanization, dam construction, agriculture) on the hydrological cycle.

The first attempt to create land use maps and to detect land use change was represented by field data and aerial photographs, that have been partially abandoned because they are time and cost consuming in case of big regions. Nowadays, the most powerful instrument for studying land use and land use change is given by remote sensing via satellite imagery. This tool provides information about the characteristic of Earth's surface based on radiation reflected or emitted from those objects that are in the Earth's surface, as land coverage and their change. The launch of the first of a series of Earth Resource Satellites (ERS) for civil purposes occurred in 1972 with Landsat project, followed by NOAA AVHRR (1978) program. These first datasets were initially available at 8 km resolution, that has been improved through the efforts of the International Geosphere–Biosphere Programme (IGBP) (Townshend et al., 1994), reaching a nominal resolution of about 1.1 km and with a global land areas coverage (Cihlar, 2000). The first global-satellite land use maps have been elaborated through the aforementioned datasets (DeFries et al., 1998; Hansen et al., 2000). Several reasons led to a wide use of remote sensing via satellite

products for land use detection: increase of computational power for data processing, huge availability and reduction of cost of satellite datasets. The quality of the satellite imagery increases through the use of new satellite sensors that inaugurate a new season of satellite products such as Landsat 7 SPOT 4 VEGETATION (VGT), Moderate Resolution Imaging Spectroradiometer (MODIS), Medium Resolution Imaging Spectrometer (MERIS) (http://envisat.estec.esa.nl/) and Global Imager (GLI) (http://hdsn.eoc.nasda.go.jp/guide/guide/satellite/sendata/gli-e.html).

Consequently, the methods and tools for processing remote sensing datasets have been developed in order to create land use maps and to study land use change. Geographic Information Systems (GIS) and platforms as Google Earth Engine are the most powerful tools to elaborate remote sensing data and they had a huge use in land use classification (Weng, 2002; Xiao et al., 2006; Shalaby and Tateishi, 2007; Dewan and Yamaguchi, 2009; Xiong et al., 2017; Liu et al., 2018; Deng et al., 2020).

Lu and Weng (2007) categorized in a review the land use classifiers. The first studies of land use detection adopted classification techniques based on the pixel as the basic unit of analysis which represent and could be divided into two main groups: unsupervised and supervised. The second one is based on the adoption of training data pixels that represent a specific land use class. Then the algorithm uses the training data as reference for individuate similar pixels that have the same characteristic of training data pixels. Maximum likelihood, minimum distance, artificial neural network and decision tree classifier are some examples of supervised techniques. In unsupervised techniques, the user defines the number of land use classes and software analyses the remote sensing

images without any training data: ISODATA, K-means clustering algorithm. Other classifications distinguish land use classification techniques by the use of different kind of information in the pixels (per-pixel vs sub-pixels classifiers), the use of parameters (parametric vs non-parametric classifiers), the kind of spatial used (object-oriented vs per-field classifiers).

Hydrologists adopt remote sensing and land use studies and products to unravel and discover possible relationship between long-term trends of hydrological variables and land use properties. For example, Zhang and Schilling (2006) shown with simple statistical analyses of the runoff and precipitation, that in the Mississippi River the conversion of perennial vegetation to season row crops caused the decreases evapotranspiration, increased baseflow and thus the runoff. Similar approach are followed in other papers (Costa et al., 2003; Jovanovic et al., 2016). Paired catchment analyses aimed at land use change influence on hydrology are been developed in a lot of studies (Stednick, 1996; Brown et al., 2013), but the modelling approach is the most adopted and intriguing for the today computational efficiency and power. Particularly, it allows to describe land use properties and their evolutions in time by parametrization of hydrological modelling. Siriwardena et al. (2006) assessed the effect of forest clearing and change in land use in a big watershed of 164000 km^2 (Comet River, Australia) using the conceptual model TANH at annual scale and the conceptual daily rainfall-runoff model SIMHYD. After different calibration process, they observed that the models, performing modification of the land use parameters, were able to clearly describe the effect of the deforestation, that induces increase in runoff, attested by higher values of

runoff coefficient (+50%) and a change in the cdf of annual runoff. Gordon et al. (2005) studied at global scale by GIS modelling, the influence of the land use change in the evapotranspiration, concluding that the irrigation and deforestation are equally important. Haddeland et al. (2007) studied the influence of human land change and water management at continental scale, in the North America and Asia in the period 1970-1992 through hydrological modelling and data from different sources. In North America and Asia, the annual runoff increased caused by conversion of forest in croplands of 2.5% and 6% respectively.

In the scientific literature there are several contributions that investigate the impact of climate and land use change in the water balance components. The hydrological modelling (for the land use change) and the observed and future climate scenarios (for the climate change) permit to describe or forecast near-future evolution of the most important hydrological quantities. Furthermore, one of the most challenging issue is to separate the contributions of land use and climate change in water balance alterations (Ye et al., 2013; Gao et al., 2016; Yang et al., 2017; Navas et al., 2019). Hydrology approaches to this theme in different ways: statistical, paired catchment approaches and physical-based modelling (Li et al., 2012; Yang et al., 2017).

Paired catchment aims to interpret the climate and land use change role in small catchments by comparison between other similar ones, but is not feasible to the large one due to the difficult in locating large basins in close proximity.

Regarding the physical-based modelling, several attempts have been done with different models (Cuo et al., 2013; Zhang et al., 2016a; Huang et al., 2019). In order to quantify

impacts of land use change and climate variability on surface hydrology, Li et al. (2009) employed SWAT model in order to model the response of an Chinese agricultural watershed, obtaining good results in the calibration phase. Particularly they were able to quantify the different contribution of land use change (from shrubland and sparse woodland to grassland, 4,5% of the basin area) and climate variability during 1981-2000: they decreased runoff respectively of the 9.6% and 95.8%. and soil moisture, respectively of 18.8% and 77.1%. The evapotranspiration was affected by land use change and climate variability respectively with an increase of 8.0 % and 103%. Other authors adopted SWAT for the same purposes (Yang et al., 2017; Mekonnen et al., 2018; Osei et al., 2019; Zhang et al., 2019). As the same way for the Ketar River basin, Legesse et al. (2003) studied the hydrologic response change, employing a modular physical-based model. They created climatic scenarios, modifying the climatic series of calibration period (1985-1986), in order to test the sensibility of the basin to climatic change and reconstruct on historical information the land use change of the basin. Applying separately the climate and land use change scenario, they obtained that supposing a decrease of 10% of mean daily rainfall all over the year and in the spring time and then a reduction of 10% of the average air temperature, the runoff changed of about 20-30% compared to the simulation period, whereas the land use (from traditionally cultivated/grazing land to woodland) increases the evapotranspiration (2.5%) and reduces the mean annual streamflow (8%). Similar studies are present in literature (Cuo et al., 2013; Zhang et al., 2016a). The future hydrologic behaviour could be investigated in the same way, considering the CGM/RCM-LAM model results under different greenhouse gas emissions (Mango et al., 2011; Cuo

et al., 2013; Serpa et al., 2015; Pan et al., 2017; Shrestha et al., 2018) as forcing of several hydrologic models.

The statistical approach is mostly related to, as Mann-Kendall (Kendall and Gibbons, 1990) and Pettit's (Pettitt, 1979) test and aims to statistical remark the trend change in the most important water balance components. This approach is often associated to the use of the elasticity of runoff calculated by Budyko's theory. For example, in a study over the Haihe basin, Xu et al. (2014) highlighted the decreasing trend (10.9 mm/decade) and the common breakpoint of the main part of subcatchments (in 1979) of annual runoff from 1956 to 2005. The variation of runoff was accountable for climate and land use change by 26.9% and 73.1% on average, respectively associated to decrease of precipitation and increase of vegetation. The same approach has been adopted for the Loess Plateu river basin by Gao et al. (2016) in an analysis for quantifying the climate and land use change variability on mean annual streamflow. The results of Mann-Kendall analysis identified a decreasing trend in the annual streamflow, that it is attributable to the extensive land cover change the main reason of significant streamflow reduction. Gao et al. (2016) pointed out by a sensitivity analysis bases on the Budyko's theory that mean annual precipitation and potential evapotranspiration are the key control of water balance. The Mann–Kendall test and Pettitt abrupt change point test were used in Weihe River Basin of China by Deng et al. (2018) to interpret the change in mean runoff due to human impact and climate change. The 1990s was identified as the abrupt change point and the calculation of elasticity of annual runoff within Budyko's theory related the downward trend of runoff mostly to precipitation, then land use and potential evapotranspiration.

The change detection and break point analyses has been adopted also for South East Asia (Lee and Yeh, 2019) and South East America (Navas et al., 2019) watersheds.

1.3. Budyko's approach

As highlighted in the previous paragraph, in the study of climate and land use change influence in large arid watershed, the aforementioned Budyko's theory (Budyko, 1974) is a valuable tool. Furthermore, distributed physical-based or semi-distributed models are a powerful instrument as well, but they have practical limitations and uncertainties related to model parametrization and might be accompanied by field measurements program (Beven, 1989). In particular, Rosso et al. (1994) stated that the basic problems of these models is the assessment of land surface hydrology and thermal properties parameters. Then, in an impact study of land use change, uncertainties could affect deeply the predictions that arises from model parametrization of large watersheds. For all these reasons, Budyko's theory is a good alternative because of the ease of application and the limited number of needed parameters for the prediction of mean annual runoff Q. Budyko's theory simplifies the water balance and defines Q as the difference between mean annual precipitation P and mean annual evapotranspiration PET. Furthermore, Budyko hypothesized a functional relationship between mean values of annual evapotranspiration, annual rainfall and potential evapotranspiration, that several authors tried to model (Schreiber, 1904; Ol'Dekop, 1911; Turc, 1953; Pike, 1964; Choudhury, 1999; Porporato et al., 2004). One of the most known model was obtained by Fu (1981), with only one parameter, commonly indicated as ω, which rules the rainfall partitioning into mean annual runoff and mean annual potential evapotranspiration. In Budyko's theory and Fu's equation, ω covers a central role in determining hydrological response.

Different attempts have been made to interpret and model ω. Using 270 Australian catchments, Zhang et al. (2004) performed a stepwise regression analysis between ω and basin properties (i.e. vegetation cover, precipitation characteristics, catchment slopes, and plant available water capacity) finding that the most significant element were average storm, depth and coefficient of variation in daily precipitation. Similarly Xu et al. (2013) linked ω with geographic and morphometric catchment properties of a dataset composed by MOPEX "small" basins (Duan et al., 2006) and "large basin" which data come from different sources (CRU TS 3.20, HYDRO1K, GIMMS). A simple stepwise regression and a more complex neural network were adopted to explain relationship between ω hydrological defined parameter and morphological basin properties finding good explanatory capacity of the two developed models for small and large group basin (R^2= 0.53 ÷ 0.83). Latitude has proved to be the best correlate with ω. As an alternative, Yang et al. (2007) selected non-linear expression for predicting ω over 180 non-humid basins in China, that was a function of infiltration capacity, soil water storage and average terrain slope. They were able to predict annual water cycle components (95.2% and 62% of the variance of mean annual evapotranspiration and runoff, respectively) just using the aforementioned morphological descriptors. Through water-soil-vegetation metrics, Abatzoglou and Ficklin (2017) studied the correlation between ω and morphological properties over United State watersheds. The relative cumulative moisture surplus ($rCMS$), the ratio of available soil water holding capacity to precipitation (AWC/P) and topographic slope were integrated in a regression model, that demonstrates to be able to simulate the spatial variability of ω (81.2%); for increasing value of $rCMS$ Fu's parameter

decreases, whereas for $AWC/P > 0.4$ has direct proportionality with ω.

To interpret the influence of climate and land use change in hydrological response in large watershed, several authors adopted the Budyko's framework. An important work about climate and land use change/human activity through Budyko's framework was done by Wang and Hejazi (2011). They used the international rainfall, runoff and potential evapotranspiration database MOPEX and they considered two periods (1948–1970 and 1971–2003) to assess the mean annual streamflow change in the USA. A decomposition method based on the Budyko hypothesis was to quantify the climate and human activity contribution to mean annual streamflow change. In the MOPEX watersheds Wang and Hejazi (2011) stated that the climate change is the most important contribution in the change of mean annual runoff due to low human impact in the analysed basin. The results showed that human impact is likely to be more influent in watersheds with urban areas because of increasing imperviousness and extensively irrigated agricultural watersheds. Jiang et al. (2015) extensively adopted the Budyko's theory to define the contribution of climate and human impact in Weihe River basin of China. Firstly, for four mono-parametric Budyko's models have been considered to represent the hydrological behaviour of Weihe River basin of China and a covariate analysis indicated that ω is related to the explanatory variables of both climate conditions and human activities. The decomposition and sensitivity analyses highlighted that the decrease of annual mean runoff is most attributable to climate more than to human activities. A Budyko's approach was adopted by Abera et al. (2019) too in northern (Tigray region) and south-eastern (Somali region) Ethiopia. Deviation and elasticity metrics have been used to interpret how

the partitioning process changed from 1990-1994 to 2010-2014. In the southern and in the south-eastern part of Ethiopia, these metrics showed higher values than in the rest of the nation, indicating that the change in water yield is more predictable than in the northern part. Furthermore, the contribution of climate and land surface change in the increase of annual runoff is almost 50% each, as attested by the sensitivity analysis.

2. Methods, models and datasets

This Chapter is composed by four Sections. The first one starts illustrating the general theory of Budyko and the related Fu's equation, that apply to dry and ungauged watersheds, as the island of Sardinia (Section 2.1). Then, moving from Budyko's theory and Fu's equation, a description of the Budyko-based approach of Caracciolo et al. (2017) is described.

The proposed approach requests as hypothesis that annual rainfall P and annual potential evapotranspiration PET empirical cumulative density function (*ecdf*) approximate gaussian shape. Then, Section 2.2 is dedicated to the methods used to test the validity of normality assumption of P and PET.

In Section 2.3, given the importance of Fu's parameter in the proposed approach, three in-silico experiments that deal with the linkage between ω and land use (LU) properties, and with the influence of basin characteristics on Q, are described. Furthermore, the procedure adopted to develop regression equations that allow to asses ω by basin characteristics and in poor or missing hydrological data, is described.

Finally, Section 2.4 describes the conceptualization behind near future climatic and LU scenarios. Each climatic scenario is represented by a set of four parameters, namely mean and standard deviation of P and PET. These parameters have been derived from

EUROCORDEX project datasets after a preliminary bias correction (BC) of the related climate modelling outputs. BC methods here adopted are described both for daily rainfall and temperature. The conceptualization behind LU scenarios and the procedure to derive the related ω is depicted in the end of Section 2.4.

Furthermore, each Section illustrates models and datasets used.

2.1. From the Budyko's theory to annual runoff distribution

The Budyko's theory, as interpreted by Donohue et al. (2007a), is based on a simple bucket model which represents large basins water balance as follows:

$$\frac{dS_w(t)}{dt} = P(t) - Q(t) - E(t) \quad (2.1)$$

where $S_w(t)$, $P(t)$, $E(t)$ and $Q(t)$ are respectively soil water storage, rainfall, evapotranspiration and runoff at a given time t.

Considering steady state conditions (Porporato et al., 2004; Donohue et al., 2007b) and neglecting the variation of water storage $\frac{dS_w(t)}{dt} = 0$ (Koster and Suarez, 1999; Zhang et al., 2004; Shao et al., 2012), which are typical of dry catchment-scale even at annual, Eq. 2.1 becomes:

$$\bar{Q} = \bar{P} - \bar{E} \quad (2.2)$$

where $\bar{Q}$, $\bar{P}$ and $\bar{E}$ refer to the mean annual values of Eq. 2.1.

Budyko also included the energy balance which is involved in the evapotranspiration processes:

$$\frac{dS_e(t)}{dt} = R_n(t) - \lambda ET(t) - H(t) \quad (2.3)$$

where $S_e(t)$, $R_n(t)$, $\lambda ET(t)$ and $H(t)$ are respectively the energy storage, the latent heat of vaporization, the fluxes of latent and sensible heat at a given time t. Over long-timescales, energy storage variations can be considered negligible:

$$\overline{R_n} - \lambda\overline{ET} - \overline{H} = 0 \quad (2.4)$$

where $\overline{R_n}$, $\lambda\overline{ET}$ and $\overline{H}$ refers to the mean annual variables of Eq. 2.3.

In detail, he related the ratio of $\overline{R_n}/\lambda$ to $\bar{P}$ that has been called as aridity index (AI) and the ratio of $\overline{ET}$ to $\bar{P}$ (called EI). R_n/λ is also intended as the annual potential evapotranspiration (PET). Budyko found a curvilinear relationship between AI and EI with only one parameter, that tuned using hydrological metrics of 1200 large Russian catchments ($A > 1000\ km^2$) and obtaining reasonable good fit.

Different expressions have been proposed to describe the relation between EI and aridity index AI (Schreiber, 1904; Ol'Dekop, 1911; Turc, 1953; Pike, 1964; Choudhury, 1999; Porporato et al., 2004); one of the most known was obtained by Fu (1981), which is a mono-parametric expression. The only parameter to assess is commonly indicated as ω, which rules the rainfall partitioning into Q and ET (see Chapter 1):

$$\frac{ET}{P} = EI = 1 + AI - (1 + AI^{\omega})^{\frac{1}{\omega}} \quad (2.5)$$

The higher the Fu's parameter, the higher EI for a given aridity index AI (Figure 2.1). Fu also derived that ω value of Budyko's empirical expression is equal to 2.6 (Choudhury, 1999; Donohue et al., 2011; Li et al., 2013). Nevertheless, the Fu's parameter has been related to morphological, geographic aspects and vegetation (Shao et al., 2012; Williams et al., 2012; Li et al., 2013; Zhou et al., 2015; Zhang et al., 2016b).

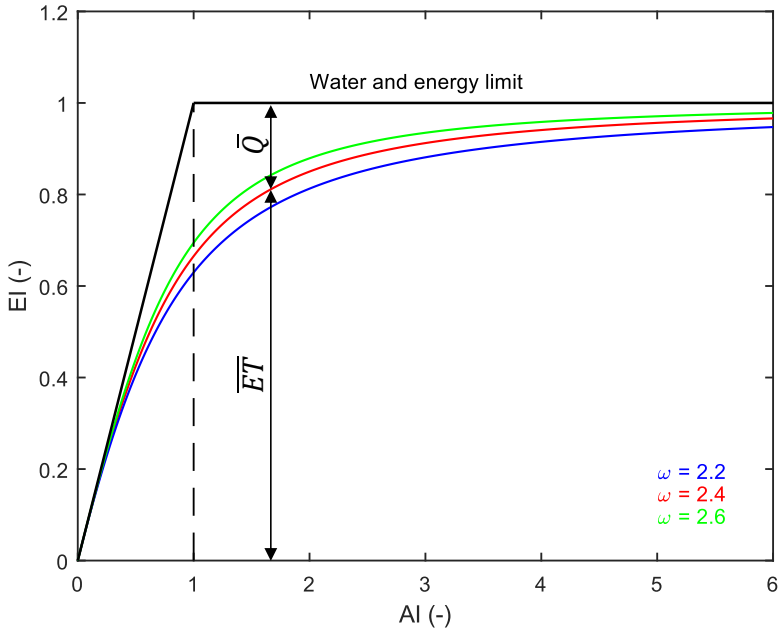

Figure 2.1. For different ω, graphical representation of Fu's equation. Given a value of AI, the partition between $\bar{Q}$ and $\overline{ET}$ changes according to ω.

In this thesis, Budyko-based method developed by Caracciolo et al. (2017) has been used, who derived the *pdf* of annual surface runoff (Q) in a closed-form for dry and ungauged basins. In detail, Caracciolo et al. (2017) linearized the Fu's equation by a first order Taylor expansion for narrow ranges of AI, as a linear equation, as follows:

$$EI = aAI + b \tag{2.6}$$

where a and b are expressed as a function of AI and the Fu's parameter ω:

$$a = 1 - (AI)^{\omega-1}(1 + (AI)^{\omega})^{\frac{1-\omega}{\omega}} \tag{2.7}$$

$$b = 1 - (1 + (AI)^{\omega})^{\frac{1}{\omega}-1} \tag{2.8}$$

Then, substituting in Eq. 2.2:

$$Q = P - ET = (1 - b)P - aPET = (1 - b) - aAI \tag{2.9}$$

where Q, P, ET, PET represent, as already stated, respectively the annual surface runoff, rainfall, evapotranspiration and potential evapotranspiration.

Caracciolo et al. (2017) characterized Q as a random variable and in particular as the difference of two terms $X = (1 - b)P$ and $Y = aPET$ which in turns represents the two variables of the joint *pdf* of Q. X and Y have been assumed independent (i.e. thus the correlation can be neglect) and statistical described by the normal distribution which parameters are the mean annual rainfall $\bar{P}$, variance of annual rainfall σ_P^2,mean annual potential evapotranspiration $\overline{PET}$ and the variance of annual potential evapotranspiration σ_{PET}^2. Under such assumptions, the *pdf* of Q reads:

$$p(Q) = c\frac{e^{-\frac{(Q-\mu_X+\mu_Y)^2}{2(\sigma_X^2+\sigma_Y^2)}}}{\sqrt{2\pi}\sqrt{\sigma_X^2 + \sigma_Y^2}} \tag{2.10}$$

where $\mu_X = (1 - b)\bar{P}$, $\mu_Y = a\overline{PET}$, $\sigma_X^2 = (1 - b)^2\sigma_P^2$, $\sigma_Y^2 = a^2\sigma_{PET}^2$ and c has been to be tuned in order to constraint the area under the *pdf* to one.

Then, in order to assess the *pdf* of Q, four parameters strictly related to the P and PET properties ($\bar{P}$,$\overline{PET}$,σ_P^2,σ_{PET}^2) and an additional parameter (ω) which is linked to climate and land use (LU) properties, as widely argued in literature (see Section 1.3), are

requested.

The proposed method has been applied by Caracciolo et al. (2017) for the assessment of the observed analytical *pdf* of Q in 27 basins of Sardinia (Italy), showing good performance in the prediction of Q distribution compared to the empirical ones. Using this method too, Viola et al. (2019) performed in-silico experiments that investigate how the Q *pdf* could vary under different climate and LU change, derived from CM outputs and LU analyses. In both studies, the authors adopted Caracciolo et al. (2017) procedure without taking into account the hypotheses of the method. Normality assumption and statistical independence of P and PET are the two main hypothesis of the proposed methods. Then, in the next Section the procedure and methods for an investigation on converge of P and PET to gaussian shape will be described.

Therefore, given the importance of Fu's parameter ω in the proposed method, the linkage between this parameter and the LU characteristics will be discussed by three consecutive in-silico experiments that will lead to an empirical expression for ω's assessment

Finally, to define future parameter values of Eq. 2.10, in Section 2.4 the description of the procedures and ideas behind climate and LU scenarios will be reported.

2.2. Normality assumption for annual rainfall and potential evapotranspiration

Most part of this Section has been submitted for publication as:

Ruggiu, D., Viola, F., Langousis, A., A non-parametric procedure to assess the accuracy of the normality assumption for annual rainfall totals, based on the marginal statistics of daily rainfall: An application to NOAA-NCDC rainfall database, submitted to Journal of Applied Meteorology and Climatology

As stated in Section 2.1, according to Caracciolo et al. (2017), the probability density function (*pdf*) of annual rainfall P and annual potential evapotranspiration PET should be assumed normal. This Chapter is dedicated to the verify such hypothesis at global level.

One of the first attempts to investigate about P distribution was conducted by Markovic (1965), who used P timeseries from 2506 stations in Western United States and the Southwestern Canada with at least 30 years of recordings, to identify the distribution model that best fits observations. The study concluded that among the normal, lognormal, and Gamma distribution models, the lognormal probability density function produced acceptable results, especially in the case when the P was positively skewed. Following the early work of (Markovic, 1965), several other studies have focused on identifying the best distribution model that fits the observed frequencies of P in different areas around the globe, including India (Mooley et al., 1981; Rodell et al., 2009), South Florida (Sculley, 1986), Costa Rica (Waylen et al., 1996), Saudi Arabia (Abdullah and Al-

Mazroui, 1998) , Israel (Ben-Gai et al., 1998), Jordan (Dahamsheh and Aksoy, 2007), Portugal (De Lima et al., 2010), Nigeria (Ogungbenro and Morakinyo, 2014), and Iran (Vaheddoost and Aksoy, 2017). The aforementioned studies concluded that the type of the distribution model that best fits the empirical frequencies of P may be well approximated by a normal distribution; see e.g. Mooley et al. (1981), Waylen et al. (1996), Abdullah and Al-Mazroui (1998), De Lima et al. (2010), and Ogungbenro and Morakinyo (2014).

The theoretical basis for the normality assumption of P arises from central limit theorem (CLT); see e.g. Parzen (1960), Fisz (1963), Feller (1968), Benjamin and Cornell (1970), and Papoulis (1990). According to this theorem, if $X_i(i = 1, \dots, n)$ are independent copies of a random variable X with finite variance, then asymptotically as $n \to \infty$ random variable $Z = \sum_{i=1}^{n} X_i$ converges to a normal distribution. Common relaxations to CLT include approximate convergence of Z to a normal distribution when n is large but finite (i.e. referred to as pre-asymptotic conditions), and when X_i are not independent and identically distributed, but exhibit similar variances with some (but not all) of X_i being inter-dependent; see e.g. Benjamin and Cornell (1970). Evidently, for the case when $X_i(i = 1, \dots, n)$ correspond to daily rainfall amounts, where seasonal periodicities and short-range dependencies are present, approximate convergence of the P $Z = \sum_{i=1}^{n=365} X_i$ to a normal shape depends highly on the local climate and the marginal and joint statistics of daily rainfall, including: seasonal variations of the empirical distributions, the increased daily skewness of positive rainfall rates in arid regions exhibiting high fraction of dry days (Wilks, 1990; Katz, 1993; Ben-Gai et al., 1998; Yoo

and Ha, 2007) and the (often non-negligible) temporal dependencies in daily rainfall series (Le Cam, 1961; Waymire and Gupta, 1981a; Waymire and Gupta, 1981b; Waymire and Gupta, 1981c; Foufoula-Georgiou and Lettenmaier, 1986; Onof et al., 2000; Veneziano and Langousis, 2010; Koutsoyiannis and Langousis, 2011).

In all cases, the rate of convergence of the distribution of Z to a normal shape decreases as the aforementioned factors intensify.

Given the importance of normality assumption of P and PET in Caracciolo et al. (2017)'s framework, this Section aims at describing the methods adopted to test normality assumption of this two variables. About P, three consecutive steps will be followed to investigate Gaussian/No Gaussian nature 1) goodness-of-fit metrics to conclude on the approximate convergence of the empirical cumulative density function (*ecdf*) of P to a normal shape, and classify P samples into the G and NG complementary groups, 2) logistic regression analysis to identify the statistics of daily rainfall that are most descriptive of the G/NG classification, and 3) a random-search algorithm to determine a set of constraints that allows classification of P samples based on the marginal statistics of daily rainrates. This latter attribute of the data allows us to study, also, how large-scale climatic features affect Gaussianity of P, such as those embedded in the Köppen-Geiger climatic classification (Kottek et al., 2006).

Convergence to normal shape of PET has been discussed in the final results moving from theoretical basis, namely CLT, and the goodness-of-fit metrics to conclude on the approximate convergence of PET *ecdf* to a normal shape in an investigation of PET samples.

2.2.1. Dataset

The analyses are conducted using 3007 timeseries of daily rainfall from the NOAA-NCDC Global Historical Climatology Network (GHCN) rainfall database (https://www.ncdc.noaa.gov/ghcn-daily-description); see Menne et al. (2012). NOAA-NCDC-GHCN contains daily timeseries from 90230 stations with Global coverage. To ensure the statistical significance of the obtained results, and similar to previous studies (Easterling et al., 1997; Papalexiou et al., 2018; Papalexiou and Montanari, 2019), the analysis have been conducted with a total number of 3007 stations with percentages of missing data below 5%, yearly completeness above 98%, and more than 30 years of recordings. The density map of the analysed stations is shown in Figure 2.2, while Figure 2.3 illustrates the percentage of stations exceeding different length requirements. Figure

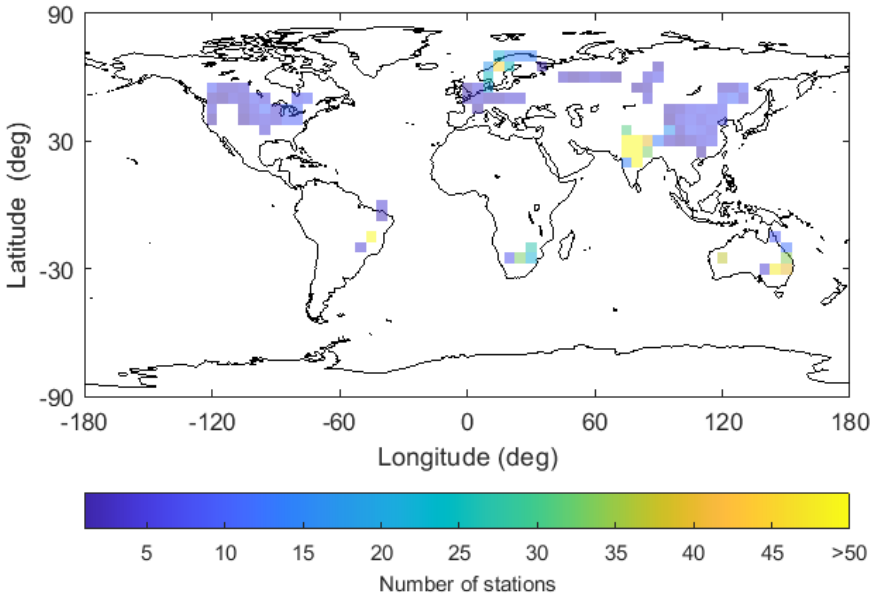

Figure 2.2. Spatial density of the 3007 NOAA-NCDC rainfall stations considered in the analysis.

2.2 highlights that Africa and South America are the less represented regions, while North America, Europe, India, China and West Australia exhibit denser station networks.

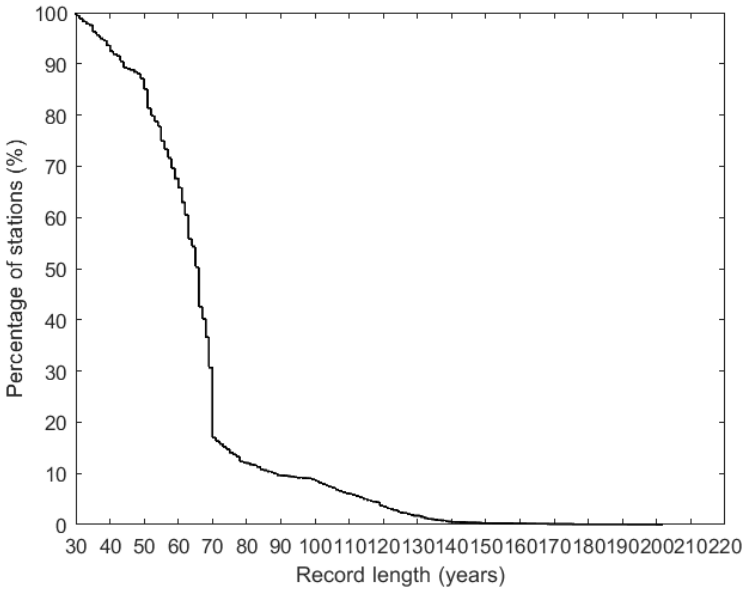

Figure 2.3. Percentage of the considered NOAA-NCDC stations exceeding different record length requirements.

2.2.2. Goodness-of-fit metrics for normality assumption

Statistical tests are based on the acceptance/rejection of a null hypothesis H_0, based on a statistical metric T, referred to as test statistic; see e.g. Fisher (1925), Neyman and Pearson (1933), Lindquist (1940), and more recently Benjamin and Cornell (1970), and Papoulis (1990). For a certain test statistic T, the level of significance α of the test is the acceptable/desired probability level to acquire type I errors (namely, H_0 is true but the

test rejects it), and it is strictly linked to the uncertainty associated with rejection of the null hypothesis. Hence, the larger the α, the higher the uncertainty in rejecting the null hypothesis. Suppose now that t is an estimate of T obtained from a sample. In this case the p-value of the sample is defined as:

$$p = Pr[T > t] = 1 - F_T(t) \tag{2.11}$$

and the null hypothesis is accepted if $p > \alpha$.

Three test statistics have been used, namely the Kolmogorov-Smirnov (KS), Anderson-Darling (AD) and Cramer-Von Mises (CVM), as implemented by Öner and Kocakoç (2017) in MatLab for the Gaussian case, to classify rainfall samples according to the approximate normality of P. More precisely, P at each station are considered to be Gaussian distributed if the calculated p-value is larger than a specified significance level α.

The first test statistic used here is the Kolmogorov-Smirnov (KS), which is widely used in hydrological applications (Heo et al., 2008; Fan et al., 2013; López-Rodríguez et al., 2019). Define $F_Z(z)$ to be the *ecdf* of a timeseries of P of length n, and denote by $G_Z(z)$ the fitted normal *cdf*. The KS test statistic D_n is defined as the maximum distance between the empirical $F_Z(z)$ and theoretical $G(z)$ *ecdfs*:

$$D_n = \max_z |F_z(z) - G_z(z)| \tag{2.12}$$

The *p*-value of the sample can be obtained from the Kolmogorov distribution as the exceedance probability of $\sqrt{n}D_n$; see e.g. Massey (1951), and Lilliefors (1967). It follows from Eq. 2.12 that D_n is suited to quantify linear deviations between the empirical and theoretical *cdfs* in the frequency domain and, therefore, the test is not very accurate in detecting deviations in the upper and lower tails of the empirical distributions; see also discussion below.

Contrary to KS test statistic, which focuses on a single point of the corresponding *cdfs*, Cramer-Von Mises (CVM) and Anderson-Darling (AD) test statistics are calculated by evaluating the integral of the weighted squared differences between the empirical $F_Z(z)$ and the fitted normal $G_Z(z)$ *cdfs* over the whole distribution range (Cramér, 1928; Von Mises, 1928; Anderson and Darling, 1952; Farrell and Rogers-Stewart, 2006):

$$A^2 = n\int_{-\infty}^{+\infty}[F_z(z) - G_z(z)]^2\psi(z)dF_z(z) \tag{2.13}$$

where $\psi(z)$ =1 for CVM, and $\psi(z) = [G_z(z)(1 - G_z(z)]^{-1}$ for AD. It follows from Eq. 2.13, and the form of function $\psi(z)$, that CVM weights equally the whole *ecdf*, while AD assigns larger weights to observations located in the distribution tails; see e.g. Laio (2004), Farrell and Rogers-Stewart (2006), and Langousis et al. (2016). Hence, AD is more restrictive in accepting the normality hypothesis than CVM. The sample *p*-values corresponding to CVM and AD test statistics, can be obtained as the exceedance probability of the calculated value of A^2; see e.g. Stephens (1986). It follows from the

discussion above that KS, AD and CVM test statistics exhibit different attributes and, therefore, they may lead to contrasting results.

Existence of inter-annual dependencies in P samples may bias the estimation of the variance from finite samples and, thus, influence goodness-of-fit testing. To avoid such issues, the standard deviation of P samples has been calculated using the formulation suggested by Koutsoyiannis (2003):

$$\sigma_H = \sqrt{\frac{n - \frac{1}{2}}{n - n^{2H-1}}}\sigma \tag{2.14}$$

where σ_H is the unbiased estimate of the standard deviation in the presence of inter-annual temporal dependencies, n is the length of the P sample, σ is the estimate of the standard deviation assuming independence of P, and H is the Hurst coefficient; see e.g. Hurst (1951), Mandelbrot and Wallis (1969), Montanari et al. (1997), and Langousis and Koutsoyiannis (2006). Hurst coefficient H quantifies the magnitude of inter-annual dependencies (Lettenmaier and Burges, 1977; Salas et al., 1979; Montanari et al., 1997; Razavi and Vogel, 2018)

H varies between 0 and 1, with H = 0.5 indicating linear independence, and H >0.5 (<0.5) indicating positive (negative) correlations in the corresponding time series. The value of H can be calculated from the empirical samples of P, by aggregating them at different temporal scales m (e.g. m = 1, 2, 3, 4 years etc.) and calculating the log-log slope of their standard deviation versus m.

2.2.3. Non-parametric procedure to assess the accuracy of the normality assumption for annual rainfall

Approximate convergence of the distribution of P to normal shape is strictly linked to the seasonal character and marginal statistics of daily rainfall rates. In order to describe basic features of daily rainfall, the fraction of dry days f_{dd} (here days with rainfall accumulation below 0.1 mm), the mean value m_{wd}, standard deviation σ_{wd}, and skewness coefficient sk_{wd} of rainfall in wet days (here days with rainfall accumulation in excess of 0.1 mm), and the precipitation concentration index (PCI) (Oliver, 1980; Michiels et al., 1992; De Luis et al., 1997; Cannarozzo et al., 2006) have been used. If the latter index is below 0.10, monthly rainfall distribution is uniform, whereas values between 0.11 and 0.2 indicate a substantial inter seasonal rainfall variability.

To quantify the effects of local climate in determining the approximate convergence of P to a normal distribution, a logistic regression analysis (Bliss, 1934; Berkson, 1944; Augustin et al., 2008; Van Steenbergen and Willems, 2013) will be used to identify the most influential daily rainfall statistics in grouping the analysed P samples into the G and NG subsets.

Then, a random-search algorithm has been combined with a proper test-based objective function to conclude on a set of constraints that allows classification of P samples based on the marginal statistics of daily rainrates.

Define A to be the event that a sample exhibits approximate Gaussian behaviour at a certain significance level α, and denote by T the event that a sample fulfils a certain set of constraints **S** regarding its marginal statistics. Evidently, the probabilities of events A and T depend on the normality test and the level of significance α used, and the set of adopted constraints **S**, respectively. To conclude on an optimal **S**, the likelihood that the identification procedure based on the selected constraints **S** produces accurate outcomes has been maximized. Along these lines, the following maximization expression have been selected to solve the problem:

$$\max_{\mathbf{S}}(Pr[A \cap T] + Pr[A^c \cap T^c]) \tag{2.15}$$

To avoid convergence problems, the optimal set of constraints was determined through random search. Specifically: 1) 10^6 threshold level combinations by uniformly sampling the corresponding regressor variables have been considered within their observed ranges, 2) for each threshold combination, the AD classification into G and NG groups of the previous Section was used to estimate the empirical probabilities $Pr[A \cap T]$ and $Pr[A^c \cap T^c]$, and 3) a set of threshold combinations as optimal was selected that maximizes the objective function in Eq. 2.15.

2.3. The linkage between Fu's parameter and land use properties as an investigation on the relationship betweem basin characteristc and annual runoff

Most part of this Section has been accepted for publication as:

Ruggiu, D., Viola, F., 2019, Linking climate, basin morphology and vegetation characteristics to Fu's Parameter in data poor conditions, Water (Switzerland), 11 (11), art. no. 2333

The role of climate, basin morphology and vegetation in characterizing long-term hydrological processes and in determining the ω value will be explored by three consequent modelling experiments, sketched in Figure 2.4.

Supposing a particular climate, defined as a characteristic seasonal pattern of potential evapotranspiration and rainfall, once defined the morphological basin and vegetation properties (model parameters), the hydrological response is supposed to be only related to the aridity index. In other words, for a given climate condition, notwithstanding the combinations between mean value of annual rainfall P and potential evapotranspiration PET are infinite, water partitioning rules are uniquely defined. In the Budyko's framework and using the Fu's equation, this means that for different casual couples of AI and EI, a unique value of ω is identifiable (Figure 2.4.a).

Namely, the same basin (the same model parameters and morphological and vegetation properties), in different geographic areas with different seasonal pattern of climatic variables, will result in different partitioning rules as a function of climate (Figure 2.4.b).

Finally, the idea of biunivocal relationship between basin morphometric and vegetation properties and hydrological response is supported (Figure 2.4.c). Numerical simulations will be run for the five climates with different basin morphological and vegetation properties (model parameter combination).

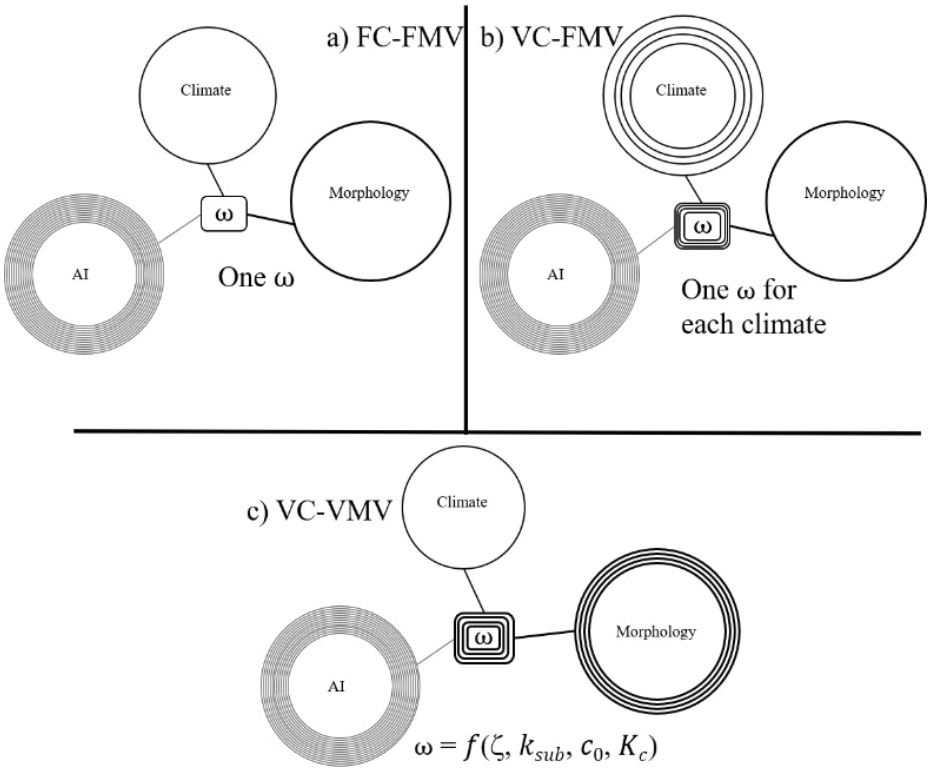

Figure 2.4. (a) Fixed climate, fixed morphology and vegetation: given a climate, given a watershed, over different annual precipitation (P) and potential evapotranspiration (PET), hydrological response follows the same law. (b) Varying climate, fixed morphology and vegetation: given a watershed, the climate drives the hydrological response in different ways. (c) Varying climate, varying morphology and vegetation: for each climate, water partitioning process is driven by morphological and vegetation properties of the basin.

Results will be used to create five linear relations (one for each climate type), namely regression equations between model parameters (that are four, representing the role of morphology and vegetation) and ω.

2.3.1. Climatic setups and weather generator

To take into account the role of climate in water partitioning five climatic setups have been considered which roughly mimic some of the most frequent climate conditions. As specified before, every climate is here characterized by different seasonal pattern of rain and potential evapotranspiration. Within a given climate, synthetic series of rainfall $P(t)$ and $PET(t)$ at daily time scale t have been generated using a weather generator. The five climatic setups are aimed to represent the seasonal variability of rain and potential evapotranspiration time patterns, as illustrated in Figure 2.5. The idea of exemplifying climate in such a simple schematization refers to Viola et al. (2017), where it has been used to investigate green roof retention performances. The first climatic setup (Figure 2.5.a) represents stationary condition of rain and potential evapotranspiration during the year. This is an ideal situation in which the variance of meteo-climatic variables is zero, being the less realistic seasonal pattern of the five proposed in this work. The second case (Figure 2.5.b) is typical of oceanic areas with almost constant precipitation during the hydrological year, while potential evapotranspiration has a peak.

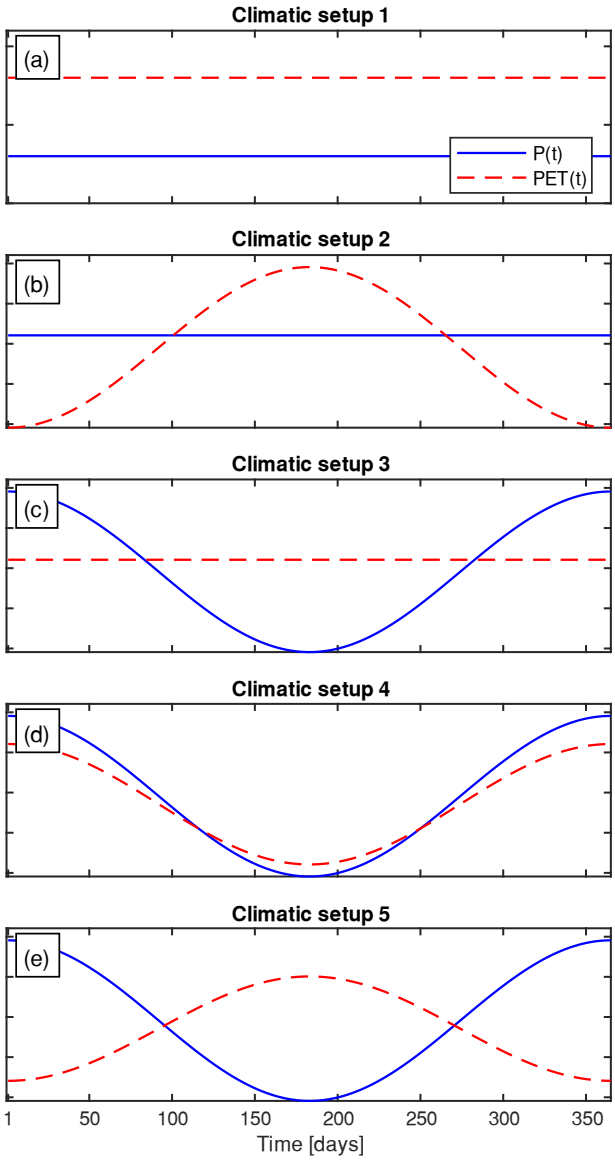

Figure 2.5. Schematic representation of seasonal time patterns of precipitation and potential evapotranspiration. Lines represent the daily mean of stochastic time series, as generated by Eqs. 2.16 and 2.17 for $P_{(t)}$ and by Eq.2.18 as regard to $PET_{(t)}$. Parameters are given in Table 2.1. Following Viola et al. (2017)

Climatic setup 3 (Figure 2.5.c) is the opposite of the last ones, namely potential evapotranspiration is almost constant and major precipitation values are observed during a specific rain season. This climatic setup is attributable to tropical climate with high constant temperatures along the year and monsoon season with precipitation peak. The feature of climatic setup 4 (Figure 2.5.d) is in-phase climatic forcing: this is a classic case of humid subtropical climates, where precipitation peak occurs simultaneously to the temperature one. The last case is the opposite of the climatic setup 4 (Figure 2.5.e), that is rainfall and potential evapotranspiration are in counter-phase during the hydrological year. Mediterranean climate is well represented by this climatic setup, because is well known that rainfall mostly occur during the winter, while temperature peak happens in summer.

In this work the synthetic time series $P(t)$ and $PET(t)$ referring to after mentioned climatic setup are created by the weather generator proposed by Viola et al. (2017), whose parameters have been calibrated according to main climatic features observed in 10,000 observational sites worldwide. The rain series are intended as daily rainfall arising from a non-stationary and cyclic Poisson point process, characterized by a frequency $1/\lambda(t)$ (rate of the Poisson process occurrences, [1/days]). The $\lambda(t)$ parameter is modelled as a sinusoidal function of time t [days], with amplitude $\bar{\lambda}$, the average interarrival time [days] between two rain events and one-year period, as described in in the following equation:

$$\lambda(t) = \bar{\lambda}\left(1 + \delta_\lambda \sin\left(\frac{2\pi t}{365} + \omega_\lambda\right)\right) \tag{2.16}$$

where δ_λ characterizes the ratio between the semi-amplitude of the annual harmonics of $\lambda(t)$ and the annual average and ω_λ is the initial phase of the sinusoidal function.

Every day with rainfall different to zero event $P(t_i)$ [mm/day], where i subscript indicates rain days in the $P(t)$ series, is simulated as a random process extracted from an exponential distribution with mean daily value $\alpha(t)$ [mm/day], modelled as follows:

$$\alpha(t) = \bar{\alpha}\left(1 + \delta_\alpha \sin\left(\frac{2\pi t}{365} + \omega_\alpha\right)\right) \tag{2.17}$$

where $\bar{\alpha}$ is the average amount of rainfall [mm/day], δ_α represent the ratio of the semi-amplitudes of the annual harmonics of $\alpha(t)$ to the annual average and ω_α is the value of phase when $t = 0$.

Therefore, Eqs. 2.16 and 2.17 allow to calculate mean interarrival times and mean daily rainfall along the year, which in turns allow to randomly obtain rain time series.

Similarly, the daily potential evapotranspiration series $PET(t)$ [mm/day] are defined as a sinusoidal function with a similar structure to the previous one:

$$PET(t) = \overline{PET}\left(1 + \delta_E \sin\left(\frac{2\pi t}{365} + \omega_E\right)\right) \tag{2.18}$$

where $\overline{PET}$ is the daily mean evapotranspiration [mm/day], δ_E the ratio of the semi-amplitude of the annual harmonics of $PET(t)$ to the annual average and ω_E is the initial phase.

Each climate is defined by a phase between rain and potential evapotranspiration (as described by ω_λ, ω_α and ω_E) and by a specific seasonal variability of rainfall (as described by δ_α and δ_λ) and potential evapotranspiration (modelled by δ_E). The values of the semi-amplitude δ_λ, δ_α and δ_E have been assessed by Viola et al. (2017) as the median of their empirical distributions, as observed in 10000 worldwide stations; for the five climate scenarios, the parameters of Eqs. 2.16-2.18 are reported in Table 2.1.

Climatic setup	$\bar{\lambda}$ [days]	δ_λ [-]	ω_λ [rad]	$\bar{\alpha}$ [mm/day]	δ_α [-]	ω_α [rad]	$\overline{PET}$ [mm/day]	δ_E [-]	ω_E [rad]
1	4,35	0	0	Variable	0	0	Variable	0	0
2	4,35	0	0	Variable	0	0	Variable	0,3	- π/2
3	4,35	0,45	-π/2	Variable	0,35	π/2	Variable	0	0
4	4,35	0,45	-π/2	Variable	0,35	π/2	Variable	0,3	π/2
5	4,35	0,45	-π/2	Variable	0,35	π/2	Variable	0,3	-π/2

Table 2.1. Parameters of the sinusoidal Eqs. 2.16-2.18 that define the particular pattern of rainfall and potential evapotranspiration, related to the considered climatic setup. δ_λ, δ_α and δ_E represent the ratio of the semi-amplitude of the sinusoidal equations to their mean value, whereas ω_λ, ω_α and ω_E are the initial phase. $\bar{\lambda}$, $\bar{\alpha}$ and $\overline{PET}$ are respectively the average interarrival time, the average amount of daily rainfall and the average daily potential evapotranspiration.

The climate definition, as given above, may embed wide geographic areas where the

seasonal pattern of rainfall and potential evapotranspiration is homogeneous, and described by the six parameters aforementioned; at the same time, annual rainfall P and potential evapotranspiration may vary within a climatic area, for instance following topographic gradients. This kind of variability is reflected in the weather generator by allowing to obtain different aridity indices (AI). Numerically, this is achieved by generating synthetic series with different values of $\bar{\alpha}$ and $\overline{PET}$; $\bar{\alpha}$ has been supposed to vary between 3.5-24 [mm/day] and $\overline{PET}$ between 0.3-5.5[mm/day]. These ranges have been selected considering a realistic range of P and potential evapotranspiration. For sake of simplicity, $\bar{\lambda}$ was assumed to be constant, and equal to 4.35 [days] (Table 2.1), in all the considered climates. This numerical value has been obtained as the mean of the global interarrival times between rainfall events; indeed, the assumption of a unique value restricts the generality of this approach because it hampers to investigate the influence of this parameter on the P partitioning, but indeed is a common and reasonable assumption (Yokoo et al., 2008). Under these conditions, the mean annual amount of rainfall P generated and used in this work can vary between 300 and 2000 mm; similarly, PET ranges from 100 to 2000 mm.

2.3.2. EHSM model

The rainfall $P(t)$ and the potential evapotranspiration $PET(t)$ time series have been then used as input to a conceptual hydrological model, namely a slight simplified version of the Ecohydrological Streamflow Model (EHSM) (Viola et al., 2014). The way of the

model to describe hydrological response is to represent a basin with two linear reservoirs, describing surface and baseflow runoff and one soil bucket split into two compartments representing impervious area c_0 and permeable area (1-c_0). The daily rainfall $P(t_i)$ that falls in the soil bucket is divided in two parts: $c_0 P(t_i)$ flows directly in the surface linear reservoir and (1-c_0)$P(t_i)$ infiltrates in the permeable soil bucket portion (1-c_0) and is accumulated into the soil bucket. Water infiltration and leakage in and from the soil bucket are regulated by 3 parameters: the active soil depth nZ_r [mm], which is the product of the soil porosity n [-] and root zone thickness Z_r [mm], the hygroscopic point s_h [-] and the soil moisture at field capacity s_{fc} [-]. In order to have only a variable that expresses hydrological soil properties, nZ_r, s_h and s_{fc} have been condensed with the following expression:

$$\zeta = nZ_r\left(s_{fc} - s_h\right) \tag{2.19}$$

where ζ [mm] is maximum water holding capacity, representative of maximum amount of water that could be stored in the soil.

The soil moisture of soil bucket regulates the partition of (1-c_0)$P(t_i)$ in runoff that flows into surface and baseflow linear reservoir. If the soil moisture content exceeds the field capacity, this water volume becomes leakage pulses that feed the linear reservoir that is responsible of baseflow conceptual description. The mean residence time of water within this bucket, has been defined as $1/k_{sub}$ [1/day], which from physical point of view is related to groundwater dynamics. When soil moisture overpasses saturation, the excess

feeds the surface linear reservoir related to annual surface runoff production. From the union of the outputs of the two linear reservoirs, the model generated the daily runoff series $Q(t)$.

The model allows to simulate soil moisture dynamics and the influence of vegetation in drying the soil during two consecutive rain events. In order to quantify the evapotranspiration process, a limitation is assumed that is induced by the soil moisture that is equal to the maximum value calculated as the product between reference evapotranspiration and the coltural coefficient K_c [-].

The model parameters describing the watershed are only four, summarizing the key processes producing, limiting and delaying runoff at long time scales. Namely, the selected descriptors are: ζ maximum water holding capacity, k_{sub} subsurface bucket parameter, c_0 impermeable area and K_c coltural coefficient. For all experiments and demonstrations conducted in this work, the model parameters can vary between physically reasonable ranges, reported in Table 2.2.

Name	Acronym	Minimum value	Maximum value	*Test-watershed*
Maximum water holding capacity	ζ [mm]	18	230	50
Subsurface bucket parameter	k_{sub} [1/day]	0.0017	0.1	0.05
Impervious area	c_0 [-]	0	0.05	0.025
Coltural coefficient	K_c [-]	0.5	1.5	1

Table 2.2. The ranges for the morphological and vegetation parameters used in this work: minimum and maximum supposed values. In the last column, it is stated the value assumed referring to the test-watershed used for leading our in-silico experiment.

It is worthy mentioning that c_0 range (less than 5%) is reasonable because Budyko's framework applies to large watersheds, in which impervious areas is often spread over the basin. This physically implies that impervious areas away from outlet, still contribute to runoff, because the routing drives water volumes to pervious areas, where infiltration occur; this physical process is not accounted in the model. Then, impervious areas in EHSM should be considered as the ones close to the outlet, therefore, the range of c_0 has been limited.

2.4. Near future climate and land use scenarios

This Section describes the procedures to obtain future climate and land use (LU) scenarios. These will be used in order to assess the five parameters of Eq. 2.10 of the proposed methods, that will be adopted to define the probability distribution function (*pdf*) of annual surface runoff Q of Sardinia, according with Caracciolo et al. (2017).

Near future values of central moments of annual rainfall P and annual potential evapotranspiration PET, namely $\bar{P}$, $\overline{PET}$, σ_P and σ_{PET}, that epitomizes climatic scenarios, are assessed by EUROCORDEX climate modelling outputs. As discussed in Chapter 1, climate modelling (CM) outputs are affected by systematic errors from different sources, and then bias correction (BC) procedure will be applied to rainfall and temperature to create the less unbiased climate scenarios. Near future LU scenarios will be represented by the possible LU maps, which effect of the water partitioning processes is here epitomized by ω's.

2.4.1. Rainfall, temperature and land use dataset

The EUROCORDEX project (Jacob et al., 2014) is from the broader family of the CORDEX project. The simulations of EUROCORDEX project have been conducted at two different spatial (EUR-44 ~ 50 km and EUR-11 ~ 12.5 km) and several temporal resolutions for different experiments families: historical (HS) and RCP (RCPS) scenarios for different representative concentration pathways RCP (4.5 and 8.5), that respectively

reproduce climatic variables in the past (before 2005) and in the future (2006-2100). Here, 14 CM daily rainfall and temperature outputs have been used to investigate future P and PET marginal statistics. The gridded CM outputs here adopted are defined in EUR-11 domain with a daily time resolution. Since RCP 8.5 scenario is the only RCP scenario here considered, it will be shortened as RCPS for brevity. The stricter RCPS has been considered in order to hypothesize the more deviated scenario from observed climate.

The list of the CMs here used is reported in Table 2.3.

The observed rainfall and temperature datasets are from the Sardinian Hydrological Service, collected by a network of 441 rain gauges and 186 thermometric stations. Both CM and observed daily temperature and rainfall datasets have been resampled spatially over the Sardinia territory following Mascaro et al. (2018), regridding the datasets in a covering grid with a spacing of 0.1°, similarly to EUR-11 domain. Each grid point i, j $(i = 1,..,30\ j = 1,..,20)$ is associated with a daily scale timeseries (t).

Climatic parameters which refers to observed rainfall and temperature dataset will be defined as baseline, because they describe the reference climatic properties that will be compared to future ones.

The CORINE Land Cover (CLC) inventory was here used to describe Sardinian LU. Five updates have been considered starting from 1990 to 2018, including 2000, 2006 and 2012. The LU map referring to 2018 has been choose as reference to describe the initial LU scenario of Sardinia (baseline LU scenario). In Figure 2.6, the covering area percentage of LU types over the Sardinian territory have been reported. Seven LU types have been used to characterize the Sardinian LU maps: urban, agriculture, low density

vegetation, agriculture, forest and sclerophyllous vegetation, water bodies and others LU types.

CM	GCM	RCM
1	CNRM-CERFACS-CNRM-CM5	CLMcom-CCLM4-8-17
2	CNRM-CERFACS-CNRM-CM5	CNRM-ALADIN53
3	CNRM-CERFACS-CNRM-CM5	SMHI-RCA4
4	ICHEC-EC-EARTH	CLMcom-CCLM4-8-17
5	ICHEC-EC-EARTH	KNMI-RACMO22E
6	ICHEC-EC-EARTH	SMHI-RCA4
7	IPSL-IPSL-CM5A-MR	SMHI-RCA4
8	MOHC-HadGEM2-ES	CLMcom-CCLM4-8-17
9	MOHC-HadGEM2-ES	KNMI-RACMO22E
10	MOHC-HadGEM2-ES	SMHI-RCA4
11	MPI-M-MPI-ESM-LR	CLMcom-CCLM4-8-17
12	MPI-M-MPI-ESM-LR	MPI-CSC-REMO2009 (r1i1p1)
13	MPI-M-MPI-ESM-LR	MPI-CSC-REMO2009 (r2i1p1)
14	MPI-M-MPI-ESM-LR	SMHI-RCA4

Table 2.3. List of the fourteen climate modelling outputs from EUROCORDEX project here used, with the respective GCM and RCM.

The classification is oriented to define LU classes which has a homogeneous response in the hydrological cycle and accordingly to similar work in literature. Urban indicates cities, low density populated and villages areas, while agriculture, low density vegetation, agriculture, forest and sclerophyllous vegetation include the natural and anthropogenic vegetated areas of Sardinia. Sclerophyllous vegetation has been classified in a proper class because it is a typical Sardinian vegetal species which deeply affect and modifies the interaction of water cycle, reducing the water amount addressed to the groundwater and surface runoff and increasing the evapotranspiration contribution. Figure 2.7

represents the CORINE Land Cover map of Sardinia in the baseline scenario (2018), according to land types here used.

For each update, the percentage of covering area of LU types varied very slowly, and every class exhibits a very smooth linear trend, except for the grassland and low density vegetation which has a significance decrease from 1990 to 2018. The prevalent LU type is the agriculture, which has a high number of employees in Sardinia, followed by the sclerophyllous vegetation, which due to their own high capacity to adapt to Mediterranean climates infest a large part of the regional territory. The last LU type in terms of covering area percentage is the grassland and low density vegetation. Because of the reduced variability and due to the low percentage of occupation of the territory, water bodies and other (i.e. beaches, dunes, sands and burnt areas) can be assumed to maintain the same percentage of covering.

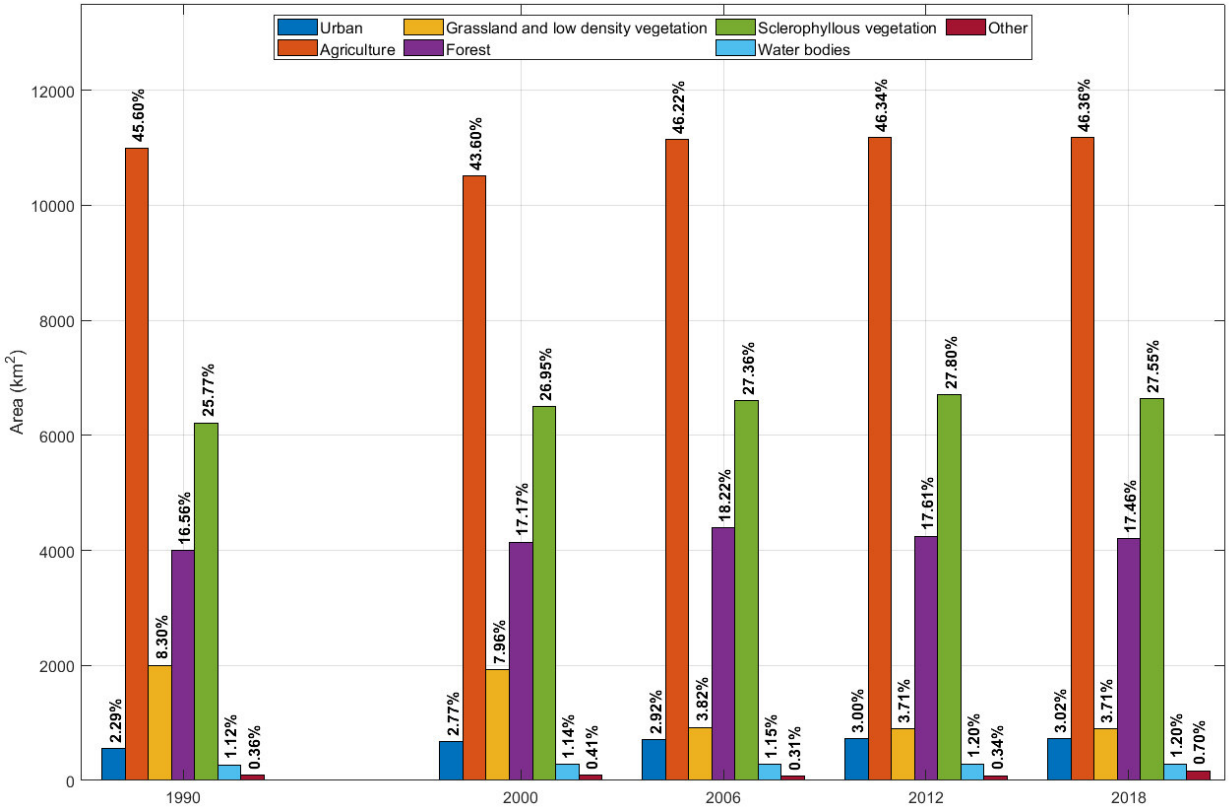

Figure 2.6. Covering area percentage of Sardinia from CORINE Land Cover (CLC) inventory for 1990, 2000, 2006, 2012 and 2018. CLC land use types have been aggregated in seven types: Urban, Agriculture, Grassland and low density vegetation, Forest, Sclerophyllous vegetation, Water Bodies and Other.

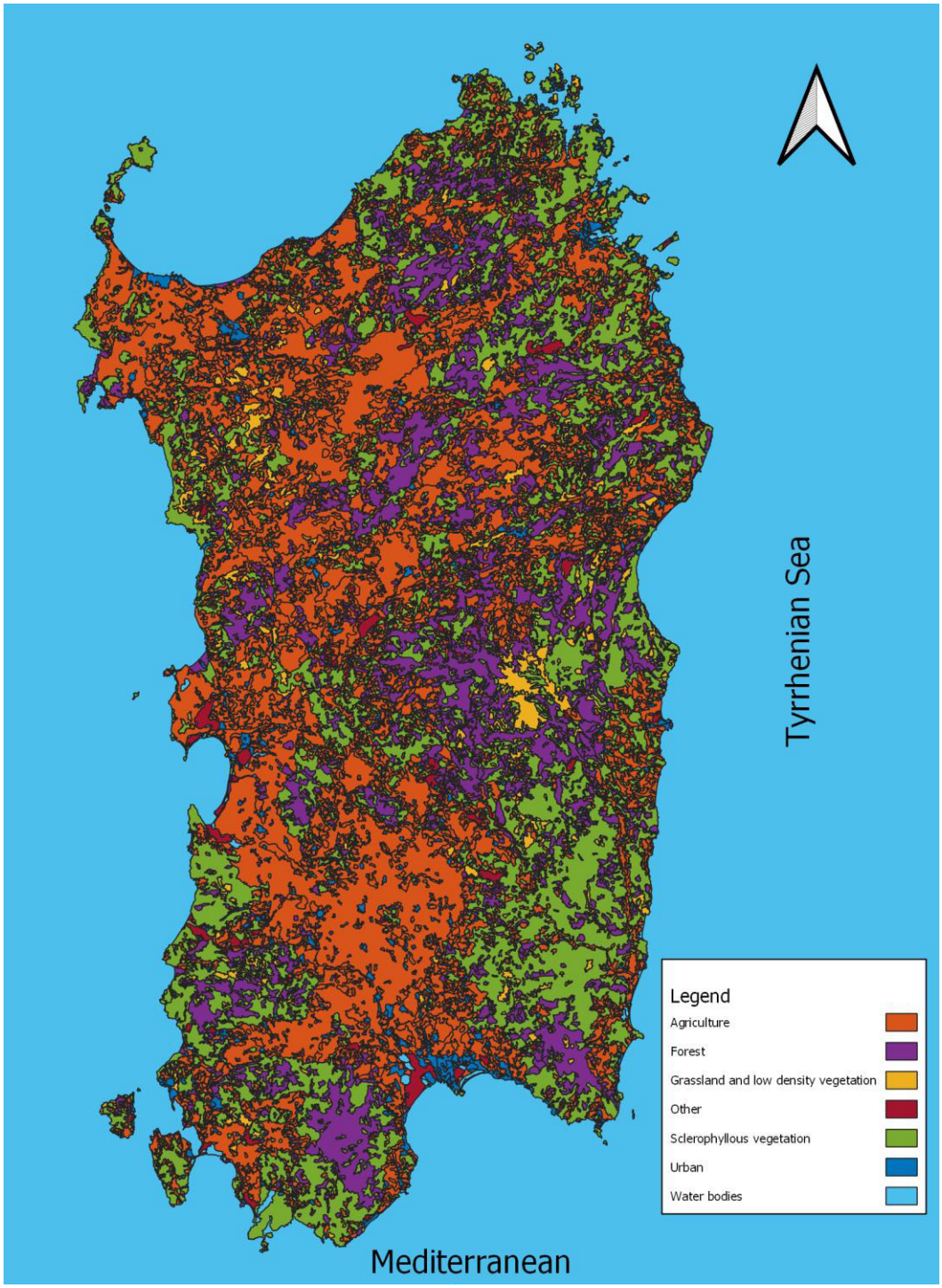

Figure 2.7. CORINE Land Cover map of Sardinia for the baseline scenario (2018), according to land types used: urban, agriculture, low density vegetation, agriculture, forest and sclerophyllous vegetation, Water bodies and Other.

2.4.2. Bias corrected near future climatic scenarios

As discussed in Chapter 1, climate modelling outputs are affected by systematic errors that arises from several sources. Then, three BC methods have been selected for rainfall and just one for the temperature in order to define unbiased near future climatic scenarios and parameters. Temperature outputs has been also considered because temperature is the main variable driver in the potential evapotranspiration. The adopted BC methods have been chosen following the criteria of the ease of application and reduced computational effort. The objective is to obtain the less unbiased near future mean and standard deviation values of P and PET ($\bar{P}$, $\overline{PET}$, σ_P and σ_{PET}), that epitomize climatic scenarios and represent the climatic parameters in the proposed method (Eq. 2.10).

As discussed in Chapter 1, for each BC method it is required a preliminary phase (hereafter parametrization phase) of evaluation of the correction parameters that have been used to remove systematic bias in the RCPS CM rainfall and temperature outputs (correction phase). The performance of the BC methods will be tested by the comparison of raw historical (HS), BC historical (HS) and observed cumulative density functions (*ecdfs*) of daily and annual rainfall P. The magnitude of deviation of BC HS *ecdfs* from observed ones will be represent a measure of the correction efficiency of BC methods adopted. The closer *ecdfs*, the more efficient the bias correction. The parameters that have been evaluated in the parametrization phase will be used to correct the RCPS CM timeseries, that allow to define near future climatic parameters.

Despite annual scale is the reference scale for Budyko's and Caracciolo et al. (2017), the BC methods here used will be applied in correcting the raw daily rainfall and

temperature outputs from EUROCORDEX project. The BC outputs will be than aggregated at annual scale as requests the proposed approach.

For each grid cell of CM outputs, BC has been implemented independently, meaning that every cell is associated to a timeseries with a daily resolution (t) in which BC has been performed (see Section 2.4.1 for clarification about CM datasets).

Regarding rainfall, three BC approaches have been considered: linear scaling (LS), power transformation (PT) and parametric distribution mapping with gamma distribution (DM-Γ).

Linear scaling approach operates on the mean daily rainfall. The RCPS outputs correction is based on a single parameter c (6.3).

$$p_{bcCM_{HS}}(t) = c \cdot p_{rawCM_{HS}}(t) \tag{2.20}$$

$$p_{bcCM_{RCPS}}(t) = c \cdot p_{rawCM_{RCPS}}(t) \tag{2.21}$$

$$c = \frac{\mu(p_{obs})}{\mu\left(p_{rawCM_{HS}}\right)} \tag{2.22}$$

where:

- $p_{bcCM_{HS}}(t)$ is the BC daily rainfall value of a given HS CM timeseries at time (t);
- $p_{bcCM_{RCPS}}(t)$ is the BC daily rainfall value of a given RCPS CM timeseries, at time t;
- $p_{rawCM_{historical}}(t)$ is the raw daily rainfall of a given HS CM timeseries, at

time (t);

- $p_{rawCM_{RCP}}(t)$ is the raw daily rainfall of a given RCPS CM timeseries, at time (t);
- p_{obs}(t) is the observed rainfall timeseries at time (t);
- c is the linear scaling parameter.

Eq. 2.22 evaluates the linear scaling parameter c, that is the ratio of the daily mean rainfall of observed timeseries to the daily mean rainfall of the raw HS CM timeseries. Then, the HS and RCPS CM daily rainfall outputs are corrected at daily scale by c (Eqs. 2.20 and 2.21).

The power transformation approach operates both on the mean and the standard deviation. The c and shape b parameters affects respectively the daily rainfall mean and standard deviation.

$$p_{bcCM_{HS}}(t) = c \cdot p_{rawCM_{HS}}(t)^b \tag{2.23}$$

$$p_{bcCM_{RCPS}}(t) = c \cdot p_{rawCM_{RCPS}}(t)^b \tag{2.24}$$

$$f(b) = 0 \quad b \rightarrow CV(p_{obs}) - CV\left({p_{rawCM_{HS}}}^b\right) = 0 \tag{2.25}$$

$$c = \frac{\mu(p_{obs})}{\mu\left({p_{rawCM_{HS}}}^b\right)} \tag{2.26}$$

c and b are the scale and shape correction parameters and CV refers to the coefficient of variation of CM daily rainfall timeseries. b is obtained under the hypothesis that the observed timeseries CV matches the HS CM one modified by the shape parameter (Eq.

2.25). c is evaluated as the same way of the linear scaling method (Eq. 2.26). The BC timeseries are derived by the scale and shape parameters (Eqs.2.23 and 2.24).

Unlike to linear scaling and power transformation methods that operate just with the daily mean and standard deviation of climatic variables, the parametric distribution mapping aims to modify the entire distribution of the CM daily rainfall timeseries in the attempt to mimic the observed one. The hypothesis under the parametric distribution mapping method is that the observed and HS CM daily rainfall timeseries are fitted by a given theoretical statistical distribution. In literature, the gamma distribution is widely adopted to describe the distribution of daily rainfall by several authors for similar purposes (Piani et al., 2010; Yang et al., 2010; Lafon et al., 2013). Of course, the reliability of the methods arises from the goodness of fit of the observed and HS CM daily rainfall outputs with the gamma distribution. In particular, here the mixed gamma distribution has been adopted to properly account for the intermittent nature of the rainfall (Li et al., 2010). The BC RCPS CM timeseries distribution will show roughly the same trend of the observed ones (Eqs. 2.27-2.29).

$$p_{bcCM_{HS}}(t) = F^{-1}\left(F\left(p_{rawCM_{HS}}(t)\middle|\alpha_{rawCM_{HS}},\beta_{rawCM_{HS}},\pi_{rawCM_{HS}}\right)\middle|\alpha_{obs},\beta_{obs,}\pi_{obs}\right) \quad (2.27)$$

$$p_{bcCM_{RCPS}}(t) = F^{-1}\left(F\left(p_{rawCM_{RCPS}}(t)\middle|\alpha_{rawCM_{HS}},\beta_{rawCM_{HS}},\pi_{rawCM_{HS}}\right)\middle|\alpha_{obs},\beta_{obs,}\pi_{\mathrm{obs}}\right) \quad (2.28)$$

$$F(p|\alpha,\beta,\pi) = \begin{cases} \pi & p = 0 \\ \pi + (1-\pi)\int_0^p \frac{\beta^\alpha p^{\alpha-1}e^{-\beta p}}{\gamma(\alpha)} & p > 0 \end{cases} \quad (2.29)$$

where α and β represented the fitted parameters of the theoretical distribution respectively of non-zero daily rainfall, while π represents the probability of zero-daily

rainfall. The non-zero distribution parameters α and β have been fitted estimated using the maximum-likelihood estimation because is more accurate than other ones (Piani et al., 2010).

Daily temperature timeseries has been bias corrected by applying the last approach adapted to the different statistical properties of this climatic variable. Indeed, instead of gamma distribution, the normal shape has been considered to statically represent the behaviour observed and CM daily temperature timeseries. The following equations represent the previous approach adapted to temperature (Eqs. 2.30-2.33).

$$t_{bcCHS}(t) = F^{-1}\left(F\left(t_{rawCM_{HS}}(t)\middle|\mu_{rawCM_{HS}}, \sigma_{rawCM_{HS}}\right)\middle|\mu_{obs}, \sigma_{obs}\right) \quad (2.30)$$

$$t_{bcCM_{RCPS}}(t) = F^{-1}\left(F\left(t_{rawCM_{RCPS}}(t)\middle|\mu_{rawCM_{HS}}, \sigma_{rawCM_{HS}}\right)\middle|\mu_{obs}, \sigma_{obs}\right) \quad (2.31)$$

$$f(t;\mu,\sigma) = \frac{1}{\sigma\sqrt{2\pi}} e^{-\frac{(t-\mu)^2}{2\sigma^2}} \quad (2.32)$$

$$F(t;\mu,\sigma) = \int_{-\infty}^{\infty} f(t;\mu,\sigma)dt \quad (2.33)$$

The BC CM temperature timeseries are just an intermediate result. Indeed, as described in Section 2.1, mean and standard deviation value of PET ($\overline{PET}$ and σ_{PET}) are two out of five parameters to predict the probability density function (*pdf*) of the annual surface runoff Q. Daily and annual potential evapotranspiration will be calculated by BC CM and observed temperature timeseries.

In details, Thornthwaite (1948)'s method has been used to evaluate BC CM and observed potential evapotranspiration timeseries, which fundamental equations are the

following ones:

$$PET_m = 16\, p_m \left(\frac{10\, t_m}{I}\right)^{(0.5+0.016\, I)} \tag{2.34}$$

$$I = \sum_{m=1}^{12} \left(\frac{\overline{t_m}}{5}\right)^{1.514} \tag{2.35}$$

where t_m is the mean monthly temperature of a given month (°C), $\overline{t_m}$ is the long-term mean temperature for the m-month (m=1,12) (°C), I is called annual heat index, p_m is a corrective coefficient that accounts for the average day length of the m-month being calculated and it is related to the latitude, and finally PET_m is the estimated i-month potential evapotranspiration (mm/monthly).

2.4.3. Near future land use scenarios

It is quite hard to image LU in the next future and the impacts of its variation on basin hydrological response. In this paragraph it is illustrated how LU scenarios have been created and how to calculate ω's value using the empirical expression related to the climate setup 5 (see Section 2.3), which mimic better main Sardinian climatic properties. Recalling Section 2.3, ω has been calculated as a function of four morphological and vegetation descriptors (ζ, k_{sub}, c_0,K_c) which will be tuned to represent several LU scenarios.

Given a baseline LU scenario, to generate LU scenarios three approaches have been taken into account:

- Constant trend scenarios (CT-S): given an observed trend of a given LU type, it is supposed that it will remain constant in the future. The other LU types are rescaled accordingly;
- Fixed change scenarios (FC-S): given some observed typical LU changes, a fixed percentage of area is removed/added to a given LU type and added/removed to another one;
- Climate-vegetation-driven scenarios (CVD-S): given some hypotheses on the interaction between vegetation and climate, some portion of vegetation-related LU types are supposed to be transformed in other ones.

For each vegetation-related type (namely agriculture, low density vegetation, agriculture, forest and sclerophyllous vegetation, see Section 2.4.1), K_c has been calculated considering the vegetation species' properties and then, a unique value is obtained by weighted-area average over Sardinia. Therefore, c_0 have been assumed to be equal to urban covering percentage. As discussed in Section 2.3.2, ζ and k_{sub} are two descriptors related to the soil properties and then are supposed to not be modified to the LU change and then constant. Summarizing, c_0 and K_c are the only two descriptors that differentiate the LU scenarios. This is an acceptable hypothesis due to the high impact of vegetation and impervious areas in the water partitioning process as deeply highlighted in the scientific literature and in Chapter 1.

3. Results

Climate and land use (LU) change are the most influential drivers of hydrological changes. Several authors tried to quantify and interpret the sign and magnitude of this change in different ways (hydrological modelling, paired catchments approach, statistical techniques).

In this thesis a different approach has been applied to assess climate and LU change effect in hydrological cycle. Indeed, this work aims to define the probability density function (*pdf*) of annual surface runoff (Q) for the island of Sardinia (Italy) in a closed-form under transient climate and LU. A Budyko-based approach has been adopted. Indeed, Caracciolo et al. (2017) method hypothesized that Q *pdf* follows a gaussian shape fully defined by five parameters: mean and standard deviation of annual rainfall P and potential evapotranspiration PET, and Fu's parameter ω. Climatic and LU scenarios have been defined and their hydrological impact have been epitomized by the previous five parameters. Climate modelling (CM) outputs from EUROCORDEX project have been adopted to define climatic scenarios, embodied by mean and standard deviation of P and PET. Several LU scenarios have been considered which have been epitomized in Caracciolo et al. (2017) approach by ω.

Given these premises, this Chapter will show the results of this thesis. Before assessing

the Q *pdf* in the near future under climate and LU change, the results of the propaedeutic study about normality assumption of P and PET (see Section 2.2) will be reported in Sections 3.1 and 3.2. The outcomes of the investigation about the linkage between ω and LU properties (see Section 2.3), that will provide a functional relation for the assessment of ω, have been illustrated in Section 3.3, divided in three subsections.

Given these two propaedeutic studies, Section 3.4 shows the climatic and LU scenarios, that lead to different sets of the five previous mentioned parameters. The results of bias correction procedures and climatic scenarios will be described in Section 3.4.1, while the conceptualization of LU scenarios and the related Fu's parameter values are reported in Section 3.4.2.

Finally, in Section 3.5 four combination of the climatic and LU scenarios will be used to define possible Q *pdf* in the near future for Sardinia, that shows the final outcomes of this thesis.

3.1. Global verification of annual rainfall normality

Most part of this Section has been submitted for publication as:

Ruggiu, D., Viola, F., Langousis, A., A non-parametric procedure to assess the accuracy of the normality assumption for annual rainfall totals, based on the marginal statistics of daily rainfall: An application to NOAA-NCDC rainfall database, submitted to Journal of Applied Meteorology and Climatology

In this Section, the evidences of the investigation about normality assumption for annual rainfall P have been reported, using methods, models and dataset described in Sections 2.2.2 and 2.2.3.

Starting from the classification of the 3007 P samples into G (approximately Gaussian distributed) and NG (non Gaussian distributed) groups, KS normality test resulted that almost all samples (i.e. 2967 out of 3007) can be considered as Gaussian distributed at the 5% significance level, while CVM and AD tests resulted that 2312 and 2213 samples, respectively, fall into the G group. Evidently, AD is the strictest and most conservative of all normality tests, as it is more sensitive to observations in the upper and lower distribution tails.

For the three normality tests considered, Figure 3.1 shows the local fractions of stations that fall within group G (i.e. exhibit P that are approximately Gaussian distributed). Apart from KS test, which results in fractions of Gaussian distributed stations

that are close to unity and globally uniform, both CVM and AD tests reveal increased fractions of normally distributed P samples in eastern and northern China, and North America, and reduced fractions of normally distributed P samples in India and eastern Australia, indicating that approximate Gaussianity of P is strongly linked to local climatic conditions.

Along these lines, and in the light of the obtained results, the link between normality patterns revealed by the KS, CVM and AD tests and the five climatic types of Köppen – Geiger climatic classification (Kottek et al., 2006): equatorial (A), arid (B), warm temperate (C), continental (D) and polar (E) have been examined (see Figure 3.2.a). Figure 3.2.b shows the fraction of stations with approximately Gaussian distributed P, on the basis of the three normality tests considered, at the 5% significance level. KS is the less conservative test in assessing the normality of P samples (see discussion above), while CVM and AD results are comparable in terms of percentages of Gaussian distributed samples, with AD being slightly stricter (i.e. leading to lower percentages) due to the increased weight imposed on observations at the upper or lower tails of the corresponding distributions. In addition, continental climate (D) exhibits the highest fraction of Gaussian distributed P samples (i.e. AD 84.3% and CVM 87.3%), followed by warm temperate (C; AD 75.8% and CVM 79.2%), equatorial (A; AD 72.5% and CVM 74.2%), and polar (E; AD 70.4% and CVM 74.1%) climates. Arid climate (B) displays the lowest fraction of Gaussian distributed P (AD 61.0% and CVM 66.4%). This is in accordance with what statistically expected, as daily rainfall timeseries in arid regions exhibit higher fractions of dry days, highly skewed distributions of positive rainfall rates

(due to the increased frequency of low rainfall intensities) and, consequently, exhibit reduced convergence rates to the normal shape when aggregated at an annual level.

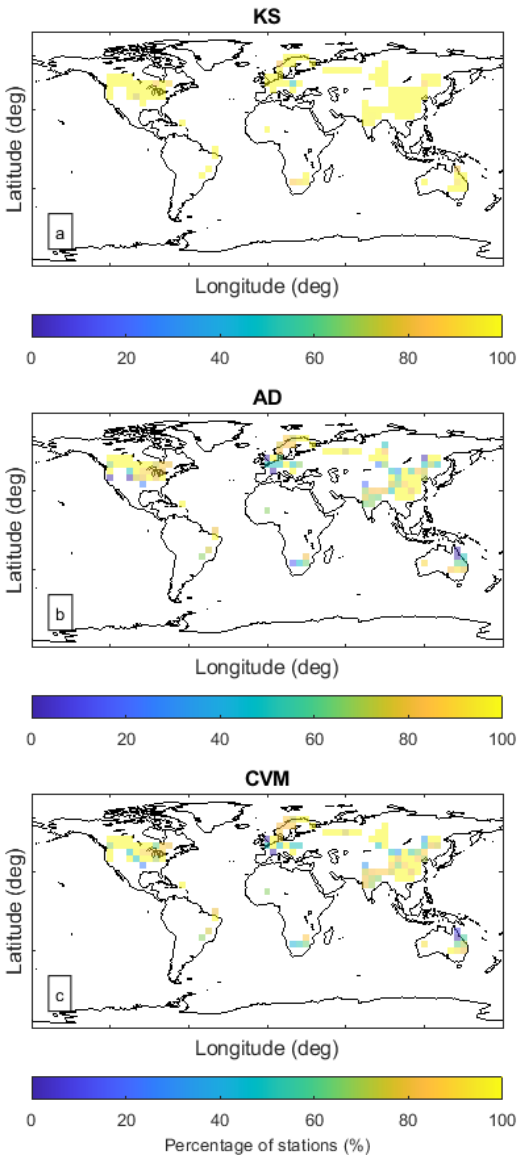

Figure 3.1. Global maps with spatial resolution 5 x 5 deg, illustrating the local fractions of stations that belong to group G (i.e. approximately Gaussian distributed annual rainfall P), according to the three normality tests considered (Kolmogorov Smirnov, KS (a); Anderson-Darling, AD (b); Cramer Von-Mises, CVM (c), at the 5% significance level.

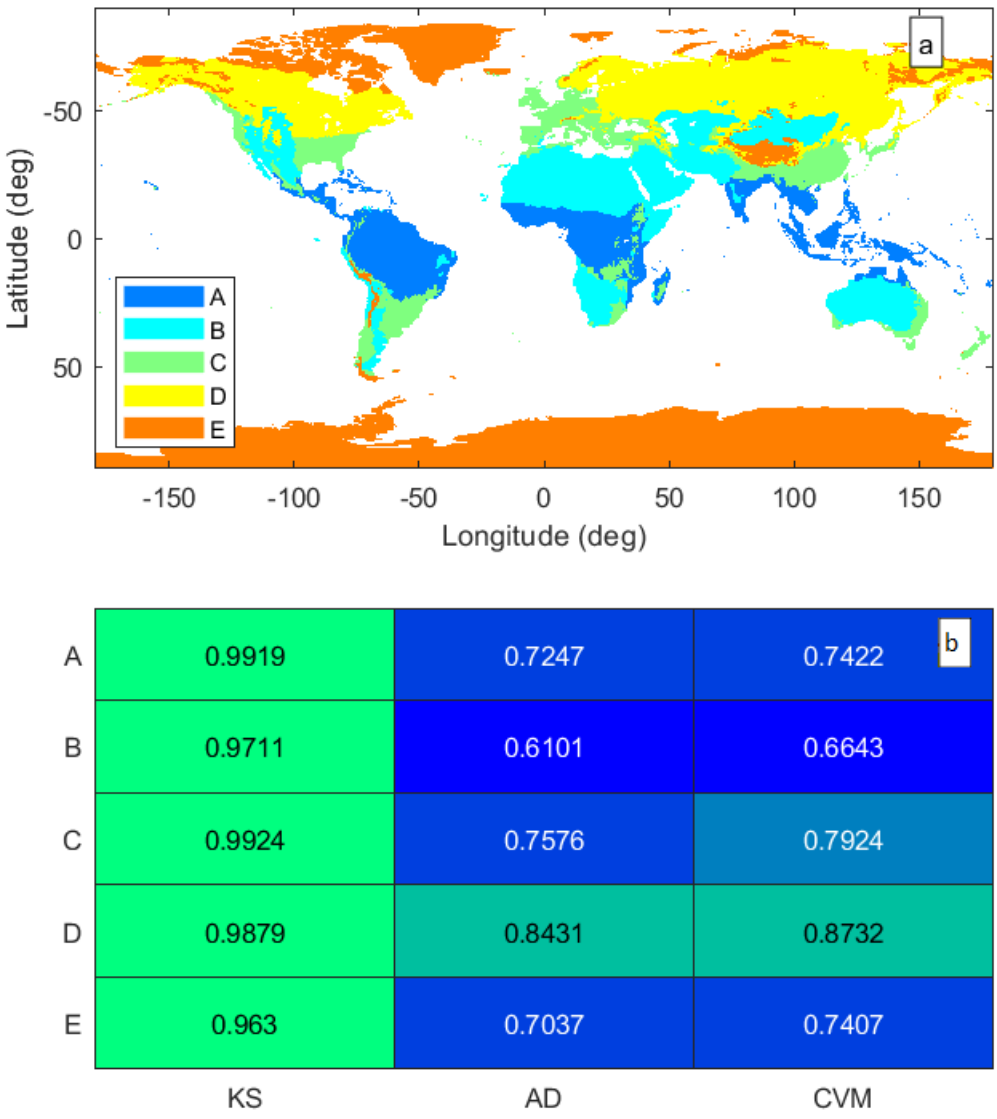

Figure 3.2. (a) Global map illustrating the Köppen – Geiger climate classification, featuring five distinct climate types: equatorial (A), arid (B), warm temperate (C), continental (D) and polar (E). (b) Fraction of stations with approximately Gaussian distributed P (group G), on the basis of the three normality tests considered (Kolmogorov Smirnov, KS; Anderson-Darling, AD; Cramer Von-Mises, CVM), at the 5% significance level.

Table 3.1 summarizes the results of the logistic regression in the form *p*-values (i.e. for the null hypothesis that a certain predictor is influential), and VIFs (Song and Kroll, 2011), for the classification based on the Anderson-Darling test statistic (the most conservative one) at 5% significance level, and for three selected sets of predictor variables (Set I: f_{dd} and sk_{wd}; Set II: f_{dd}, sk_{wd}, and σ_{wd}; Set III f_{dd}, PCI, and sk_{wd}). Lower *p*-values indicate higher significance of the corresponding predictor in the regression, whereas VIF values close to unity indicate approximate linear independence of the predictors (Chatterjee and Price, 1991; O'Brien, 2007; Song and Kroll, 2011). It is clear that Set I, which consists of two predictor variables, namely the fraction of dry days $f_{dd}$and the skewness coefficient of rainfall in wet days sk_{wd}, is the best performing one, with the two regressors exhibiting approximate linear independence.

		f_{dd}	PCI	sk_{wd}	σ_{wd}
p-value	Set I	1.38E-18	--	3.74E-11	--
	Set II	8.69E-12	--	7.24E-10	1.32E-02
	Set III	6.004906e-06	5.502648e-03	7.057651e-11	--
VIF	Set I	1.000032	--	1.000032	--
	Set II	1.310212	--	1.024746	1.333897
	Set III	1.984055	1.985027	1.001464	--

Table 3.1. Results of the logistic regression analysis in the form p-values, and VIFs (Variance Inflation Coefficients), for the classification of the considered NOAA-NCDC rainfall stations into G and NG subsets, based on the Anderson-Darling test statistic at 5% significance level, and for three selected sets of predictor variables (Set I: f_{dd} and sk_{wd} ; Set II: f_{dd} , sk_{wd} , and σ_{wd} ; Set III f_{dd} , PCI, and sk_{wd}); see main text for details.

In what follows, a random-search algorithm has been combined with a proper test-based objective function to conclude on a set of constraints that allows classification of P samples based on the marginal statistics of daily rainrates. Figure 3.3 illustrates histograms of the fraction of dry days f_{dd}, and the skewness coefficient sk_{wd} of rainfall in wet days for the 3007 daily rainfall series analyzed, while Figure 3.4 shows how the selected optimal thresholds of the aforementioned marginal statistics vary with the level of significance α of the AD normality test in the range 2% -15%. As expected, when the level of significance α increases, the optimal thresholds for the fraction of dry days f_{dd}, and the daily skewness coefficient sk_{wd} tend to drop. More precisely, the threshold for the fraction of dry days f_{dd} is approximately constant and equal to 0.9 up to $\alpha \approx 7\%$, and decreases to 0.88 at $\alpha = 15\%$. Regarding sk_{wd}, it is approximately constant and equal to 5.92 up to $\alpha \approx 10\%$, and decreases to 5.7 at $\alpha = 15\%$.

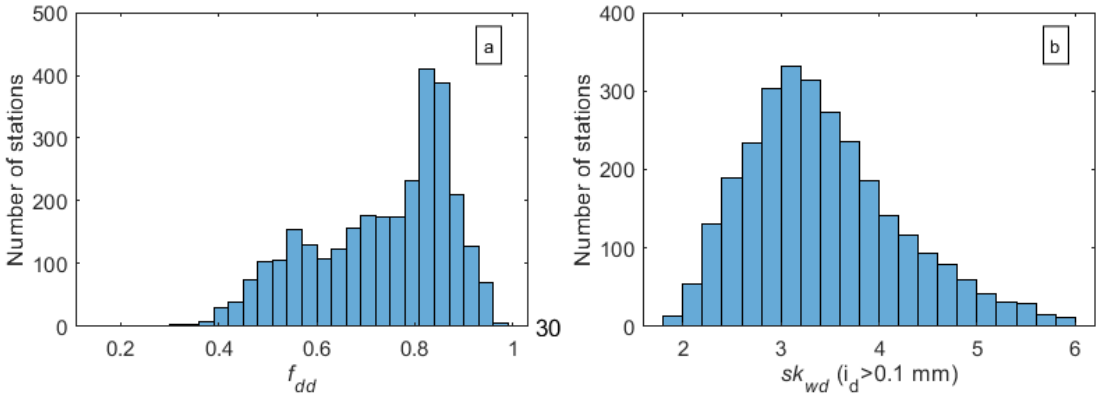

Figure 3.3. Histograms of the fraction of dry days (left panel), and the skewness coefficient (right panel), for the 3007 NOAA-NCDC daily rainfall timeseries analyzed.

Figure 3.4 highlights that irrespective of the significance level α of the AD test, both conditional probabilities exhibit higher values relative to their respective marginals, indicating the significant information value of the non-parametric procedure. Figure 3.5 compares the conditional probabilities $Pr[A|T]$ and $Pr[A^c|T^c]$ with the marginal probabilities $Pr[A]$ and $Pr[A^c]$ = 1-$Pr[A]$, as a function of the level of significance α used for the AD test.

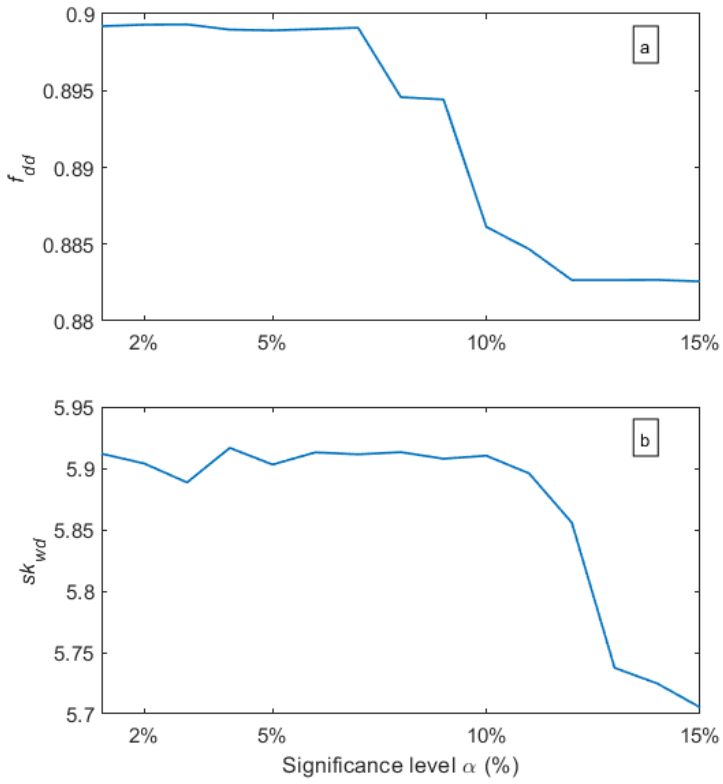

Figure 3.4. Dependence of the optimal thresholds of the fraction of dry days (a), and skewness coefficient of rainfall in wet days (b), on the level of significance α of the Anderson-Darling (AD) test, for the 3007 NOAA-NCDC daily rainfall timeseries analysed.

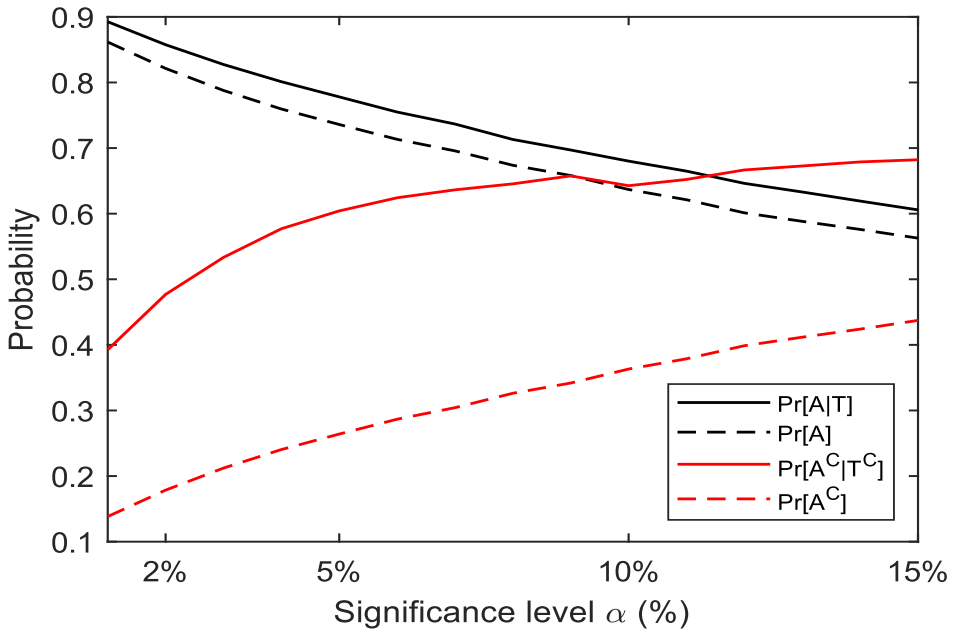

Figure 3.5. Comparison of the conditional probabilities $Pr(A|T)$ and $Pr(A^c|T^c)$, with the marginal probabilities $Pr(A)$ and $Pr(A^c)$ = 1-$Pr(A)$, as a function of the level of significance α used for the Anderson-Darling (AD) test, for the case when the two most influential predictor variables (i.e. Set I: f_{dd}, sk_{wd}) are used to constraint classification to G and NG groups; see main text for details.

Figures A.1-A.4 in the Appendix, show similar plots to Figures 3.4 and 3.5, but for the case when three predictor variables are used (i.e. Set II: f_{dd}, sk_{wd}, and σ_{wd}; Set III f_{dd}, PCI, and sk_{wd}; see Table 3.1). It is evident that the results obtained using three regressors are virtually identical to those obtained using solely f_{dd} and sk_{wd} as independent variables, thus, verifying their significance in determining the approximate convergence of the distribution of P to a normal shape.

3.2. Annual potential evapotranspiration normality assumption

A discussion on the validity of normality assumption for annual potential evapotranspiration PET is reported in this Section. Goodness-of-fit metrics analysis will support the discussion.

In the proposed Budyko-based approach, PET covers a critical role. Generally, potential evapotranspiration is a key factor in drought processes that hugely influences the water balance (Zhou et al., 2020). PET could be defined as the amount of water that evaporate and transpire in a year from soil and vegetated areas without restrictions other than atmospheric demand. Different approaches are available in literature to estimate PET and they can be divided in temperature-based (Thornthwaite, Hamon and Hargreaves-Samani) and radiation-based (Turc, Makkink, and Priestley-Taylor) (Lu et al., 2005).

In this thesis, Thornthwaite's method have been adopted to calculate PET samples, which is based on the idea that monthly potential evapotranspiration is related to monthly temperature (Thornthwaite, 1948). In detail, given a reference area, monthly potential evapotranspiration is exponentially dependent on the monthly temperature as marked in Section 2.4.2. Therefore, normality assumption of PET is strictly connected to temperature. Moving from monthly to annual scale, for a given year, PET could be expressed as:

$$PET = \sum_{m=1}^{12} PET_m = \sum_{m=1}^{12} 16\, p_m \left(\frac{10\, t_m}{I}\right)^{(0.5+0.016\, I)} \tag{3.1}$$

$$t_m = \frac{\sum_{d=1}^{n} t_d}{n} \tag{3.2}$$

where t_d is the daily mean temperature (°C), n is the number of days in a month and t_m is monthly mean temperature (°C). Given Eqs. 2.34-2.35 and 3.1-3.2, daily mean temperature rules the question of normality assumption of PET.

PET's normality assumption raises less concerns than P. Firstly, daily mean temperature is a no-zero bounded variable, it is not characterized by intermittency as daily rainfall and has a small variability in Mediterranean area, as in the island of Sardinia. All these evidences lead to believe that, accordingly to central limit theorem (CLT), the speed of convergence of daily mean temperature to gaussian shape is higher than daily rainfall. This means that temperature at daily scale already could be more suitable for gaussian distribution than daily rainfall.

In addition, moving from monthly mean temperature to monthly potential evapotranspiration, the variance of the considered variable remains still limited in Mediterranean area and then still suitable for normal shape. Despite the skewed nature of daily rainfall, P has been proved to be gaussian within optimal threshold related to daily and intra-annual marginal statistics of rainfall (see Section 3.1). According to this outcome, moving from monthly potential evapotranspiration to PET, remembering CLT, in comparison to rainfall, PET seems to be a more suitable candidate for normality assumption.

To support the hypothesis of normality assumption of PET, Anderson-Darling (AD) test ($\alpha = 0.05$) has been applied on 120 PET samples from Sardinia Hydrological Survey

thermometric stations network (see Section 2.2.1). To ensure the statistical significance of the obtained results, PET samples have been selected by stations that recorded more than 20 years of recordings. 102 out of 120 PET samples can be considered gaussian in accordance with AD test. Figure 3.6 represents the frequency distribution of one of the 120 PET samples and graphically highlights how the selected PET sample approximates the gaussian distribution.

For all these reasons, in this thesis it is supported the idea that empirical cumulative density function (*ecdf*) of PET could fit the gaussian distribution since, compared to P and following CLT, seems to be more suitable for convergence to normal shape.

These evidences and considerations strengthen the validity of normality assumption of PET, although in future more detailed analyses should be done to reinforce this hypothesis.

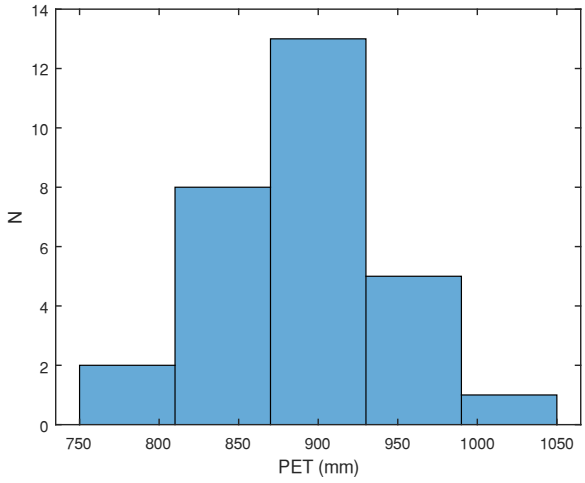

Figure 3.6. Histogram of a PET sample for a thermometric station from Sardinia Hydrological Service thermometric network

3.3. The linkage between land use and Fu's parameter

Most part of this Section has been accepted for publication as:

Ruggiu, D., Viola, F., 2019, Linking climate, basin morphology and vegetation characteristics to Fu's Parameter in data poor conditions, Water (Switzerland), 11 (11), art. no. 2333

This Section shows the results of the investigation about the linkage between ω and land use (LU) properties.

Results are presented in three parts: i) in the first part it will be shown how ω is unique for a given climate and watershed morphological and vegetation characteristics; ii) in the second it will be explicated the effect of climate in water partitioning and iii) in the last part it will be quantified the role of basin morphology and vegetation in driving water partitioning for different climate, providing practical expression of ω that will be adopted in the next Section to calculate this parameter for different land use (LU) scenarios.

3.3.1. Fixed climate, fixed morphology and vegetation (FC-FMV)

Under a climate scenario and for a given watershed, the first assumption to test is the univocity of Fu's parameter over a wide range of aridity indices (see Figure 2.4.a).

Following the method described in Section 2.3, 50 series of daily rainfall and potential evapotranspiration have been generated from a given climatic setup with duration equal to 100 years. Every couple of these climatic forcings identified an aridity index's value AI. These time series have been used as meteoclimatic input to a *test-watershed*, which morphological and vegetation properties are summarized by model parameters reported in Table 2.2, last column. Using the model described in Section 2.3.2, that represented the hydrological response of the *test-watershed*, 50 daily time series have of runoff $Q(t)$ and then evapotranspiration series $ET(t)$ have been obtained, which in turns has been summed at yearly time scale and averaged and divided by the related yearly averaged P to obtain 50 values of evaporative index, EI. The 50 AI-EI's couples may be interpreted as different hydrological behaviour of the same basin under different aridity index conditions, but under the same climate. The 50 AI-EI's couples were plotted and the Fu's equation has been fit to data maximizing the coefficient of determination R^2 (Figure 3.7).

After the optimization process, coefficient of determination R^2 obtained is very high for the *test-watershed* (namely 0.93) meaning that Fu's equation is a good estimator of water partitioning processes and that the Fu's parameter could be seen as the hydrological signature of a given basin over different aridity indices within a certain climate. Only few points, with high values of aridity index, departs from Fu's curve in Figure 3.7. This fact is due to the conceptual model used for describing hydrological processes that allocates a constant percentage of rainfall to surface runoff regardless by the soil and vegetation dynamics under dry conditions (high aridity index values).

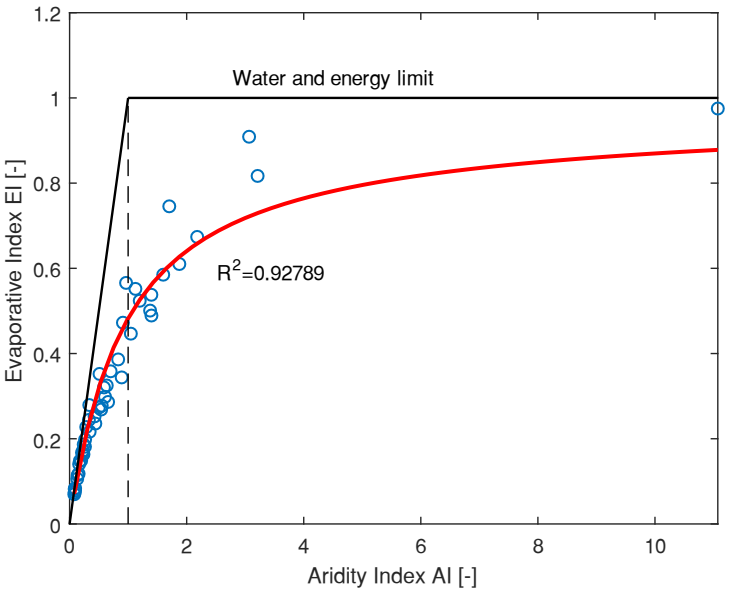

Figure 3.7. AI-EI's couples into the Budyko's domain generated by the combination of weather generator and conceptual model EHSM, the optimised Fu's curve, and the related coefficient of determination value R^2 for the climatic setup 5 and the test-watershed (see Table 2.2).

In order to generalize this result, starting from the *test-watershed* configuration, morphological and vegetation parameters have been tuned, once at time, at the minimum/mean/maximum values (reported in Table 2.2). The number of test-watersheds became nine, for which has been conducted the previous experiment (i.e. the climatic setup is fixed), in order to demonstrate what has been said in all morphological and vegetation parameter domain.

The results are shown in Figure 3.8, where AI-EI's couples fit very well to the optimized Fu's curves, highlighting the generality of the proposed method and the validity of first assumption.

Furthermore and finally, 50000 combinations of random morphological and vegetation characteristics, extracted from Table 2.2, and climatic setups, have been tested to verify that the coefficient of determination is high in every case, no matter of the watershed properties and climate. The number of combination has been sat equal to 50000 for a robust demonstration and in order to limit computational time. Results are presented as the probability distribution of R^2, shown in Figure 3.9. It is easy to note that almost all the examined cases exhibit high correlation of determination, giving further prove that Fu's law and ω are good descriptors of water partitioning process. Generally, once defined a climate and basin morphological and vegetation properties, the hydrological behaviour is a function of the aridity index and the long term water partitioning rules can be described with low uncertainties by the Fu's curve.

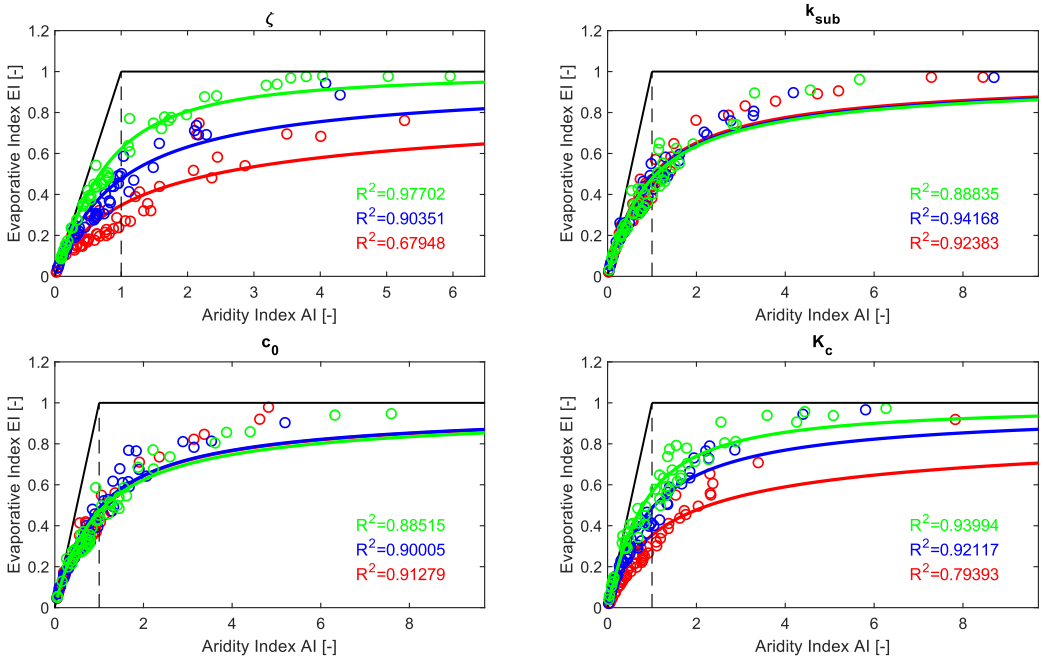

Figure 3.8. Fu's curves obtained considering the test-watershed parameters (blue line, Table 2.2, last column) and perturbating one parameter at time (one for each panel), testing their minimum (red line, Table 2.2 second column) and maximum values (green line, Table 2.2 third column). R^2 has been reported for the associated curves.

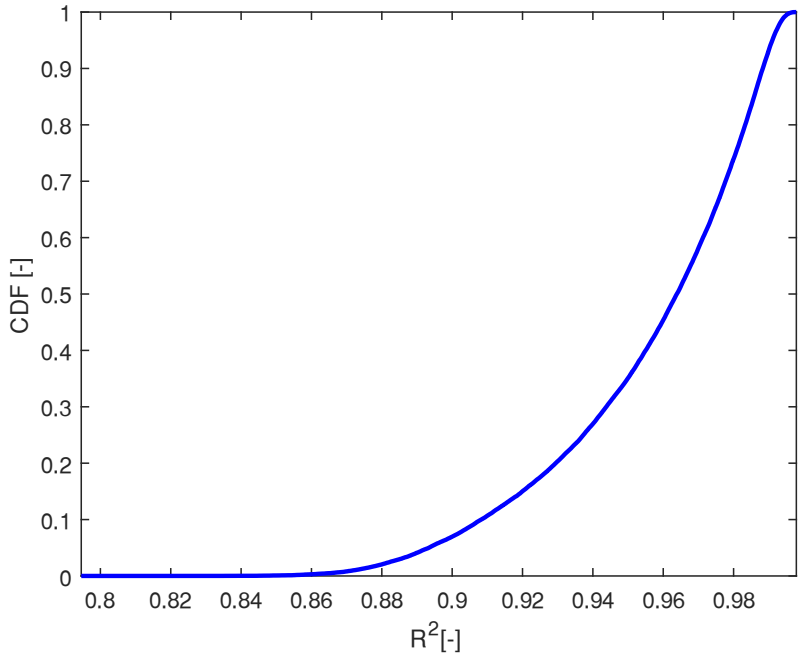

Figure 3.9. Cumulative distribution frequency (cdf) of R^2 of a sample of 50000 random generated basins. The coefficient of determination describes the goodness of Fu's equation in describing water partitioning over wide range of aridity indices.

3.3.2. Varying climate, fixed morphology and vegetation (VC-FMV)

In Section 3.3.1, it was shown that, for a given watershed and climate, only the aridity index drives the rainfall partitioning. Now the influence of climate in water partitioning processes has been explored (see Figure 2.4.b). As in the last Section, the same methodology is recursively applied for the *test-watershed* for the 5 different climatic setups and are compared the different Fu's parameters obtained. It was basically supposed

to transpose the *test-watershed* in different geographic areas (with different climate) and observe the long-time hydrological responses. The 5 analytical Fu's curves associated to the five-climatic setups and ω are reported in Figure 3.10.

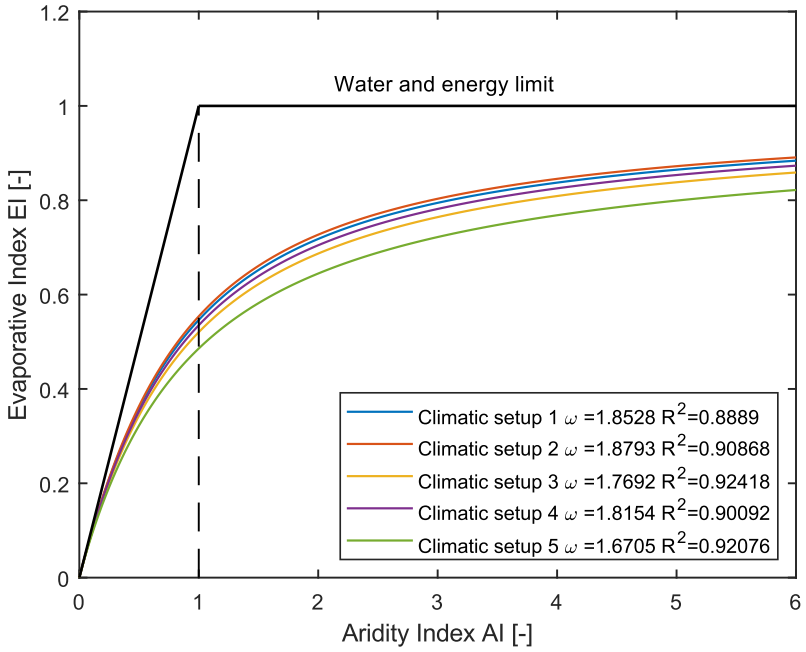

Figure 3.10. The five associated Fu's equations related to the test-watershed in 5 different climatic setups. In the inset it is reported the optimized ω and the R^2 referred to the five curves.

In line with what has already been seen in the previous Section, for each climate scenario R^2 has a value close to one, demonstrating that the univocal hydrological response is a condition independent of the climate scenario considered.

Observing the five curves, it has been highlighted that climate is an important driver in runoff (and evapotranspiration) generation. The climate seems to define different hydrological behaviour for the same watershed, as already pointed out by (Budyko,

1974); Potter et al. (2005). Under climate scenarios 1,2 and 4 the *test-watershed* results in less mean annual runoff Q (higher ω's values) than in the 3 and 5 cases. The physical explanation lies in potential evapotranspiration seasonal pattern: indeed, high evapotranspitative demand during the rain season prevents the soil saturation and consequently disadvantage subsurface and surface runoff generation. The climatic setups 3 and 5 induces the opposite hydrological behaviour due to the aforementioned mechanism. Under these climate conditions, the soil moisture is often equal to the maximum water holding capacity, that implies frequent surface and subsurface runoff production and then higher mean annual runoff Q. This happens because in the wettest periods of the year, potential evapotranspiration assumes its minimum value.

Fu's parameter are strictly correlated to the rain and evapotranspiration seasonal patterns, as demonstrated by Feng et al. (2015). Particularly in the climatic setup 5, characterized by out-of-phase rain and potential evapotranspiration, the ω value is the lower (1.67) while in the case 4, in-phase rain and potential evapotranspiration, ω is almost equal to 1.88.

3.3.3. Varying climate, varying morphology and vegetation (VC-VMV)

In this Section, it will be shown how basin morphological and vegetation properties are significant in water partition process, creating an instrument for assessment of Fu's parameter (see Figure 2.4.c). To describe such a relation it was decided to proceed as

follows: for all climatic setups, 10000 random watersheds have been considered, creating 10000 independent morphological and vegetation parameter sets, each chosen within ranges reported in Table 2.2. By means of the procedure described in Section 2.3 and already used in Section 3.3.1 and Section 3.3.2, for each morphological and vegetation parameter set, the relative Fu's parameter has been evaluated. The intermediate results are 5 databases, made by 10000 parameter sets and the associated ω values. To investigate relationship between hydrological response (represented by ω) and morphological and vegetation descriptors (ζ, k_{sub}, c_0,K_c), A stepwise linear regression has been applied for mathematically investigate the links between the after mentioned groups.

Results of linear regressions are reported in Table 3.2 for all considered climates, where a_i coefficient associated to morphological and vegetation parameter, intercept β and R^2 are reported, whereas colours refer to p-values. More precisely, white cells represent p-value equal to 0, light grey cells represent p-value higher than 0 and lower than 0.25 and dark grey cells p-value bigger than 0.25.

Generally, there is a good correlation between ω and basin morphological and vegetation descriptors for every climate, how demonstrated by elevate values of R^2. The best result is obtained for climatic setup 5, where R^2 is equal to 0.901.

For different variables the order of significance alternates according to the climatic setups. The most significative parameter is K_c, the coltural factor (p-values=0, for all climates). This means that the vegetation plays a significate role in water partitioning processes; according with the positive sign of the related coefficient/weight (Table 3.2), K_c is the most important contributor to evapotranspiration. k_{sub}, instead, has not a critical

role in water partition processes as stated by related p-value. The subsurface bucket parameter does not appear as a key descriptor of long-term water balance dynamics.

In order to explicit the role of each morphological and vegetation descriptor in determining ω, a simple sensitivity analysis (Figure 3.11) has been performed. Of course, being the relation linear, results are immediate.

	a_i				β	R^2
	ζ	k_{sub}	c_0	K_C	Intercept	[-]
Climatic setup 1	0.008699	1.207	-5.532	2.623	-0.576	0.784
Climatic setup 2	0.008379	0.044	-5.853	2.484	-0.385	0.809
Climatic setup 3	0.005831	-0.179	-5.697	1.979	-0.035	0.867
Climatic setup 4	0.007851	0.214	-5.939	2.405	-0.393	0.837
Climatic setup 5	0.003725	0.177	-3.475	1.287	0.516	0.901

Table 3.2. Results of the regression equations between morphological and vegetation parameters and Fu's parameter for all the considered climates. The a_i, β and R^2 represent respectively the coefficients related to each morphological and vegetation parameter, the constant term and the coefficient of determination of the linear equations that allow obtaining an empirical estimate of ω. All terms of the equation are obtained by stepwise regression, linking the random generated morphological and vegetation parameters' sets (which value's range are reported in Table 2.2) and the associated ω. The colors of the cells are related to p-value: white cells represent p-value equal to 0, light grey cells represent p-value higher than 0 and lower than 0.25 and dark grey cells p-value bigger than 0.25.

The variation of morphometrical and vegetation variables conditions the water portioning process vary. This analysis is an attempt to represent the influence of the EHSM parameters on ω. Fu's parameter is particularly sensitive to the coltural coefficient K_c: assuming an increasing (decreasing) from the value of the *test-watershed* to the

related extreme, both defined for the coltural coefficient in Table 2.2, it influences ω in +23÷43% (-23÷43%). Effects on ω due to increase (decrease) of ζ has the same sign of the latter, but this parameter seems to be less sensitive, as shown by lower slopes of the related sensitivity curves in Figure 3.11. The effect of vegetation and hydraulic soil capacity is fundamental in the water partitioning processes and particularly the change of type and quantity can modify the runoff and evapotranspiration relative magnitude (Wigmosta et al., 1994; Donohue et al., 2007a; Li et al., 2013; Zhang et al., 2016b). The influence of impervious areas c_0 is less pronounced than the last two variables, but it plays an important role in hydrological response. The influence of k_{sub} is negligible because subsurface runoff timing has not a fundamental role in long term hydrological processes. A maximum delay for transformation of subsurface flow in runoff is considered equal to 600 days (k_{sub} = 1/600 = 0.017). This means that most of the water becomes runoff Q in about two years; this does not influence the water balance in a long-time period and thus it could be considered a constant background noise that does not affected the rules of water partitioning. Known the effect of different parameters and in order to demonstrate how morphological and vegetation parameter influence runoff, the latter results in an additional analysis have been used. Morphological and vegetation parameters have been perturbated one at the time from the same *test-watershed* reported in Table 2.2; then ω is evaluated using the linear regression previously obtained and is evaluated the mean annual runoff alteration ΔQ due to morphological and vegetation parameters variation for all climatic setups.

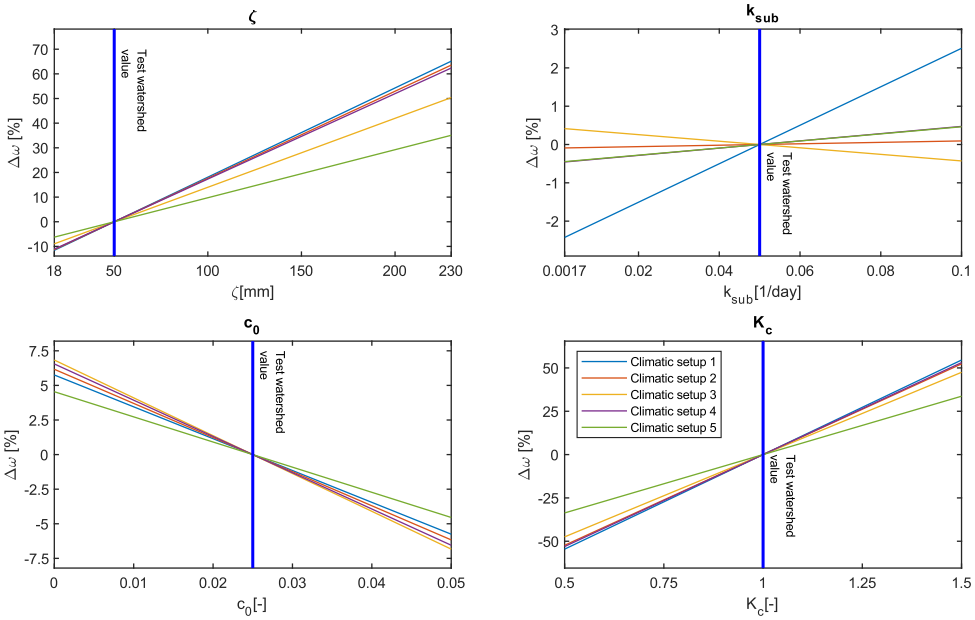

Figure 3.11. Sensitivity analysis on morphological and vegetation linear expressions relating model parameters to ω, in different climates. Coefficients are reported in Table 2.3. The percentual alteration Δω due to variation of each morphological and vegetation descriptors from the configuration of test-watershed setting, between the ranges reported in Table 2.2.

Figure 3.12 represents the influence of parameters on mean value of annual runoff Q for positive and negative variation of these of 10,20 and 30 per cent. As each of the considered variable increases or decreases, Figure 3.12 shows how runoff is modified from the reference condition, as a function of the aridity index. Results of climate scenario 5 (Mediterranean climate) are reported but similar results have been obtained for the other considered ones.

For all morphological and vegetation parameters the pattern of curves is the same and related to magnitude of ω's variation. Clearly, moving from low to high AI's values, the

magnitude of runoff variation ΔQ is always raising. This means that, in climate change conditions, as annual rainfall is decreasing and potential evapotranspiration is increasing (Viola et al., 2016), non-negligible runoff changes are foreseen, leading important economic and environmental impacts.

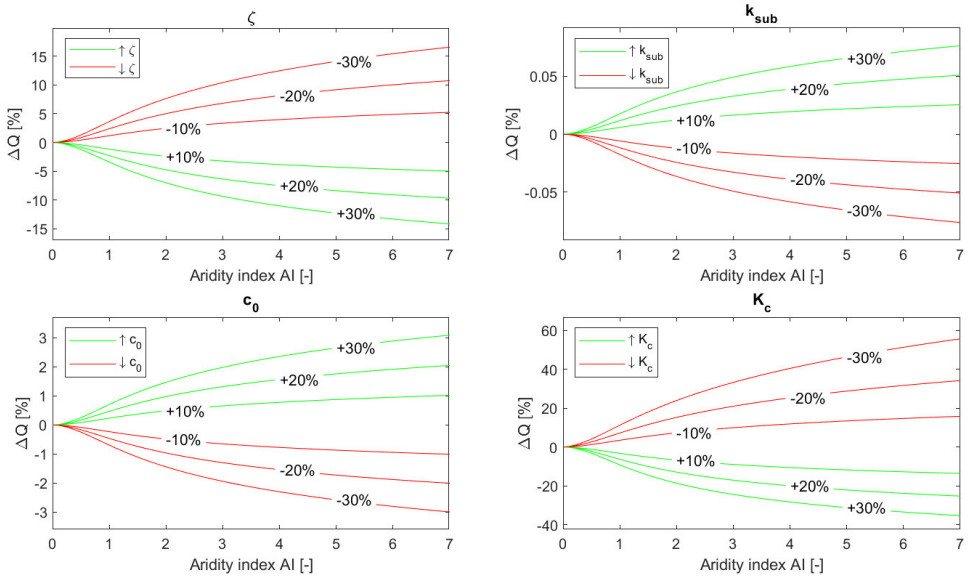

Figure 3.12. Runoff alteration, under different AI, referring to the climatic setup 5 and supposing an increment/decrement of 10, 20 and 30 per cent of the four morphological and vegetation descriptors from the test-watershed configuration. The curves associated to positive alteration of the morphology and vegetation parameters are reported in green and the ones associated to negative variation are in red.

The coltural coefficient K_c has tremendous effect on ΔQ: remarkably, positive or negative variations have not the same impacts. For instance, deforestation or afforestation on the same area induces different runoff change. Negative alteration of K_c: (i.e. deforestation) induce annual runoff increases larger, as percentage, than the ones obtained with positive K_c: variations (i.e. afforestation).

3.3.4. Validation of regression equations

In order to demonstrate the ability of the obtained regression equations to reproduce ω in different climates in the real world, four catchments, associated to four climatic setups (as defined in 3.2.1) are analysed; the first scenario has been not considered since it is an ideal condition. The parameters values as resulted from regression equations (named "assessed ω") have been compared with the ones calculated by fitting the Fu's curve to hydrological data (named "hydrological ω").

The first case study is Saline River Basin at Rye, Arkansas (USA) and it is a sub-catchment of Ouachita River with an extension of 2102 km^2. The climate is Atlantic-oceanic with constant rainfall during the year and potential evaporation that has a peak in summer months (June -August). Climatic condition of this watershed is associable to climate scenario 2. Mean annual rainfall $\bar{P}$ is 1314 mm with runoff coefficient of 0.33; mean annual potential evapotranspiration $\overline{PET}$ is 945 mm, near to real evapotranspiration ET (883.6 mm). Evergreen forest is the most prevalent LU coverage (96 %) and the remaining part is urban and built-up areas.

The second case is the Parana River at Guaira, which is in the South America and pass through Brazil, with an approximate area of 830 000 km^2. The climate is tropical with a constant value of potential evapotranspiration and a precipitation peaks in December, following seasonal pattern of climate scenario 3. $\bar{P}$ is pretty high (1469.7 mm), as $\overline{PET}$ (1368.15 mm); the runoff coefficient is about 0.22, also due to high mean annual evapotranspiration (1144.15 mm). The largest part of the basin is covered by pasture

(44%), while annual crop and sugar cane occupy the 27% and 9% of the watershed, respectively; finally, forest is only the 9% of total of Parana basin.

The third case study is a tributary of the Missouri River and its basin covers three USA states: Montana, North and South Dakota with a catchment area of 1970 km^2. Climate refers to climate condition 4, with the most important precipitations in summer months and mean annual value of 394.2 mm. Precipitation is in-phase with the potential evapotranspiration that has a maximum in the middle of the year, with a mean annual value of 1022 mm. Runoff coefficient is 0.06 and mean annual evapotranspiration is 372.3 mm. The vegetation consists of permanent wetland (61%) and woody savannah (37%).

The latter case study refers to a watershed in California, namely the Santa Ysabel Creek, with a typical Mediterranean climate, characterized by wet winter/autumn and dry summers, attributable to climate scenario 5. Santa Ysabel Creek has an extension of 112 km^2, P is 521.95 mm; only a small fraction of rainfall, namely 6%, is transformed into discharge. $\overline{PET}$ is 1405.25 mm due to high temperature and only 489.1 mm becomes real evapotranspiration ET because of soil moisture limitation. Forest and shrubland are the prevalent land cover type (51% and 46%), with little percentage of savannas. Monthly rainfall and temperature in the four considered case study are represented in Figure 3.13. Starting from the basin morphological and vegetation characteristics, the 4 aforementioned model parameters (ζ, k_{sub}, c_0 and K_c) have been calculated. The maximum water holding capacity ζ is calculated using different soil parameters, according to Eq. 2.19. n, s_{fc} and s_h were obtained from soil type info, while Z_r has been related to the vegetation type within the considered basin following Yang et al. (2016).

The evaluation of the subsurface parameter k_{sub} has been done using the global maps provided by Beck et al. (2013).

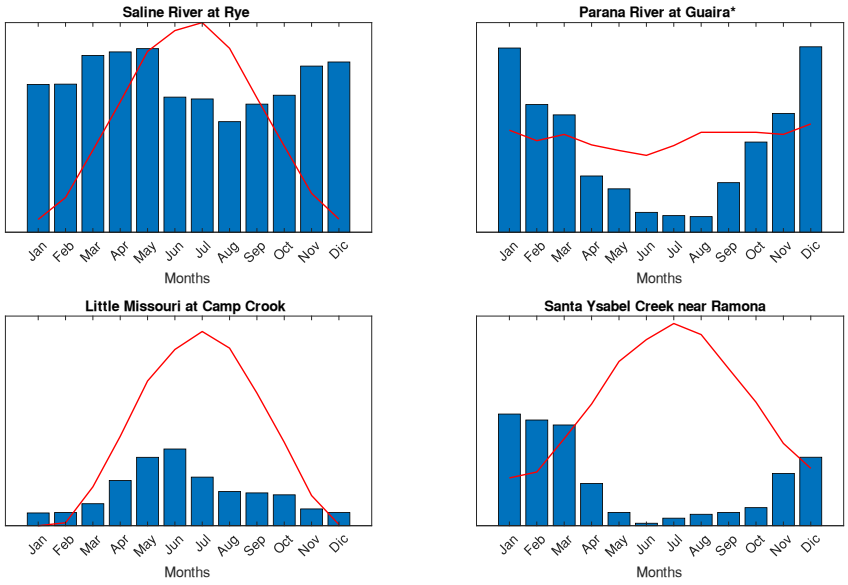

Figure 3.13. Seasonal patterns of monthly rainfall and potential evapotranspiration in the four considered case study basins. The red line represents the mean monthly potential evapotranspiration, whereas the blue bar the mean monthly precipitations from MOPEX database (Duan et al., 2006). Case study with asterisk: precipitation and potential evapotranspiration dataset come respectively from CRU TS version 4.00 (Harris et al., 2014) and CGIAR-CSI Global Aridity Index (Global-Aridity) and Global Potential Evapo-Transpiration (Global-PET) Climate Database (Trabucco et al., 2008; Zomer et al., 2008)Climatic data are provided by different sources: for the 3 US watershed (Saline River Basin at Rye, the tributary of the Missouri River and Santa Ysabel Creek) Model Parameter Estimation Experiment (MOPEX) (Duan et al., 2006) is used, while for the Parana at Guaira basin CRU TS version 4.00 (Harris et al., 2014) and CGIAR-CSI Global Aridity Index (Global-Aridity) and Global Potential Evapo-Transpiration (Global-PET) Climate Database (Trabucco et al., 2008; Zomer et al., 2008) have been adopted. In order to give a morphological and vegetation characterization of the study cases, different sources of data have been used: for the 3 US watershed, MOPEX (Duan et al., 2006) database and for Parana at Guaira basin the info reported by Melo et al. (2016) and soil maps.

The percentage of impervious area c_0 has been obtained from soil use info reported within the mentioned database. The coltural coefficient K_c has been supposed to be related to vegetation type; the value for forest is set equal to 1.5, 1.25 for shrubland and savannahs, 1 for cropland and grassland and 0.5 for bare soil. Then a weighted average provided a unique value over the considered basins.

Once calculated the model parameters, ω has been calculated through the regression equations of Section 2.3 and reported values in the column "Assessed ω" in Table 3.3. On the other hand, climatic and hydrological data allow to define AI and EI for each of the case study, and consequently ω can be assessed by making the Fu's curve pass through those points. A simple comparison has been carried out between the "hydrological" and "assessed" ω values, while the relative percentual difference $\Delta\omega$ is assessed and reported in Table 3.3. For the considered case study, errors are indeed limited, only 3% for the Santa Ysabel Creek near Ramona.

The results are encouraging, but it is however necessary to underline some limitations of the proposed method. First, the definition of a climatic pattern may be too simplistic in representing seasonal behaviour of rainfall and potential evapotranspiration worldwide. In addition, the daily rainfall representation as a Poissonian process, with constant interarrival time, could result in errors in streamflow estimation. In fact low values of $\bar{\lambda}$ imply elevate soil moisture and more runoff production and viceversa. Thus, a correct characterization of $\bar{\lambda}$ is crucial for a precise description of long-term hydrological dynamics.

Case study	Climatic setup	ζ [mm]	k_{sub} [1/day]	c_0 [-]	K_c [-]	Hydrologic ω	Assessed ω	$\Delta\omega$ [%]
Saline River near Rye	2	155,05	0,08	0,03	1,50	4,50	4,44	1,21%
Parana River at Guaira	3	146,95	0,08	0,02	1,13	2,96	2,92	1,25%
Little Missouri at Camp Crook	4	44,41	0,17	0,01	1,25	2,92	2,90	0,60%
Santa Ysabel Creek near Ramona	5	96,35	0,09	0,00	1,38	2,72	2,63	3,10%

Table 3.3. Case study basins, their associated climatic setup and morphological and vegetation parameters, evaluated by a "general database", composed by MOPEX database (Duan et al., 2006), Padrón et al. (2017), Melo et al. (2016) and other mixed information. The last three columns point out the results of comparison between "hydrological ω" (obtained by the Fu's expression) and "assessed ω" (obtained by the proposed linear regression expressions).

3.4. Near future climatic and land use scenarios

In this thesis, climate and land use (LU) represent the only drivers of the hydrological response in Sardinia. Therefore, several climatic and LU scenarios will be taken into account to consider the highest number of possible evolutions of the near future hydrological behaviour of Sardinia.

Within Caracciolo et al. (2017)'s approach, climatic scenarios are represented by four out of five parameters of the analytical expression of probability density distribution (*pdf*) of annual surface runoff Q. Remembering Eq. 2.10, each climatic scenario will be associated to a set of mean and standard deviation values of annual rainfall P and potential evapotranspiration PET ($\bar{P}$,$\overline{PET}$,σ_P^2,σ_{PET}^2).

These parameters will be evaluated at regional scale to provide a general estimate of hydrological behaviour and water availability in Sardinia in the near future. EUROCORDEX climate modelling (CM) outputs have been used to characterize near future climate.

As stated in Chapter 1 and in Section 2.4.2, CM outputs are affected by systematic errors from different sources, so bias correction (BC) methods have been adopted to define the less unbiased future climatic scenarios. BC results and climatic scenarios will be illustrated in Section 3.4.1.

LU scenarios, epitomized in the proposed method by Fu's parameter ω, will be hypothesized following three approaches described in Section 2.4.3. LU maps from CORINE Land Cover (CLC) inventory have been used to depict ongoing modification of

LU in Sardinia. Then, LU scenarios will be associated to ω's values to be representative of LU effect at regional scale within Caracciolo et al. (2017)'s approach. LU scenarios and the related ω will be reported in Section 3.4.2.

The five parameters will be assessed for two periods: 2006-2050 and 2051-2100.

3.4.1. Climatic scenarios

To define climatic scenarios, the preliminary phase is the BC of CM rainfall and temperature outputs.

Firstly, in the parametrization phase, the observed timeseries have been adopted to calibrate the BC methods as described in Section 2.4.2. The performances of BC methods are evaluated by the comparison of the observed, raw and BC HS CM empirical cumulative density distributions (*ecdfs*) of climatic timeseries, at daily and yearly scale. These results will allow to quantify the magnitude and the sign of CM systematic errors, to highlight BC methods performance. Then, after the parametrization phase, to predict near future rainfall and temperature trends, raw RCPS CM rainfall and temperature outputs will be corrected by the calibrated parameters, calculated during the parametrization phase. Again, the *ecdfs* of observed and BC RCPS P and PET will be compared to understand the near future behaviour of rainfall and temperature. Given BC RCPS temperature dataset, BC RCPS potential evapotranspiration outputs will be calculated by the Thornthwaite's formula (Eqs. 2.34-2.35 and 3.1-3.2).

Finally, given BC P and PET timeseries, spatial-averaged values of the climatic

parameters ($\bar{P}$,$\overline{PET}$,σ_P^2,σ_{PET}^2) will be calculated and they will defined the set of parameter associated to a climatic scenario. This procedure will be repeated for 14 different CM, then 14 climatic scenarios will be created.

The results of BC procedures for CM rainfall and temperature outputs will be shown

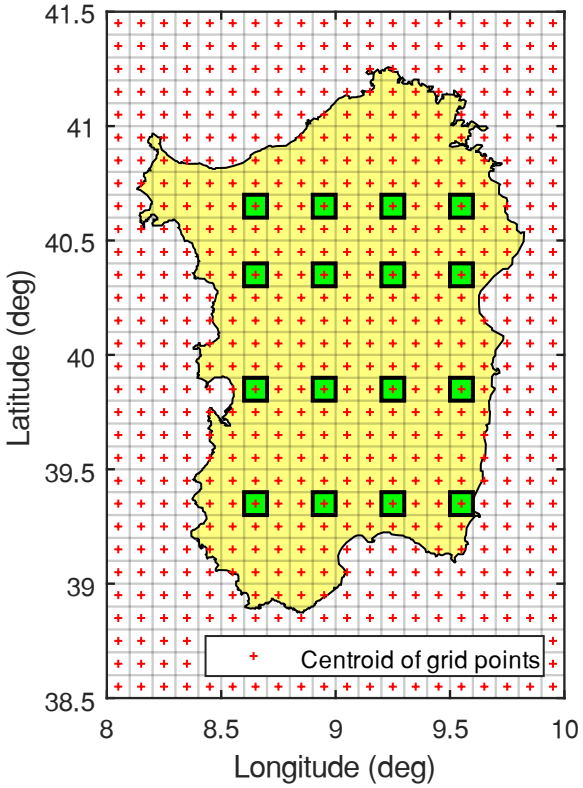

Figure 3.14. Centroids of grid points Grid points of the regular grid at 0.1° (~50 km) used to interpolate the observed and CM datasets. Green cells represent the test grid points adopted to test bias correction performance.

referring to 16 test grid points (Figure 3.14) of the regridded-data of EUROCORDEX project (see Section 2.4.1). The test grid points have been selected following the idea to take into account the meteo-climatic variability inside the Sardinian territory.

In this Section, only the results of CM#13 will be displayed for the sake of brevity.

For each test grid point (Figure 3.14) and given a CM (CM#13), Figure 3.15 shows the observed (dashed black line), raw (continuous black line) and BC HS (coloured lines) daily rainfall *ecdf*. Regarding BC *ecdf*, the red, violet and green ones are associated to HS rainfall timeseries corrected respectively by linear scaling method (LS), power transformation method (PT) and distribution mapping method with gamma distribution (DM-Γ).

There is not a clear trend in the sign of the correction, meaning that in the selected grid points BC methods both reduce and increase quantiles associated to each percentile. However, this variability is attributable to the attempt of BC methods to reproduce orographic effect, that CMs do not fully represent as attested by Mascaro et al. (2018).

Generally, all BC methods corrected well the raw HS CM daily *ecdfs* except for the right tails, namely high extreme events (Figures 3.15). This result is expected because all the BC methods here adopted do not account for extremes and the interdependence effects. Under the hypothesis that the BC HS and observed timeseries well fit a given theoretical distribution, the idea of DM method is to modify the distribution of BC daily rainfall timeseries. Then, the performances are strictly related to the DM approach adopted (Li et al., 2010) and to the selected theoretical distribution. Gamma distribution is widely adopted to fit the daily rainfall events, however other distributions as exponential, Pareto, GEV and Weibull (Wilks, 1998; Deidda and Puliga, 2006; Ye et al., 2018) are more suitable for extreme events.

Despite PT is rougher than DM-Γ, the performance in reproducing observed daily

rainfall *ecdfs* are comparable to the last one. LS showed the worst performances between BC methods here considered as attested by the LS HS daily rainfall *ecdfs*' departure to the observed one.

Since the BC has been applied at daily scale, the BC HS *P ecdfs* diverge more than daily ones by the respective observed *ecdfs* (Figure 3.16). As for the daily scale, BC HS *P ecdfs* displayed the higher deviations to the observed ones in the higher percentiles.

General effect of BC is to shift BC *ecdfs* closer to the observed ones, thus correcting the median (and the mean) and variance of timeseries. BC performance decreases moving from daily to annual scale as expected, but mean and standard deviation, which are statistics parameter of interest in this thesis, are corrected and reproduced with satisfaction.

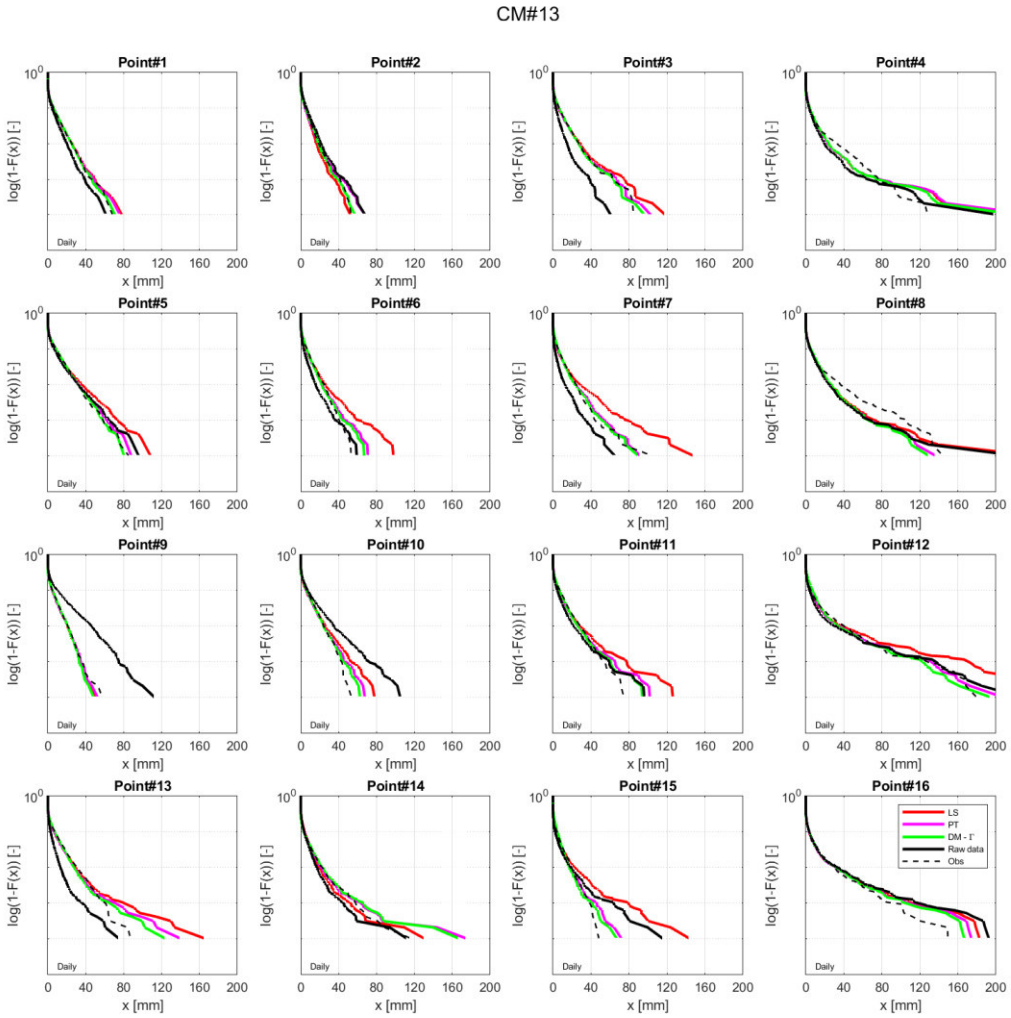

Figure 3.15.Comparison between observed (dashed black), HS raw biased (solid black) and HS bias corrected (BC) (solid coloured) daily rainfall empirical cumulative empirical density functions (ecdfs) for the sixteen test grid points considered of the CM#13. Red, violet and green lines represent the HS BC daily rainfall ecdfs by linear scaling (LS), power transformation (PT) and distribution mapping (DM-Γ) approaches. x refers to daily rainfall.

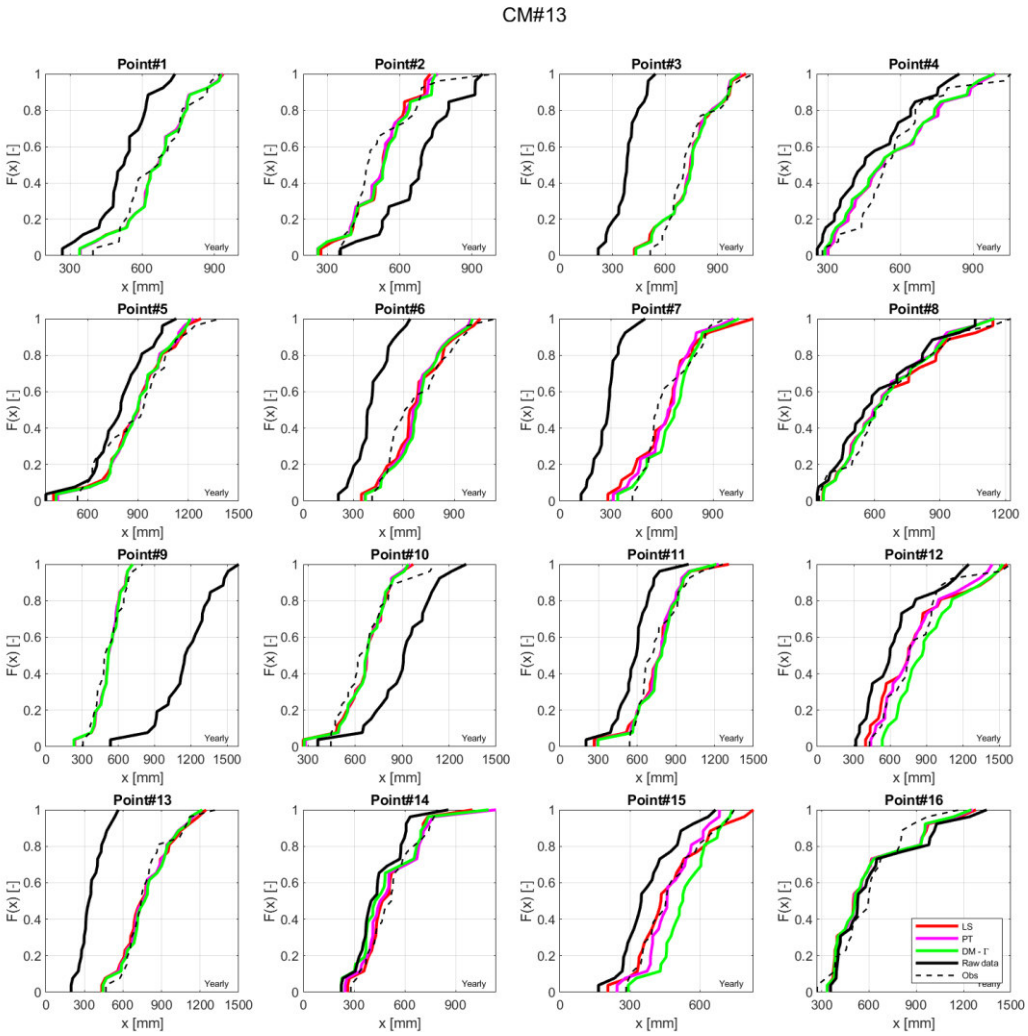

Figure 3.16. Comparison between observed (dashed black), HS raw biased (solid black) and HS bias corrected (BC) (solid coloured) annual rainfall (P) cumulative empirical density functions (ecdfs) for the sixteen test grid points considered of the CM#13. Red, violet and green lines represent the HS BC annual rainfall ecdfs by linear scaling (LS), power transformation (PT) and distribution mapping (DM-Γ) approaches. X refers to P.

For the 16 test grid points, in Figure 3.17, BC HS daily temperature *ecdfs* of CM#13 are reported. The observed (dashed black line), raw HS (continuous black line) and BC HS (red lines) *ecdfs* are displayed, highlighting that in the case of temperature the only BC method adopted corrects well the raw HS *ecdf* with a simple distribution as Gaussian. This is due to the statistical properties of temperature, that differently to rainfall, is not a zero-bounded and intermittent climatic variable, reason why good fitting performances are easier to achieve.

Differently to rainfall, the divergence of the BC HS daily temperature *ecdfs* by the observed ones is more reduced, but, similarly to rainfall, is higher in the extreme quantiles.

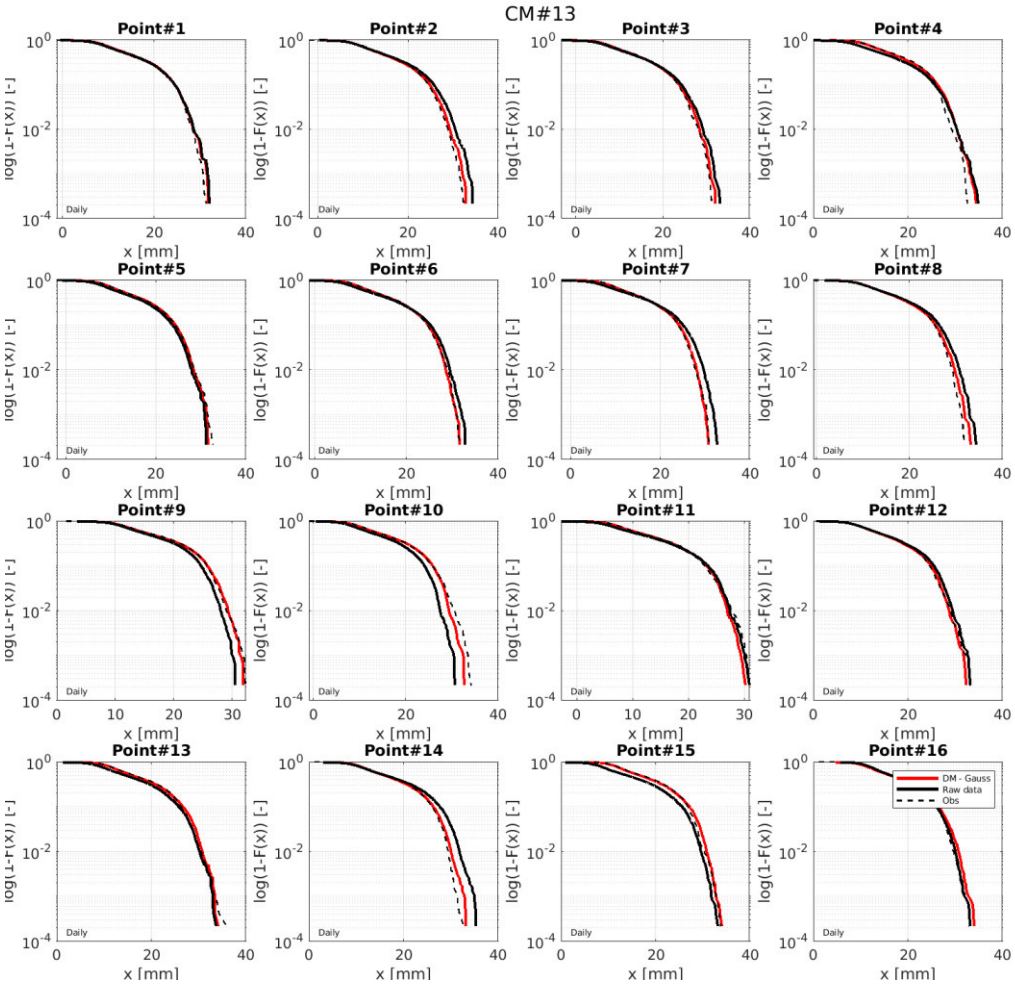

Figure 3.17. Comparison between observed (dashed black), HS raw biased (solid black) and HS bias corrected (BC) (solid red) daily temperature cumulative empirical density functions (ecdfs) for the sixteen test grid points considered of the CM#13. The BC approach adopted is the distribution mapping (DM-Gauss).x refers to daily temperature.

Given the purpose to reproduce BC mean and standard deviation of HS and RCPS P and PET (temperature), the results just showed can be considered satisfactory. BC performances are better at daily scale because obviously BC methods here adopted operate at that scale. Future improvements could be oriented to correct CM outputs at different scales (Johnson and Sharma, 2012; Mehrotra and Sharma, 2016; Mehrotra and Sharma, 2019). Other efforts could be done in future to improve BC taking into account the intermittence nature of rainfall and extreme events for both the considered meteo-climatic variables.

After the parameterization phase, the BC procedures have been applied to correct the raw RCPS CM outputs (correction phase).

As done previously, for each selected test grid point in Figure 3.18 BC RCPS daily rainfall *ecdfs* are reported together with raw RCPS and observed ones. Generally, the effect of BC is to reduce the deviation of BC RCPS daily rainfall *ecdfs* to observed ones. For this reason, the quantile range consequently changes, becoming more comparable with the observed *ecdfs*. This suggests that BC operates on variance of the process. PT and DM-Γ *ecdfs* are similar and comparable to observed *ecdfs*, despite it is evident that BC RCPS *ecdfs* represent wetter climatic conditions. In some test grid points, LS *ecdfs* deviate significatively to the last ones probably to inability to represent extreme events properties.

Therefore, LS, PT and DM-Γ P *ecdfs* are comparable and do not diverge from each other like at daily scale as shown in Figure 3.19.

The deviation between the raw RCPS temperature *ecdfs* and the BC ones is not

pronounced as for the rainfall, meaning that systematic errors of CM are lower than the CM rainfall dataset, as highlighted in Figure 3.20.

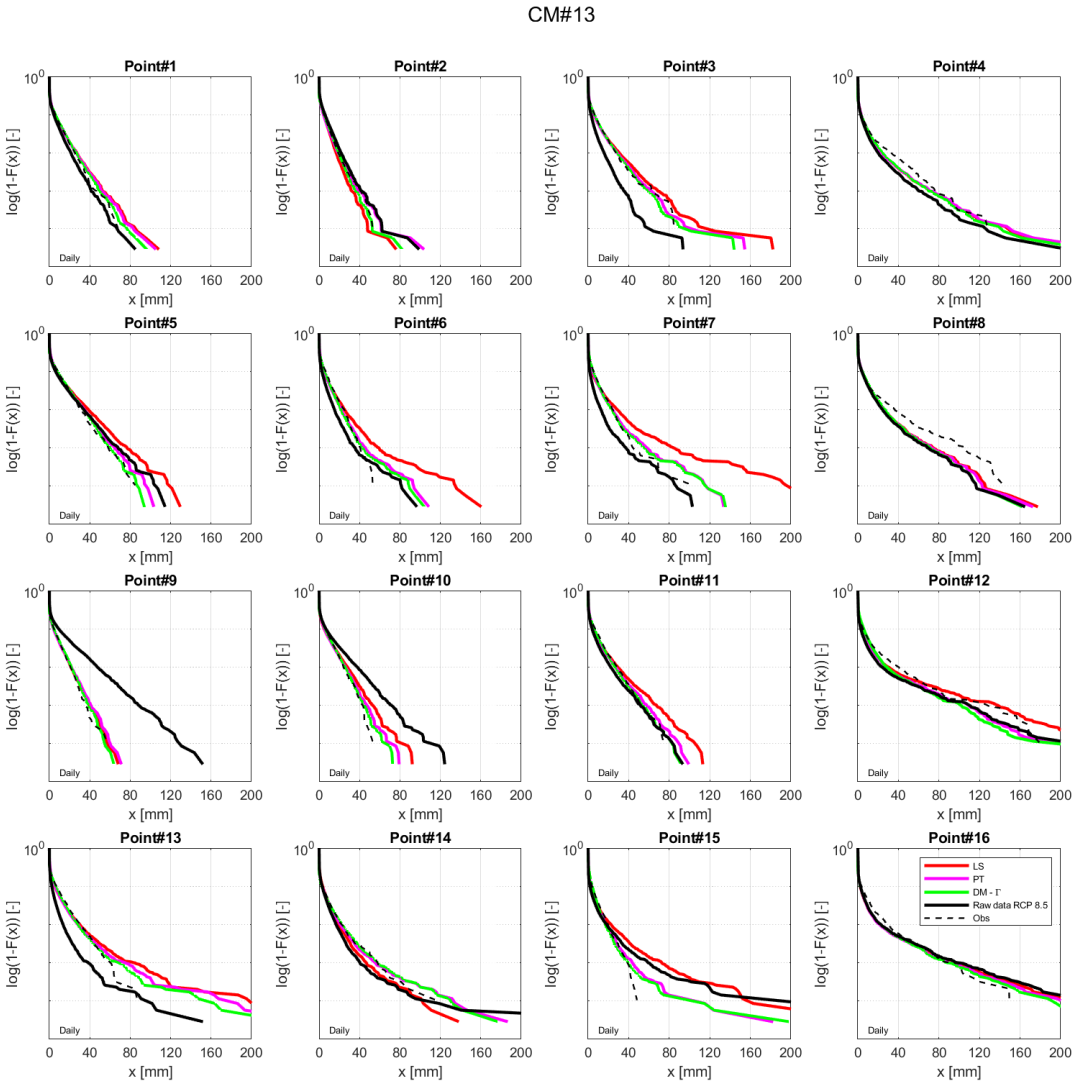

Figure 3.18. Comparison between observed (dashed black), RCPS raw biased (solid black) and RCPS bias corrected (solid coloured) daily rainfall cumulative empirical density functions (ecdfs) for the sixteen test grid points considered of the CM#13. Red, violet and green lines represent the RCPS bias corrected daily rainfall ecdfs by linear scaling (LS), power transformation (PT) and distribution mapping (DM-Γ) approaches. X refers to daily rainfall.

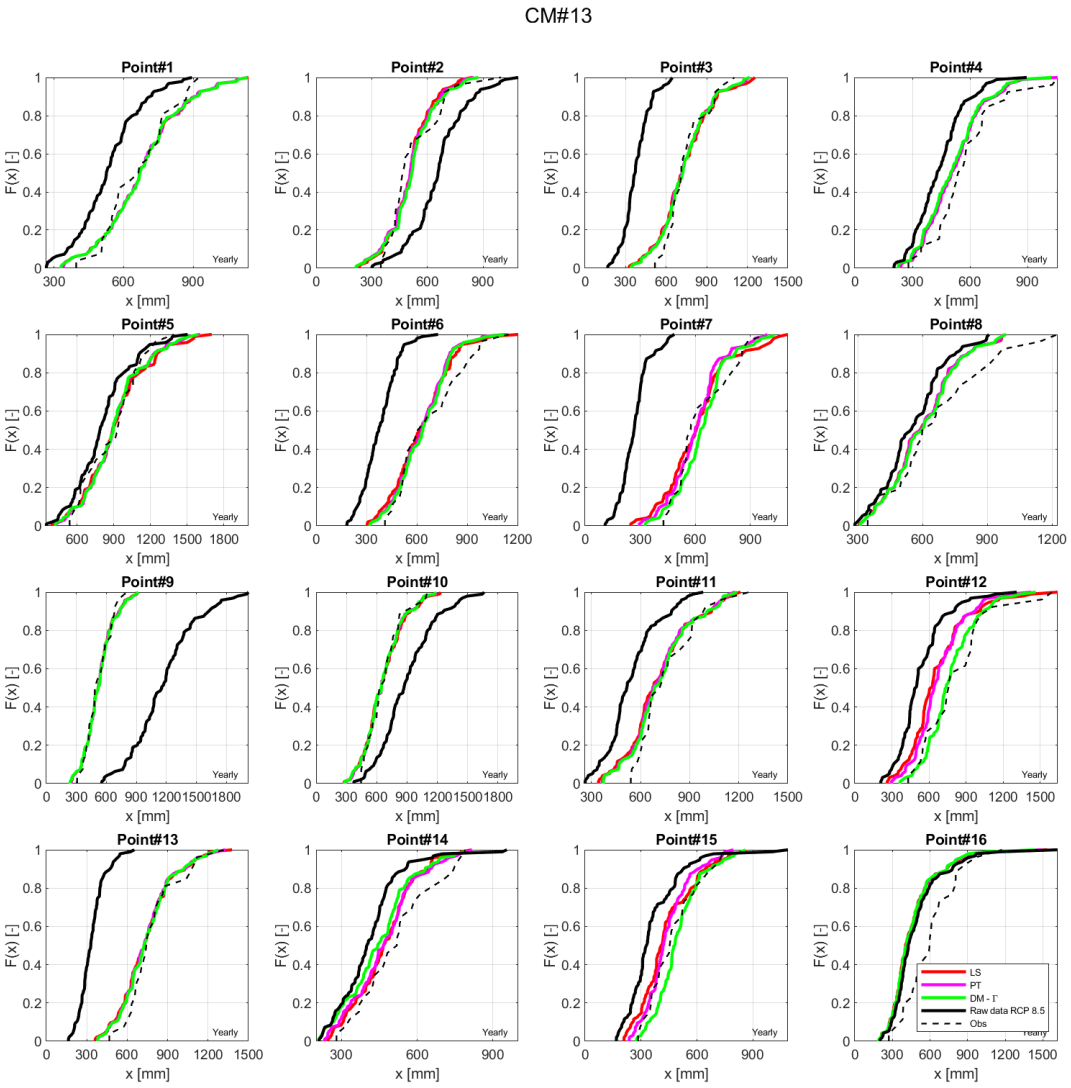

Figure 3.19. Comparison between observed (dashed black), RCPS raw biased (solid black) and RCPS bias corrected (BC) (solid coloured) annual rainfall (P) cumulative empirical density functions (ecdfs) for the sixteen test grid points considered of the CM#13. Red, violet and green lines represent the HS BC annual rainfall ecdfs by linear scaling (LS), power transformation (PT) and distribution mapping (DM-Γ) approaches. x refers to annual rainfall (P).

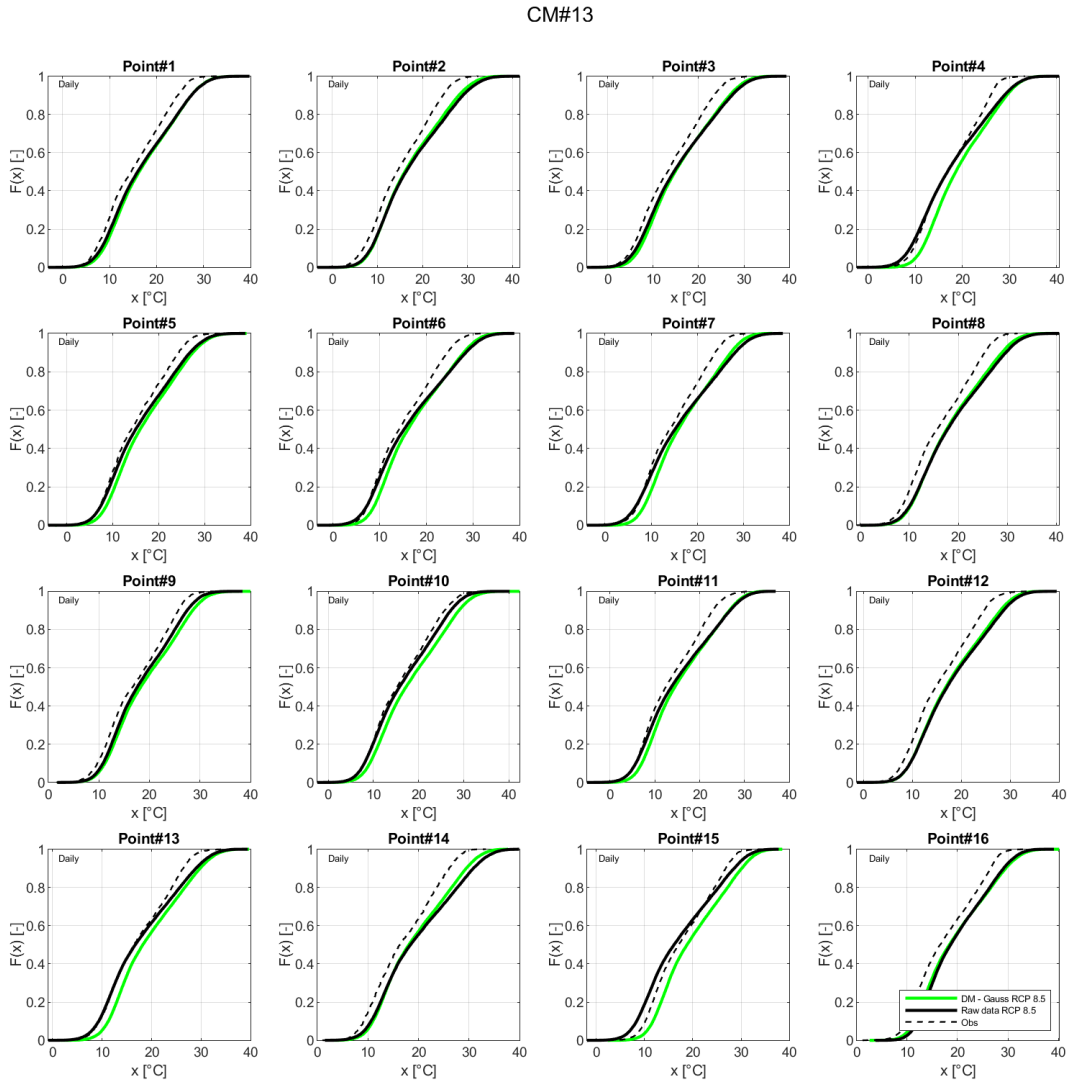

Figure 3.20. Comparison between observed (dashed black), RCPS raw biased (solid black) and RCPS bias corrected (BC) (solid green) daily temperature cumulative empirical density functions (ecdfs) for the sixteen test grid points considered of the CM#13. The BC approach adopted is the distribution mapping (DM-Gauss RCPS). x refers to daily temperature.

Since this work is oriented to define the mean and standard deviation of P and PET ($\bar{P}$, $\overline{PET}$, σ_P and σ_{PET}) here intended as four out of five parameters of the proposed method to estimate Q *pdf*, Figures 3.21 and 3.22 represent BC spatial-averaged P and daily temperature t_d statistical moments for Sardinia in 2006-2051 and 2051-2100 period. Spatial-averaging operation is intended as the mean of a given parameter associated to all grid points inside the Sardinian territory. Despite the research is oriented to define near future PET central moments, in this step temperature outcomes are reported to give a more general idea of future climate trends. In the following steps, analogous results of PET will be showed.

Therefore, for the sake of clarity, it is worth to highlight that from now on the results refer to the BC RCPS (RCP 8.5 scenario) CM rainfall and temperature outputs that have been bias corrected by distribution mapping with gamma and gaussian distribution respectively for rainfall and temperature. These results have been selected because they showed the best performances, as highlighted in the previous paragraphs.

Regarding rainfall (Figure 3.21, first row), all CMs agree in reduction of $\bar{P}$ in the future compared to the baseline value (710.2 mm), ranging from 608.70 mm (CM#14) to 699.2 mm (CM#2) in 2006-2050 and from 507.8 mm (CM#7) to 696.0 mm (CM#2) in 2051-2100. In 2006-2050 period for every CM, spatial-averaged σ_P (Figure 3.21, second row) is on average lower than the observed one (baseline value) (189.10 mm) and vary significatively between CMs, ranging from 159.6 mm (CM#7) to 190.60 mm (CM#7). Generally, σ_P increases in the 2051-2100 (minimum 167.20 mm, CM#1, maximum 200.90 mm CM#12).

On the other hand, for each CM, spatial-averaged mean temperature $\overline{t_d}$ will increase in both future periods (16.06 °C reference value), ranging from 16.88 °C (CM#12) to 17.79 °C (CM#9) in 2006-2050 and from 18.89 °C (CM#3) to 22.22 °C (CM#8) in 2051-2100 (see Figure 3.22, first row). Same trend has been observed for the spatial-averaged standard deviation of daily temperature σ_{t_d}, that in 2006-2050 period it is rather close to the observed one (6.49 °C reference value, minimum 6.42 °C CM#6, maximum 6.78 °C CM#12) and increase in 2051-2100 period (minimum 6.68°C CM#6, maximum 7.37°C CM#8) (see Figure 3.22, second row).

Figure 3.23 shows the gridded map of ensemble mean of $\bar{P}$ and the comparison with baseline values in 2006-2050 and 2051-2100 periods. This is a graphical representation of the spatial distribution of the parameter $\bar{P}$.

Given a grid point and a parameter associated with it, the ensemble mean is the mean of all values of that parameter associated to the different CMs here considered.

As previously remarked, BC allowed to reproduce orographic effect on BC CM P (Figure 3.23, first row). Figure 3.23 (second row) shows the gridded map of the difference between baseline and ensemble mean of $\bar{P}$ which assumes only negative values in 2051-2100 in all Sardinia, while, even if in limited areas, a slight increase is observed in 2006-2050. Generally, $\Delta\bar{P}$ ranges from -30% to 5% with a negative gradient moving from the west coast to the east coast, following the observed trend of Sardinian rainfall.

Similar to P, BC does not alter the altitude-mean temperature relation (Figure 3.24). In 2006-2050 period (Figure 3.24, second row), despite in some areas the ensemble mean of $\overline{t_d}$ is higher than the baseline values, the gridded map reflect the increase of

temperature in the future. This trend is more emphasized in 2051-2100 period and the difference between ensemble mean and baseline $\overline{t_d}$ is spatially homogeneous in both periods.

Figures 3.25 and 3.26 display the same results for standard deviation. The gridded map of the ensemble mean of σ_P is similar for both periods here considered. σ_P on average ranges between 150 and 180 mm in 2006-2050 and between 140 and 160 mm in 2051-2100. Extremes values are observed in the east coast attributable to board effects/extreme rainfalls. Referring to the baseline σ_P, Figure 3.25 (second row) displays an increase in standard deviation more pronounced in the west coast up to a maximum of 30%. Regarding temperature (Figure 3.26), ensemble mean of σ_{t_d} is higher in the internal areas with an increasing trend through the time. σ_{t_d} ranges approximately between 5.9 and 7.4 °C in 2006-2050 and 6.3 and 7.4 °C in 2051-2100. The deviation from the baseline σ_{t_d} is homogenous in both periods.

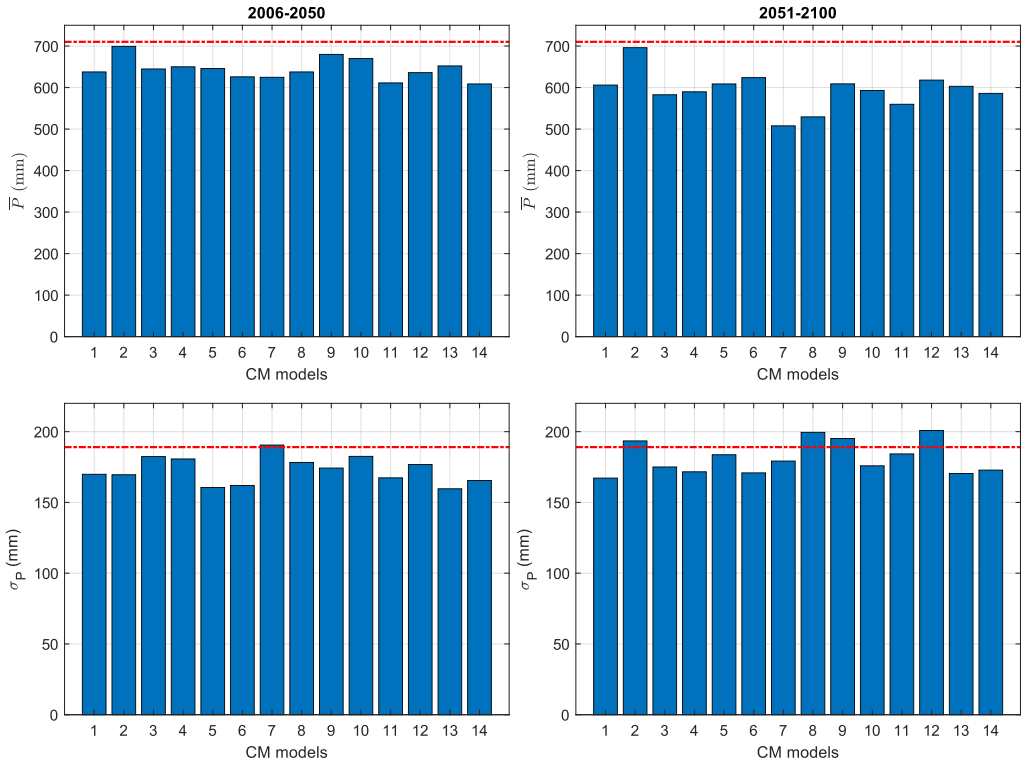

Figure 3.21. Spatial-averaged bias corrected (BC) mean (first row) and standard deviation (second row) of annual rainfall (P) of 14 CM rainfall outputs for Sardinia. The dashed red line represents the baseline value.

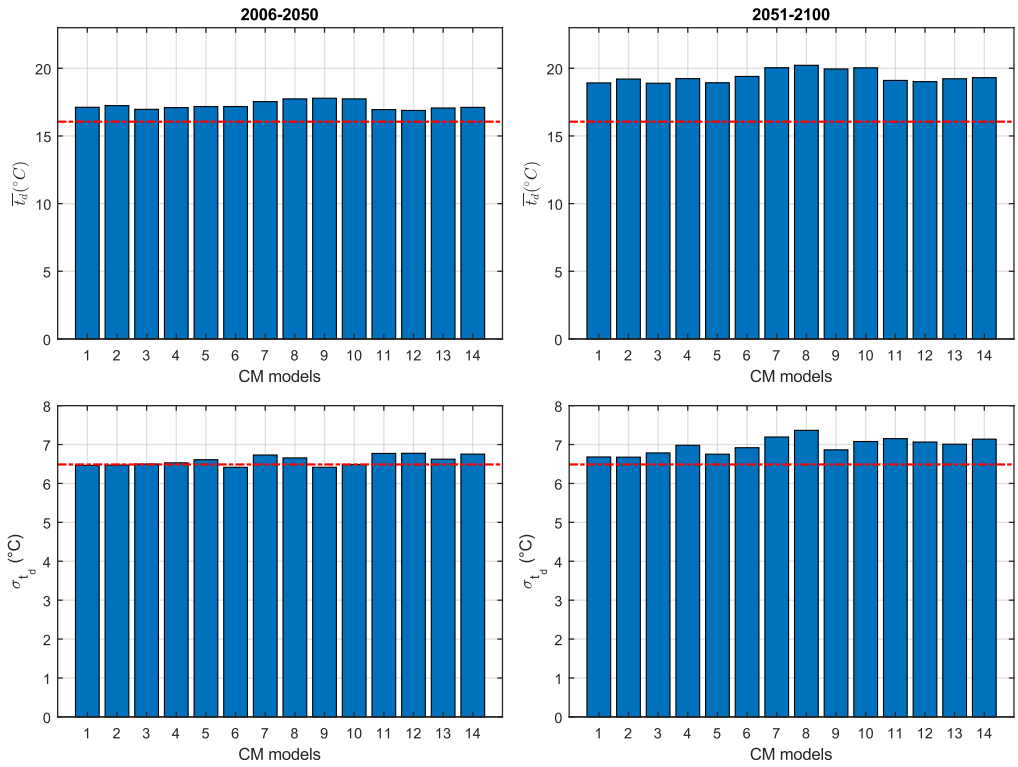

Figure 3.22. Spatial-averaged bias corrected (BC) mean (first row) and standard deviation of daily temperature (t_d) of 14 CM temperature outputs for Sardinia. The dashed red line represents the baseline value.

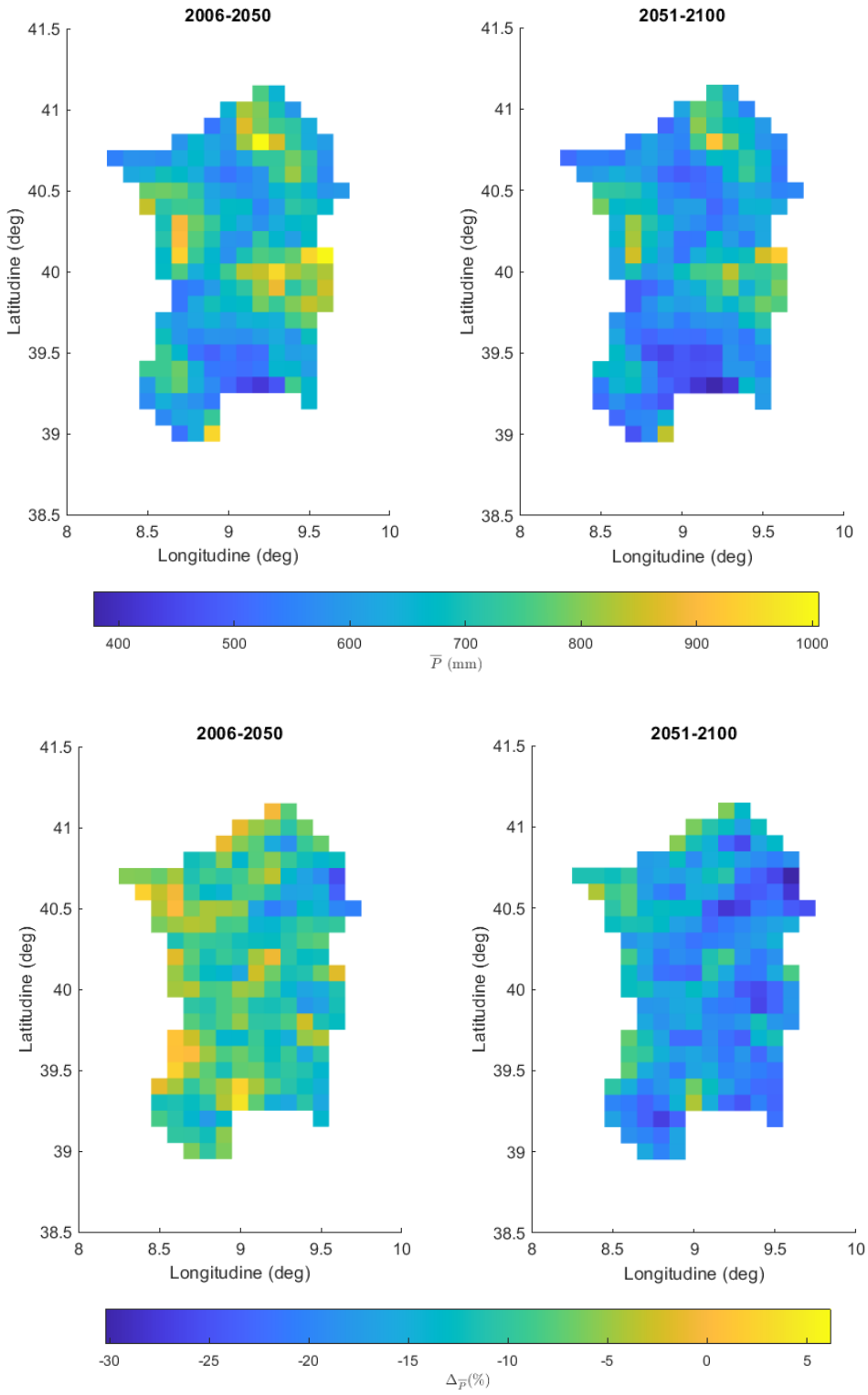

Figure 3.23. Gridded maps of bias corrected (BC) ensemble mean of mean (first row) and percentage difference from baseline values (second row) of annual rainfall (P) for Sardinia in 2006-2050 and in 2051-2100.

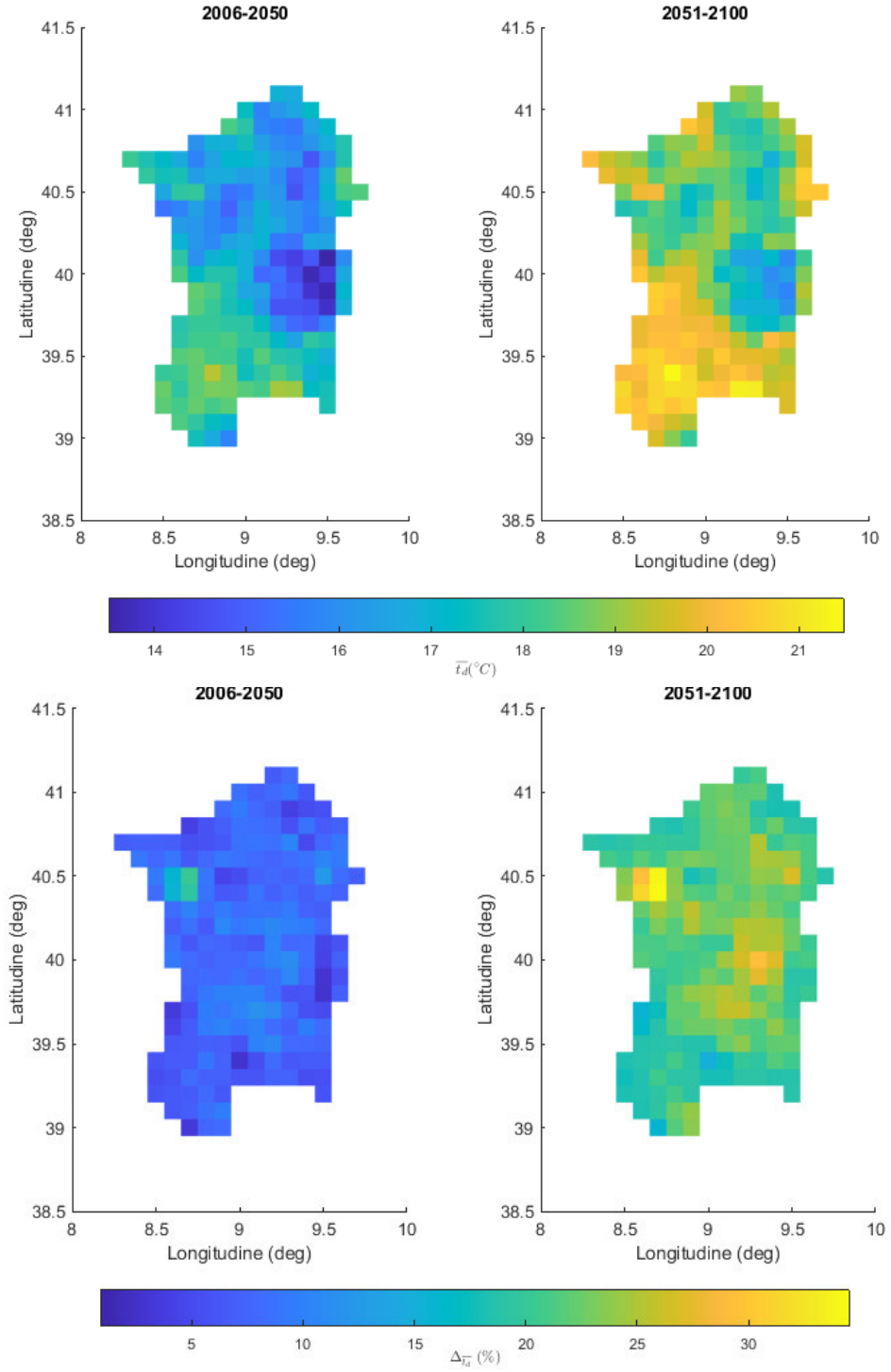

Figure 3.24. Gridded maps of bias corrected (BC) ensemble mean of mean (first row) and percentage difference from baseline values (second row) of daily temperature (t_d) for Sardinia in 2006-2050 and in 2051-2100.

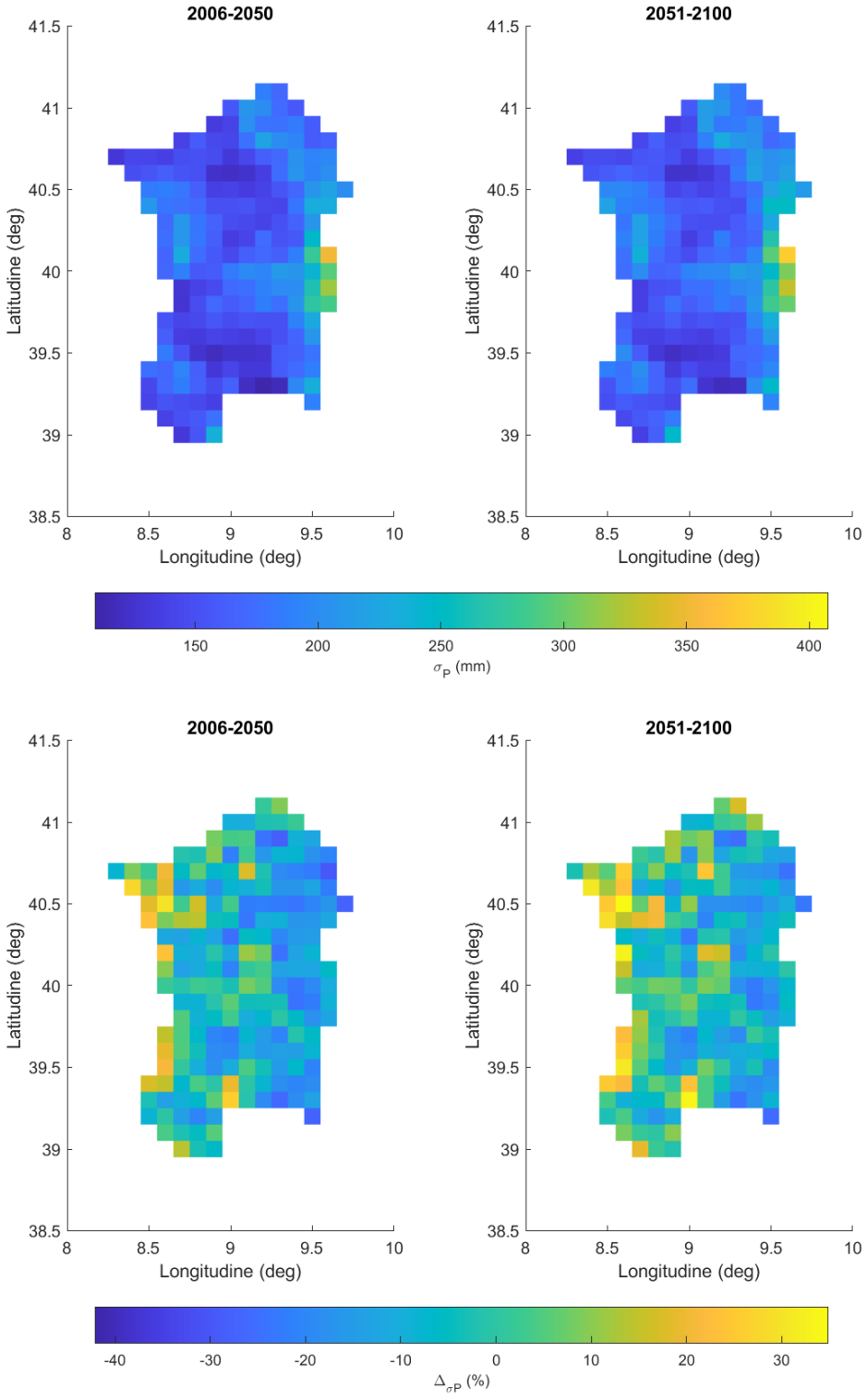

Figure 3.25. Gridded maps of bias corrected (BC) ensemble mean of standard deviation (first row) and percentage difference from baseline values (second row) of annual rainfall (P) for Sardinia in 2006-2050 and in 2051-2100.

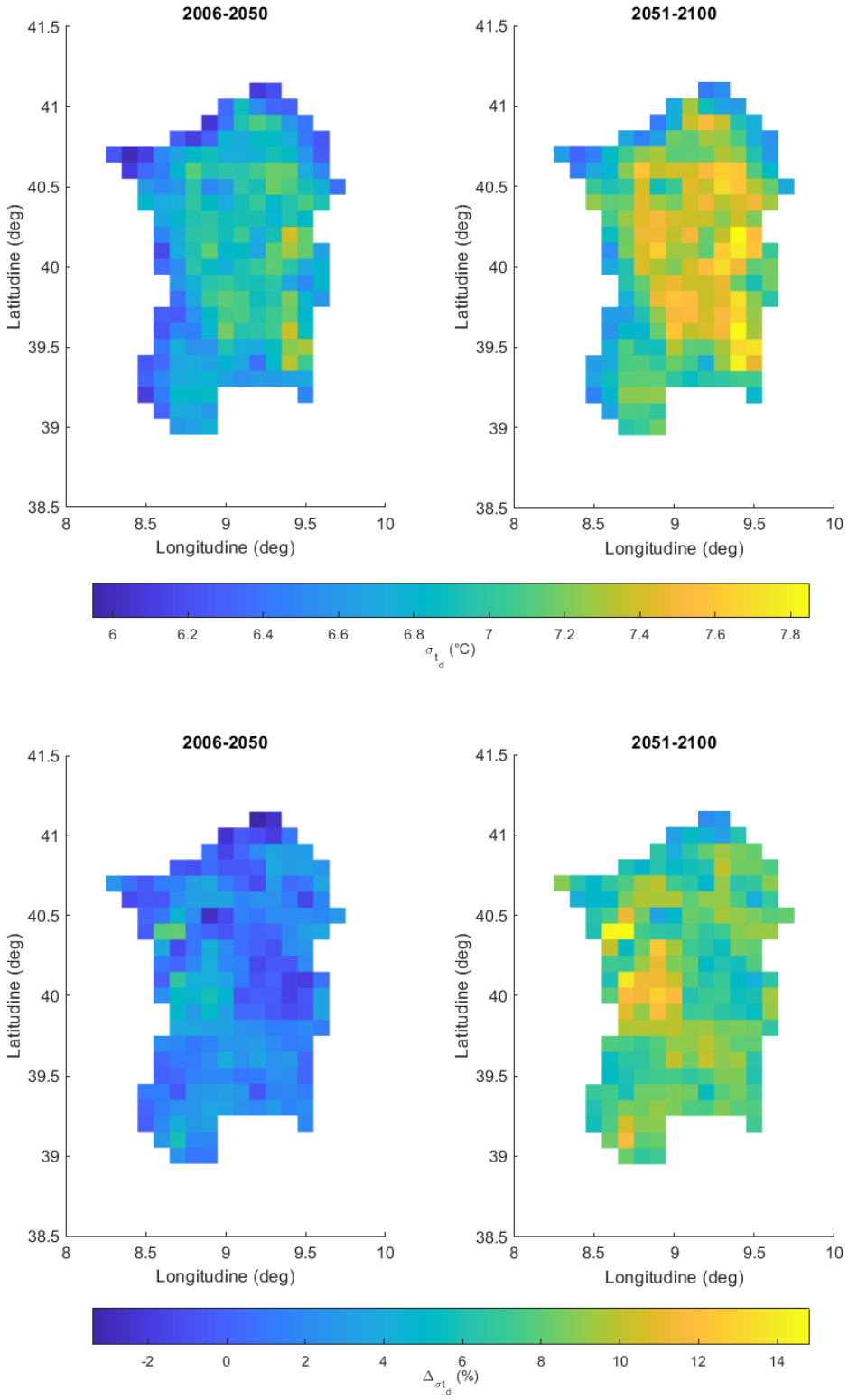

Figure 3.26. Gridded maps of bias corrected (BC) ensemble mean of standard deviation (first row) and percentage difference from baseline values (second row) of daily temperature (t_d) for Sardinia in 2006-2050 and in 2051-2100.

After BC of CM temperature outputs, the associated potential evapotranspiration timeseries have been evaluated by Thornthwaite (1948) (see Section 2.4.2). In Figures 3.27 and 3.28, the gridded map of ensemble mean of mean and standard deviation of PET ($\overline{PET}$ and σ_{PET}) have been reported. The trend of $\overline{PET}$ is coherent with the increase of mean temperature that becomes more relevant in 2051-2100 period and follows the temperature (altitude) spatial distribution (Figure 3.27 first row). The change $\overline{PET}$ and σ_{PET} compared to the baseline ones range from -5% to 5% in the 2006-2050, while it is more pronounced in 2051-2100 (Figure 3.28). σ_{PET} showed an important deviation from the baseline values (Figure 3.28 second row).

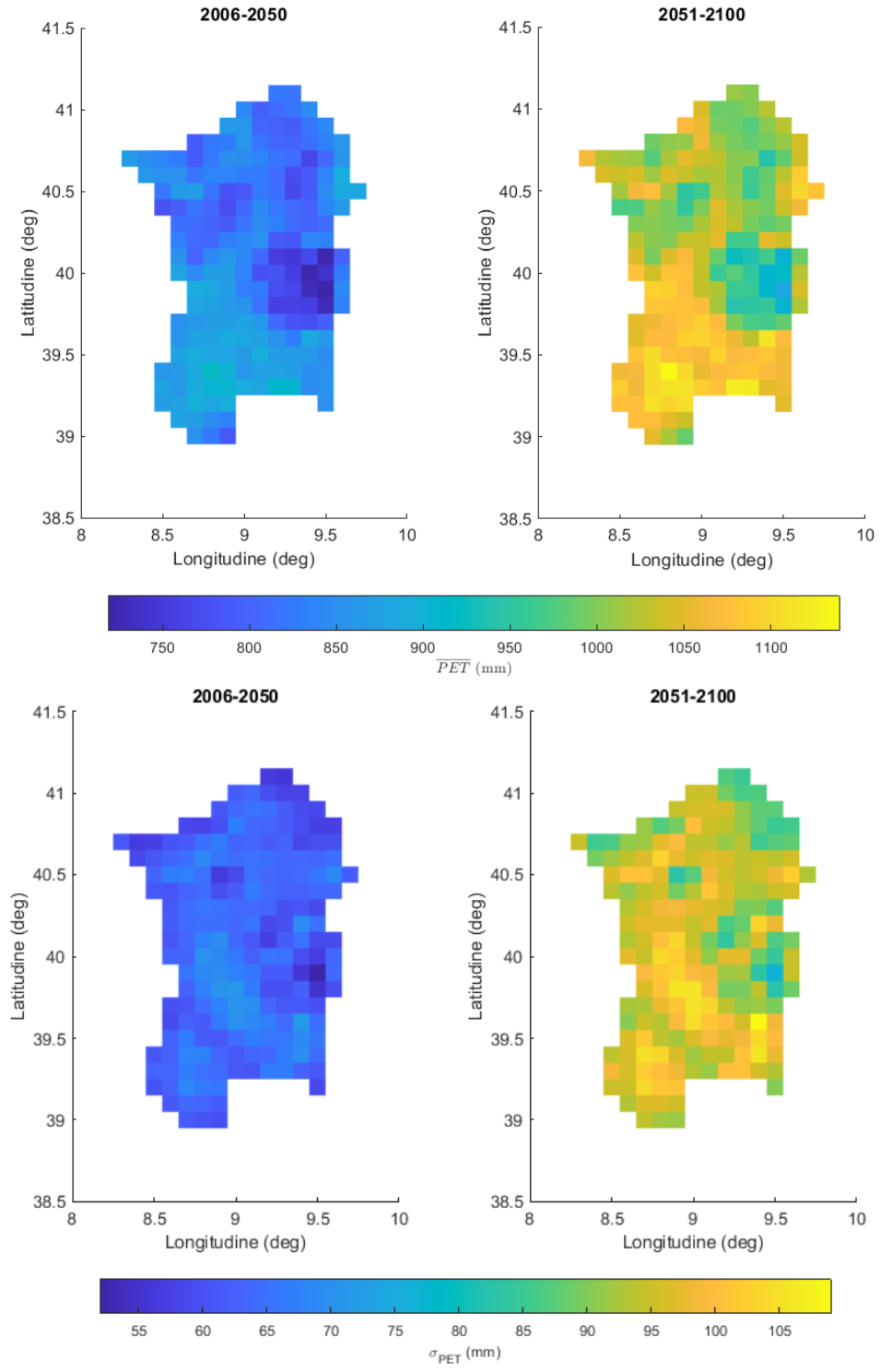

Figure 3.27. Gridded maps of bias corrected (BC) ensemble mean of mean (first row) and standard deviation (second row) of annual potential evapotranspiration (PET) in 2006-2050 and in 2051-2100.

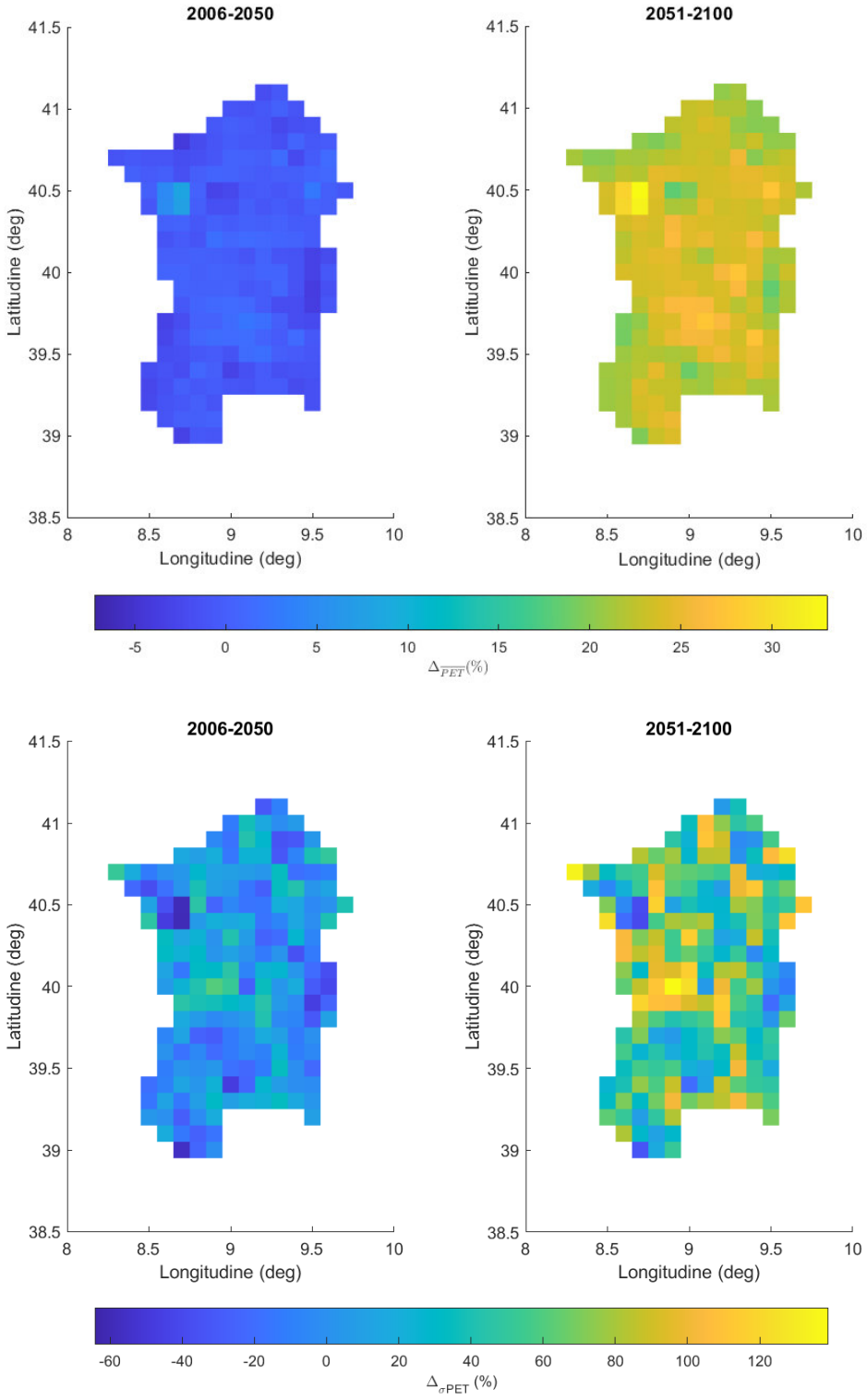

Figure 3.28. Gridded maps of bias corrected (BC) percentage difference between ensemble mean and baseline values of mean (first row) and standard deviation (second row) of annual potential evapotranspiration (PET) in 2006-2050 and in 2051-2100.

All these analyses have been conducted to characterize the future climate and to define climatic parameters of Caracciolo et al. (2017)'s framework. Then, for each CM, BC statistics (spatial-averaged mean and standard deviation σ) are reported in Table 3.4 which correspond to $\bar{P}$, $\overline{PET}$, σ_P and σ_{PET}, meaning four out of five of the parameters of Eq. 2.10 . In Table 3.5 the baseline values of spatial-averaged mean and standard deviation of P and PET are reported. These parameters have been calculated at regional scale (spatial-average) to provide a general estimate of hydrological behaviour and water availability in Sardinia.

As previously said, the future trend for P is decreasing as attested by the CM spatial-averaged $\bar{P}$, while conversely, the increase in the temperature determines higher values of spatial-averaged $\overline{PET}$. The variability of P is limited than the observed one, but with an increasing trend, as attested by σ_P, while for PET, σ_{PET} is comparable to the baseline value in 2006-2050 and then raises in the 2051-2100.

	2006-2050				2051-2100			
	$\bar{P}$	σ_P	$\overline{PET}$	σ_{PET}	$\bar{P}$	σ_P	$\overline{PET}$	σ_{PET}
	(mm)	(mm)	(mm)	(mm)	(mm)	(mm)	(mm)	(mm)
CM#1	634.91	161.14	844.99	55.19	598.96	158.21	1004.89	77.25
CM#2	680.65	116.78	851.45	50.40	662.92	123.58	1027.45	85.20
CM#3	645.16	153.47	839.60	53.53	581.52	146.12	1013.57	82.76
CM#4	648.77	184.45	836.65	61.18	592.48	178.74	1036.96	90.03
CM#5	646.81	137.02	856.38	53.91	607.19	153.46	1009.60	95.92
CM#6	627.85	150.80	836.86	58.38	617.90	156.60	1047.95	93.06
CM#7	617.47	192.43	853.12	59.57	509.07	195.33	1093.07	98.44
CM#8	639.28	187.48	842.91	69.92	537.59	211.34	1089.43	108.54
CM#9	685.16	158.01	849.88	62.07	615.65	177.84	1055.59	102.23
CM#10	671.75	170.89	845.29	65.68	594.22	163.94	1068.78	101.93
CM#11	608.59	164.13	837.21	73.18	556.36	181.46	1033.88	96.46
CM#12	606.80	189.24	836.63	64.94	596.34	217.17	1027.41	101.20
CM#13	630.78	167.00	838.65	80.37	583.49	180.22	1035.34	91.01
CM#14	613.04	146.94	845.76	61.85	578.93	153.09	1050.49	96.48
EM	639.79	162.84	843.96	62.16	588.04	171.22	1042.46	94.32

Table 3.4. For 2006-2050 and 2050-2100, spatial-averaged mean and standard deviation values of annual rainfall (P) and annual potential evapotranspiration (PET) calculated by the 14 RCP 8.5 scenario (RCPS) bias corrected (BC) climate modelling (CM) outputs from EUROCORDEX project. In the last row ensemble mean (EM) values of the previous statistics are reported.

Baseline	$\bar{P}$	(mm)	710.1529
	σ_P	(mm)	189.0843
	$\overline{PET}$	(mm)	850.063
	σ_{PET}	(mm)	65.42338

Table 3.5. For baseline period, spatial-averaged mean and standard deviation of annual rainfall (P) and annual potential evapotranspiration (Q) calculated by the observed rainfall and temperature datasets.

3.4.2. Land use scenarios

Ten future LU scenarios have been considered starting from the Sardinia LU map of 2018, that here has been defined as baseline LU scenario. As reported in the LU maps from Corine Land Cover's project, in the baseline LU scenario the predominant LU type is agriculture (46.36%), followed by sclerophyllous vegetation with a percentage of 27.55%. Due to the low population density, urban type is the least common in Sardinia (3.02%), while the grassland and low vegetation covers 3.71% of the island. Water bodies and other LU types are present for 1.9% altogether. The covering percentage for the baseline and for future LU scenarios are reported in Table 3.6. The future LU scenarios refer to different periods (2006-2051 and 2051-2100), likewise which characterize future climate.

Five future LU scenarios (Scenario 1-5) have been created, here called constant trend scenarios (CT-S), under the hypothesis that, the covering percentage of a land cover type varies in the future following a trend given by past LU evolution. The other covering percentages associated to the other LU types, except for water bodies and other LUs that are supposed to be equal to the baseline value, have been rescaled accordingly from the baseline LU scenario. The past Sardinia LU maps have been defined by the information of Corine Land Use dataset which contains six European LU maps starting from 1990 to 2018. All LU types showed a linear trend except for grassland and low vegetation which LU covering percentage has a decreasing power function evolution. For the five CT-S LU scenarios, all covering percentages associated are reported in Tables 3.6 and 3.7.

Scenarios from 6 to 9, fixed change scenarios, are defined arbitrarily

subtracting/adding covering percentage from a given LU type and adding/subtracting to another ones, trying to reproduce detected and common LU changes. In particular, Scenario 6 represents a massive abandonment of agriculture lands (-15% in 2050 and -30% in 2100, with reference to baseline) that will change in sclerophyllous vegetation and grassland and low density vegetation (+15% in 2050 and +30% in 2100, with reference to baseline). The opposite trend is represented in the Scenario 7, where spontaneous vegetation is replaced by agriculture (+2.5% in 2050 and +5.0% in 2100, with reference to baseline). In the Scenario 8, the forest is converted to agriculture (+5.0% in 2050 and +10.0% in 2100, with reference to baseline), while in the Scenario 9, the urban development is represented at the expense of sclerophyllous vegetation and grassland and low density vegetation (-2.5% in 2050 and -5.0% in 2100, with reference to baseline).

Finally, the LU Scenario 10 is a CVD scenario where the complex relation between climate (mean temperature) and vegetation (forest) have been simplified. Figure 3.29 reports the relation between observed and ensemble mean values of temperature in 2006-2050 and in 2051-2100, and altitude both associated to grid points. Despite R^2 has a low value due to the high climatic variability, for every temperature-altitude combination it is clear that exists a negative linear relation, meaning that also BC CM reproduce correctly the well-known and observed negative temperature gradient. In addition, the dashed lines represent the linear regressions between temperature and altitude, that they will be adopted to describe the relation between the climatic and morphological variables. However, as remarked in Section 3.4.1, RCPS CM dataset forecast an increasing in mean

temperature. This finding implies that under the same altitude in the future higher mean temperature will be recorded as shown in Figure 3.29.

The last evidence could influence the stress of vegetation due to climate. The survival of some plant species is strictly linked to the mean and the extremes of temperature. Forest vegetation is typical related to cold climates, while sclerophyllous vegetation suits to dry climates. Due to the temperature-altitude relation future shift-up (Figure 3.29), under the same altitude, some kind of vegetation could not have the ability to survive more since exposed to high climatic stress. Therefore, the main hypothesis was to define altitude-threshold (meaning temperature-threshold) that define the minimum altitude (temperature) for the survival of forest vegetation, which could be the most affected by future increase of temperature. In Figure .3.30, the cumulated number of cells associated to forest LU type is associated to the altitude, referring to the baseline LU scenario (2018). This relation has been assumed fixed in the future too. Therefore, an initial altitude-threshold has been defined for reference LU scenario, equal to 100 m and the associated baseline mean temperature has been obtained from Figure 3.29. From the RCPS 2006-2050 temperature-altitude relation, the altitude associated to the previous temperature has been calculated, which indicates the new altitude-threshold for forest vegetation survive. This last value has been reported in Figure 3.30, obtaining a different cumulated number of cells associated to forest LU type. The difference between the numbers of cells associated to RCPS 2006-2051 scenario and baseline altitude-threshold defines the reduction of covering percentage of forest due to the climate change. The second hypothesis was to suppose that the missing forest LU type is substituted by sclerophyllous

vegetation. This procedure has been replied to calculate the reduction of forest in 2051-2100, where the baseline altitude-threshold is evaluated from the one of RCPS 2006-2051.

Under these hypotheses, the forest will decrease by 7.68% in 2050 (covering percentage will be 9,78% in 2050) and by 8.51% (covering percentage will be 1.27% in 2100). On the other hand, sclerophyllous vegetation will take the place of the forest, following the idea that it can handle higher mean temperature.

Given these future LU scenarios, as described in Section 2.3, the corresponding ω have been obtained (Tables 3.6 and 3.7).

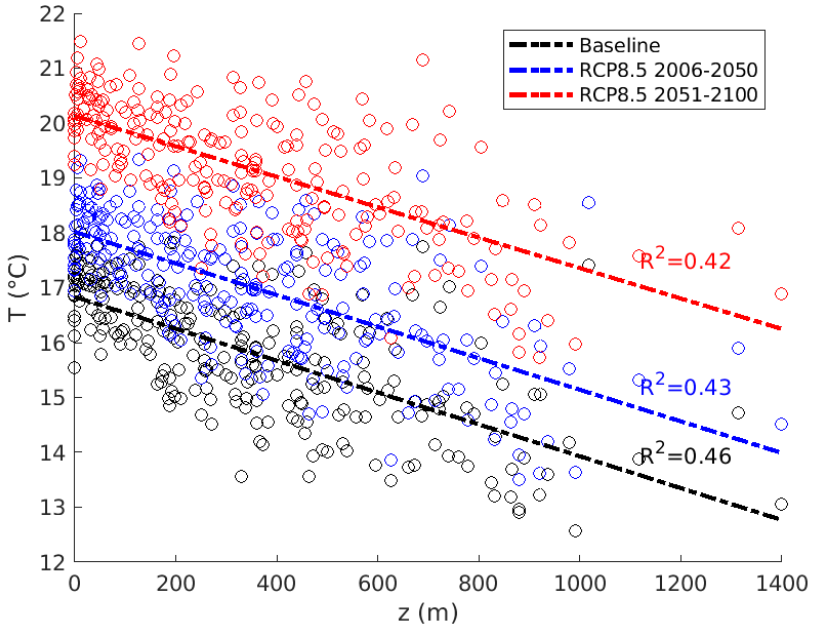

Figure 3.29. Scatter and regression analysis between altitude and mean temperature. Black, red and blue colour refer respectively to baseline, RCPS in 2006-2050 and RCPS in 2051-2100.

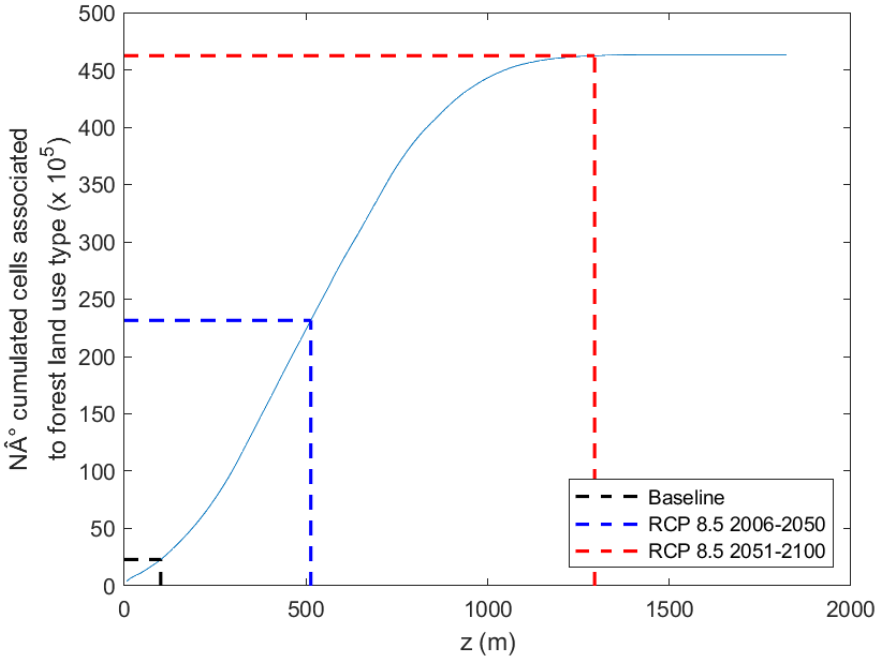

Figure 3.30. Cumulated number of grid cells associated to forest land use type (CORINE land use map 2018) for each altitude (solid light blue line). Dashed vertical blue and red lines highlight altitude that in 2006-2050 and 2051-2100 (RCPS 2006-2050 and RCPS 2051-2100) will indicate the minimum altitude at which forest land use type could survive due to climate change in Sardinia. The hypothesised reduction of coverage area of forest in 2006-2100 and 2051-2100 will be proportional to the difference between cumulated cells marked by horizontal dashed blue and red lines and the black one representing the baseline value.

Land use scenario/ Land use scenario type	Urban		Agriculture		Grassland and low density vegetation		Forest		Sclerophyllous vegetation		Water bodies		Other		ω	
1/CT-S	▲	3.96%	—	45.50%	—	3.76%	—	17.94%	—	26.94%	—	1.20%	—	0.70%	▼	2.32
2/CT-S	—	2.79%	▲	48.08%	—	3.65%	—	17.42%	▼	26.16%	—	1.20%	—	0.70%	▼	2.35
3/CT-S	—	2.99%	—	47.30%	▼	1.16%	▲	18.65%	—	28.00%	—	1.20%	—	0.70%	▲	2.37
4/CT-S	—	2.88%	—	45.51%	—	3.76%	▲	19.01%	▼	26.94%	—	1.20%	—	0.70%	▼	2.36
5/CT-S	—	2.79%	▼	44.14%	—	3.65%	—	17.40%	▲	30.12%	—	1.20%	—	0.70%	▲	2.38
6/FC-S	—	3.02%	▼	31.36%	▲	11.21%	—	17.46%	▲	35.05%	—	1.20%	—	0.70%	▲	2.39
7/FC-S	—	3.02%	▲	48.86%	▼	2.46%	—	17.46%	▼	26.30%	—	1.20%	—	0.70%	—	2.35
8/FC-S	—	3.02%	▲	53.86%	—	3.71%	▼	9.96%	—	27.55%	—	1.20%	—	0.70%	▼	2.32
9/FC-S	▲	5.52%	▼	45.11%	▼	2.46%	—	17.46%	—	27.55%	—	1.20%	—	0.70%	▼	2.28
10/CVD-S	—	3.02%	—	46.36%	—	3.71%	▼	9.78%	▲	35.23%	—	1.20%	—	0.70%	▲	2.36
Baseline	3.02%		46.36%		3.71%		17.46%		27.55%		1.20%		0.70%		2.35	

Table 3.6. For each land use (LU) scenario and 2006-2050, the Fu's parameter ω is reported (last column). Every row reports for each LU scenario the kind of conceptualization (Land use scenario/Land use scenario type) and the percentage of covering area of LU type (Urban, Agriculture, Grassland and low density vegetation, Forest, Sclerophyllous vegetation, Water bodies and Other).

Land use scenario/ Land use scenario type	Urban		Agriculture		Grassland and low density vegetation		Forest		Sclerophyllous vegetation		Water bodies		Other		ω	
1/CT-S	▲	5.26%	▼	44.87%	—	3.71%	—	17.69%	▼	26.56%	—	1.20%	—	0.70%	▼	2.32
2/CT-S	▼	2.64%	▲	50.81%	—	3.45%	—	16.47%	▼	24.73%	—	1.20%	—	0.70%	▼	2.35
3/CT-S	—	3.02%	▲	47.76%	▼	0.22%	▲	18.83%	—	28.27%	—	1.20%	—	0.70%	▲	2.37
4/CT-S	—	2.81%	▼	44.48%	—	3.68%	▲	20.80%	▼	26.33%	—	1.20%	—	0.70%	▼	2.36
5/CT-S	▲	2.65%	▼	41.95%	—	3.47%	—	16.54%	▲	33.50%	—	1.20%	—	0.70%	▲	2.38
6/FC-S	—	3.02%	▼	16.36%	▲	18.71%	—	17.46%	▲	42.55%	—	1.20%	—	0.70%	▲	2.39
7/FC-S	—	3.02%	▲	51.36%	▼	1.21%	—	17.46%	▼	25.05%	—	1.20%	—	0.70%	—	2.35
8/FC-S	—	3.02%	▲	61.36%	—	3.71%	▼	2.46%	—	27.55%	—	1.20%	—	0.70%	▼	2.32
9/FC-S	▲	8.02%	▼	43.86%	▼	1.21%	—	17.46%	—	27.55%	—	1.20%	—	0.70%	▼	2.28
10/CVD-S	—	3.02%	—	46.36%	—	3.71%	▼	1.27%	▲	43.74%	—	1.20%	—	0.70%	▲	2.36
Baseline	3.02%		46.36%		3.71%		17.46%		27.55%		1.20%		0.70%		2.35	

Table 3.7. For each land use (LU) scenario and 2051-2100, the Fu's parameter ω is reported (last column). Every row reports for each LU scenario the kind of conceptualization (Land use scenario/Land use scenario type) and the percentage of covering area of LU type (Urban, Agriculture, Grassland and low density vegetation, Forest, Sclerophyllous vegetation, Water bodies and Other).

3.5. Influence of the climate and land use on annual surface runoff distribution of Sardinia in the near future

Sections 3.1 and 3.2 showed that the normality assumption of annual potential evapotranspiration PET and rainfall P is a reasonable hypothesis, as highlighted by goodness-of-fit metrics and the non-parametric test results. These findings ensured the validity of the hypothesis of Caracciolo et al. (2017) approach (see Section 2.1).

In Section 3.3 the linkage between Fu's parameter and land use (LU) properties has been highlighted and regression equations have been developed (Section 3.3). The last ones provided the instrument to evaluate Fu's parameter in ten LU scenarios (Section 3.4.2).

14 bias corrected climatic scenarios have been determined in Section 3.4.1, each of which is represented by four parameters (mean and standard deviation of P and PET), evaluated at regional scale.

Therefore, given the climatic and LU scenarios, represented by the five parameters of the proposed method (Caracciolo et al., 2017), in this Section near future probability density function (*pdf*) of annual surface runoff Q for Sardinia will be reported. As stated in Section 2.1, Q is supposed to be a random variable that fits gaussian distribution following the expression of Caracciolo et al. (2017) (Eq. 2.10).

Despite several climatic and LU scenarios have been considered and hypothesized,

four different combination of future/baseline climate and LU scenarios have been considered to estimate possible future *pdf* of Q:

a) $EM_P\ BC + LU\ scenarios$: future BC ensemble mean of P and future LU scenarios affect *pdf* of baseline Q. PET is assumed to be equal to the baseline value;

b) $EM_{PET}\ BC + LU\ scenarios$: future BC ensemble mean of PET and future LU scenario affect *pdf* of baseline Q. P is assumed to be equal to the baseline value;

c) $P\ +\ PET\ \ BC$: The influence of each climate model is here considered. The effect of LU change is neglected and equal to the baseline one.

d) $EM_P\ BC + EM_{PET}\ BC + LU\ scenarios$: Climate (BC ensemble mean values) and LU scenarios are all considered.

In order to guide the reader, Table 3.8 resumes and clarify the values that the five parameters in Eq. 2.10 assumes for each combination.

Given the four combinations of climate and LU scenarios previously listed and the associated values of the five parameters requested in Eqs. 2.10 ($\bar{P}$, σ_P, $\overline{PET}$, σ_{PET} and ω, Tables 3.4-3.7), Figures 3.31 and 3.32 report the *pdf* of Q of Sardinia respectively for 2006-2050 and 2051-2100 periods. For each combination and both periods, the common effect in Q *pdf* is a left-shift, meaning that in future the water availability will be more limited than in the baseline period.

Combination	Name	P		PET		Land use scenario	N° pdf
		$\bar{P}$	σ_P	$\overline{PET}$	σ_{PET}	ω	
a	$EM_P\ BC + LU\ scenarios$	EM	EM	Baseline	Baseline	All (11)	11
b	$EM_{PET}\ BC + LU\ scenarios$	Baseline	Baseline	EM	EM	All (11)	11
c	$P\ +\ PET\ BC$	All from CMs (14)	All from CMs (14)	All from CMs (14)	All from CMs (14)	Baseline	14
d	$EM_P\ BC + EM_{PET}\ BC + LU\ scenarios$	EM	EM	EM	EM	All (11)	11

Table 3.8. Summary of the four combinations considered to represent near future possible pdf of annual surface runoff (Q). For each combination, values of parameters in Eq. 2.10 are reported. "EM" refers to the value of spatial-averaged ensemble mean mean/standard deviation from CMs, "Baseline" indicates the value assumed in the observation period. "All from CMs (x)/All (x)" indicate that for each couple of mean and standard deviation values from CMs (equal to x) and each Fu's parameter from land use (LU) scenario (equal to x), an assessment of the pdf of Q will be done. "N° pdf" refers to the set of pdfs that will be considered for each combination.

The reduction of Q for Sardinia is more critical moving from 2006-2050 to 2051-2100 period, according with climatic trends. This fact is related to the combined effect of the decrease of P and the raise of PET: the first reduces the meteo-climatic inputs in hydrological system and the second one diminishes subsurface runoff contribution in the water balance and then in the *pdf* of Q.

In all combinations, variability in Q is more reduced than in the baseline *pdf*. This is attributable to lower spatial-averaged standard deviation of P and PET, as highlighted by RCPS BC CM outputs (Tables 3.4 and 3.5).

Generally, the effect of LU change on the Q is smaller than climatic one. As attested

in $EM_P\ BC + LU\ scenarios$ (Figure 3.31.a and Figure 3.32.a) and $EM_{PET}\ BC + LU\ scenarios$ (Figure 3.31.b and Figure 3.32.b), Q *pdfs* are so close each other under a fixed climatic configuration and different LU scenario. In addition, these combinations highlight that Q will be more sensitive to P changes than to PET. This is related to the higher future variation of P compared to PET, meaning that P will be the main driver in changes in hydrological response.

Regarding $P\ +\ PET\ BC$ combination in which effect of LU change is neglected (ω is equal to baseline value), generally all climatic inputs from BC CM outputs cause a reduction of mean and variance of Q. There is disagreement between CMs as attested by different *pdfs* generated by Caracciolo et al. (2017)'s methods. These issues are related mostly to the disagreement between P, rather than PET, CM outputs as shown in Section 3.4.1.

In Figure 3.31.d and 3.32.d, climate and LU change are considered to affect the Q *pdf*. The *pdfs* show that Q on average in the near future will decrease (left-shift) with an increase in frequency around the average value with a consequent reduction in variance. This trend becomes stricter from the first period (2006-2050) (Figure 3.31.d) to the second one (2051-2100) (Figure 3.32.d).

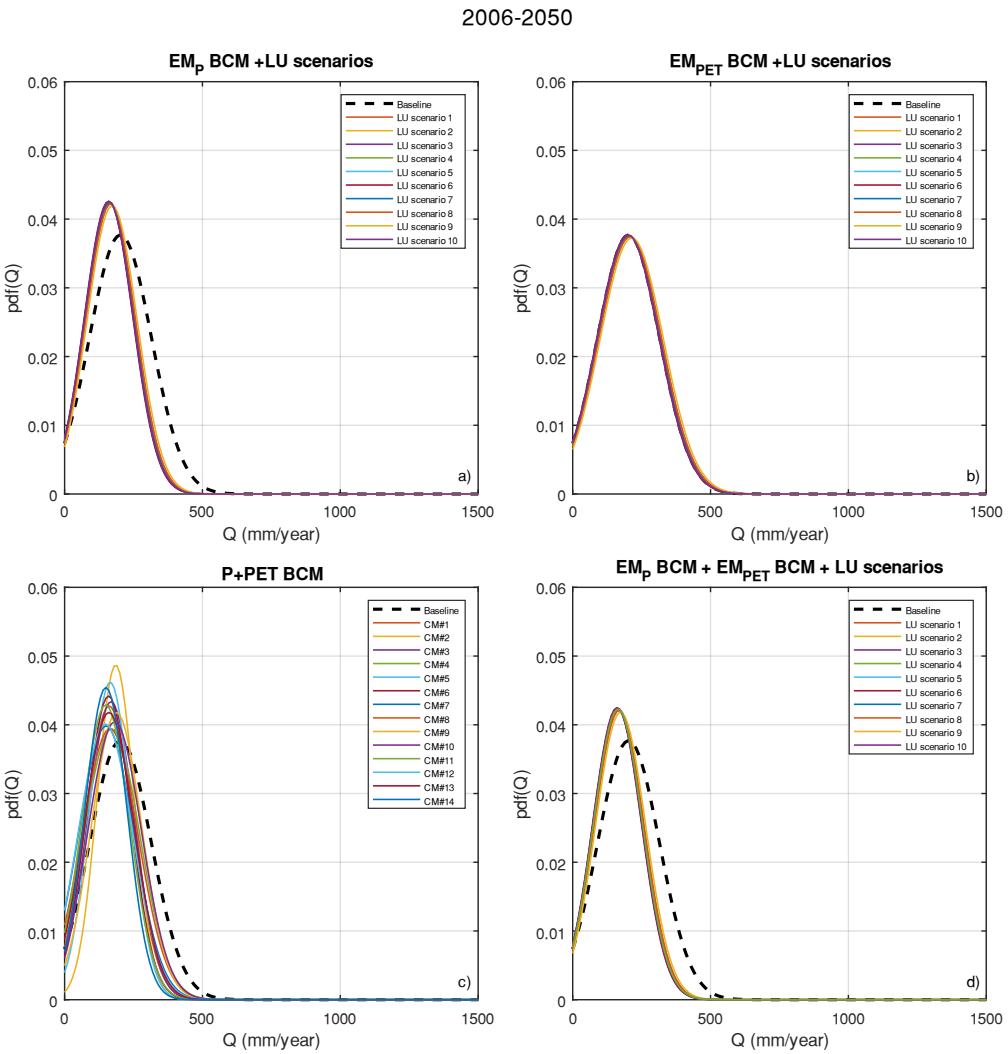

Figure 3.31. Regional distributions of annual surface runoff (Q) for Sardinia in 2006-2050, assessed by Caracciolo et al. (2017). The four plots refer to four combination of climate and land use change and have been created to highlight near future trends in Q of Sardinia. Detailed information about the four combination are available in Table 3.8.

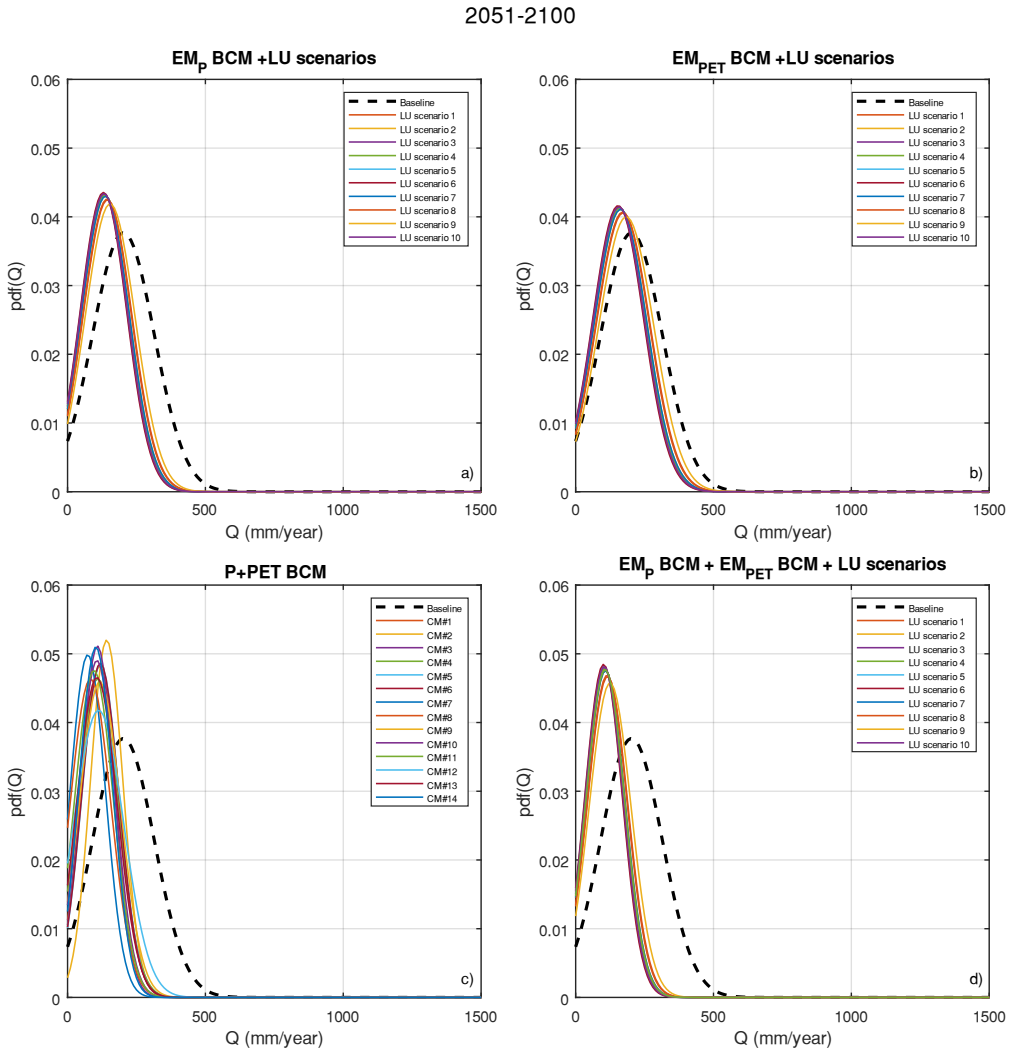

Figure 3.32. Regional distribution of annual surface runoff (Q) for Sardinia in 2051-2100, assessed by Caracciolo et al. (2017). The four plots refer to four combination of climate and land use change and have been created to highlight near future trends in Q of Sardinia. Detailed information about the four combination are available in Table 3.8.

4. Conclusion and future research

This thesis has been focused on the probability density function (*pdf*) of annual surface runoff Q in the island of Sardinia (Italy) under transient climate and land use (LU). Moving from Budyko and Fu's theory, Caracciolo et al. (2017)'s framework supposes a gaussian *pdf* in a closed-form for Q. Five parameters are requested to estimate the Q *pdf*, which are annual rainfall P and potential evapotranspiration PET central moments ($\bar{P}$,$\overline{PET}$,σ_P^2,σ_{PET}^2) and Fu's parameter ω. These parameters have been associated to several climatic and LU scenarios. Some propaedeutic analyses have been conducted. Indeed, the validity of P and PET's normality assumption has been argued, which represents a hypothesis of the proposed method for the assessment of Q *pdf*. The relationship between Fu's parameter ω and LU watershed properties has been discussed and regression equations for the calculation of ω have been developed.

Starting from ten possible LU configuration for Sardinia, this tool has been used to determine ω for ten near future LU scenarios. From bias corrected EUROCORDEX climate modelling (CM) outputs it was possible to define 14 climatic scenarios, which one associated to a set of four climatic parameters of the proposed methods.

Regarding gaussian assumption for P and PET have been discussed and tested moving from theoretical basis, namely Central Limit Theorem (CLT). Regarding P, this was done

by combining: 1) goodness-of-fit metrics to conclude on the approximate convergence of the empirical cumulative density function (*ecdf*) of P to a normal shape, and classify P samples into two complementary groups, 2) logistic regression analysis to identify the statistics of daily rainfall that are most descriptive of P convergence to a normal shape, and 3) a random-search algorithm to conclude on a set of constraints that maximizes the likelihood that the identification procedure produces accurate outcomes. The analysis was conducted using 3007 timeseries of daily rainfall rates obtained from the NOAA-NCDC GHCN database, with global coverage, which also allowed us to study how approximate Gaussianity of P is affected by large-scale climatic features, as those embedded in Köppen-Geiger climatic classification (Kottek et al., 2006). Continental climate (D) exhibits the highest fraction of Gaussian distributed P samples (i.e. 84.3%, AD test at α = 5% significance level), followed by warm temperate (C, 75.8%), equatorial (A, 72.5%), continental (E, 70.4%), and arid (B, 61.0%) climates. The analysis also showed that the Anderson-Darling (AD) statistical test is the most conservative one in determining approximate Gaussianity of P samples (followed by Cramer-Von Mises, CVM, and Kolmogorov-Smirnov, KS tests), and that the fraction of dry days f_{dd}, and skewness coefficient sk_{wd} of rainfall in wet days suffice to determine approximate convergence of P to the normal shape.

Under this setting, a powerful tool in determining the probability that P samples in data poor regions exhibit approximately Gaussian behaviour, based on the marginal statistics of daily rainfall, has been created. The methods is based on two fundamental curves that represent the linkage between f_{dd} and sk_{wd} threshold and

$Pr(A|T)$/$Pr(A^c|T^c)$, and significance level. The procedure can be outlined as follows: 1) the definition of the optimal thresholds of f_{dd} and sk_{wd}, as a function of the desired level of significance α of the Anderson-Darling (AD) test. 2) In the case when both f_{dd} and sk_{wd} sample estimates exceed the corresponding thresholds obtained from (1), one uses the $Pr(A|T)$-curve to calculate the probability that the sample is Gaussian distributed at the corresponding significance level α. 3) In the case when either f_{dd} or sk_{wd} (or both) sample estimates do not exceed the corresponding thresholds obtained from (1), then one uses the $Pr(A^c|T^c)$-curve to obtain the probability that the sample deviates significantly from the normal shape at the corresponding significance level α. For example, daily rainfall time series with fraction of dry days $f_{dd} > 0.9$ and daily skewness coefficient of positive rainrates $sk_{wd} > 5.92$ deviate significantly from the normal shape according to the Anderson-Darling statistical test at the 5% significance level.

Regarding PET, statistical properties have been argued and the discussion showed that PET suit more than P to normal distribution. Potential evapotranspiration, according to Thornthwaite (1948), depends on monthly temperature which in turns depends on daily temperature that is an unbounded variable and characterized by small variance in Mediterranean area. In accordance to CLT, mathematical operators of mean and sum strengthen and increase the speed of converge to normality shape. Given that, despite intermittency and high variance of daily rainfall, P converges to normal shape under properties of daily rainfall samples. Then, it is believed here that also PET could satisfy the normality assumption hypothesis because still daily temperature seems to suit more to convergence to normal shape than daily rainfall. To support this idea, Anderson Darling

test (α=0.05) has been performed for a set of 120 annual evapotranspiration timeseries, obtained from Sardinian Hydrological Survey thermometric network dataset. The analysis demonstrated that 102 out of 120 PET sample exhibit a gaussian distribution.

The discussion about the validity of normality assumption for P is more exhaustive than for PET. Therefore, not enough attention has been paid to the question of interdependence between PET and P. Then, future research will be oriented to dig deeply in the convergence of PET to normal shape and to test the hypothesis of interdependence of between PET and P.

After investigating in the validity of normality assumption of PET and P, the linkage between Fu's parameter and LU properties have been discussed by three in-silico experiments. Therefore, these experiments aimed to investigated deeply also the water partitioning processes and the influence of climate and LU in long-term hydrological variables, as well as Q.

Five seasonal patterns of rainfall and potential evapotranspiration (called climatic setups) have been used and 4 basin morphological and vegetation descriptors (ζ, k_{sub}, c_0 and K_c) have been selected to summarize climate and basin characteristics. First, given a climate and a basin, it was demonstrated that water partitioning is only related to the aridity index, that is a measure of local climatic conditions. This is a different point of view about the Budyko's theory: water partitioning rules for a given basin, in a given climatic setup, forced by different couples of stochastic $P(t)$ and $PET(t)$, are well described by a Fu's curve, as stated by the high values of coefficient of determination R^2.

Second, an experiment was made to assess the climate effect in determing ω;

hydrological behaviour of the same watershed was simulated within different climate scenario. As expected, water partition is heavily affected by climate: under Mediterranean climate the highest mean annual runoff Q is observed, while the oceanic climate is the driest among the considered climatic setups. This means that seasonal patterns and the phase between rainfall and potential evapotranspiration (temperature) play a non-negligible role in long term water partitioning.

Third, it was evaluated how the morphological and vegetation properties influence water partitioning. Then, given different climate and different watershed, the effect of morphological and vegetation descriptors in water partitioning processes was mathematically described. Five linear regressions between the four model parameters and ω have been calculated, one for each climatic setup, providing an optimal tool for assessment of Fu's parameter. The coltural coefficient K_c and the maximum soil water holding capacity ζ has been observed that are the most important in influencing long term hydrological processes.

Finally, the regressions equations performances have been validated for four basins in US and South America obtaining encouraging results. Obviously, the range within which regression equations have been tuned and the limited number of parameters are a limitation for the presented method, that introduce further approximation within Budyko's theory. Nevertheless, the regression equations enlarge the feasibility of Fu's equation, providing a roughly assessment of annual runoff in limited data conditions and with a low computational effort.

Given these propaedeutic results (normality assumption of PET and P, and Fu's

parameter estimation equations by LU properties), reliable near future climate and LU scenarios have been created for the study case, the island of Sardinia (Italy). Regarding climate scenarios, daily rainfall and temperature outputs of EUROCORDEX project have been considered to predict near future P and PET trends over Sardinia. 14 historical (HS) and RCP 8.5 (RCPS) scenarios CM outputs have been bias corrected at daily scale by different BC approaches (three for rainfall, linear scaling LS, power transformation PT and distribution mapping DT-Γ, and just one for temperature, distribution mapping DT-Gauss). For rainfall, DT is the best method for correcting HS outputs at daily scale within the BC approaches adopted. PT method achieved good results as well. Nevertheless, given the approaches here adopted, BC did not perform well for right tails. In addition, for rainfall, moving from daily to annual scale, BC achieved worst performances since BC approaches here adopted operate at daily scale. BC of CM temperature outputs showed better results than rainfall, except for extreme temperatures.

Future research should be oriented to remove systematic errors of climate models even in extremes quantiles and possibly at different time scale. Here, due to research purposes, BC results could be considered satisfactory because BC approaches reproduced observed mean and standard deviation accurately. In the correction phase, as attested by BC RCPS outputs, for the future (2006-2100) a reduction of P and an increase of PET will be expected over Sardinian territory in reference to baseline. The gridded map of ensemble mean of $\bar{P}$ highlighted the good performances of BC methods to reproduce orographic effect. This finding was observed also for BC CM temperature.

Regarding land use, ten LU scenarios have been proposed which have been

hypothesised following three approaches here called constant trend scenarios (CT-S), fixed change scenarios (FC-S), climate-vegetation-driven scenarios (CVD-S). For each LU scenario, a value of Fu's parameter has been calculated by stepwise regression equations of Section 3.3.3.

Spatial-averaged future climate (mean and standard deviation of P and PET) and LU scenarios (Fu's parameter ω) parameters have been evaluated referring to two periods (2006-2050 and 2051-2100).

From the ten near future LU scenarios and the climatic scenarios, four different combinations of climate and LU forcings have been created and for each one, a set of *pdfs* of Q for Sardinia have been defined. The first combination which represents the effect of future ensemble mean of P and LU scenarios on *pdf* (PET is supposed to be equal to baseline values), showed a reduction of Q as attested by the left-shift of the associated *pdf* compared to the reference one. The deviations from the baseline *pdf* are mostly related to the variation of the P statistical moments ($\overline{P}$ and σ_P). The second combination which represents the effect of near future ensemble mean of PET and LU scenarios (rainfall is supposed to be equal to baseline values), highlighted that in 2006-2050 there are no significant deviation from the baseline *pdf*. $\overline{PET}$ and σ_{PET} are close to the baseline values. This evidence highlighted that LU change affects the Q *pdf* with a smaller magnitude than P. The climate seems to be the main driver in the change of Q *pdf*, according to the related *pdf* by Caracciolo et al. (2017)'s method. In 2051-2100 due to the increase of $\overline{PET}$, the *pdf* of Q shifts to left, meaning a reduction of mean value.

The third combination embodies all 14 CM outputs considering both P and PET (Fu's

parameter is supposed to be equal to baseline value). The combinate effect of near future P and PET determines the left-shift of *pdfs* as well.

The last combination represents the combinate effect of climate and LU change. For climate, both future P and PET ensemble mean parameters and for LU, all Fu's parameter values are considered. The result is the left-shift of the *pdfs* of Q as well.

The results of Chapter 3 highlighted that the near future water resources are going to decrease due to the expected reduction of annual rainfall and the increase of mean temperature. Mean annual surface runoff will decrease as the variability of Q will do, as highlighted by the reduction of extreme quantiles. The effect of LU change is significative and depends on LU scenarios, but in terms of the modification of the shape of Q *pdfs* is not comparable to climate influence (annual rainfall and potential evapotranspiration), that affects more deeply water resources distribution.

In relation to what has been shown in the last and conclusive Chapter, the reduction of mean annual surface runoff could lead to criticisms in the management of water resources in Sardinia. Water resources scarcity will result in a more difficult management of the regional water supply system, that could lead to more frequent crises and stress in the regional agricultural and socio-economic system.

The proposed methodology has been applied at regional scale providing a general indication of the near future water availability in Sardinia. Although the obtained results could be considered satisfactory and interesting, future research will be oriented to adapt this approach at basin scale. In particular, the proposed framework might suit to large watersheds of Sardinia, which are of absolute interest because they provide the largest

part of water resources in the island. Obviously, thorough downscaling and bias correction techniques should be used to adapt climate forcings from CM outputs at basin scale. Therefore, in these lines, a deeper investigation in the ongoing Sardinia LU change processes are requested, that should account for the regional land use guidelines, environmental and urban plans. More accurate near future assessment of water resources in this way will be available to water management agencies of Sardinia.

Appendix

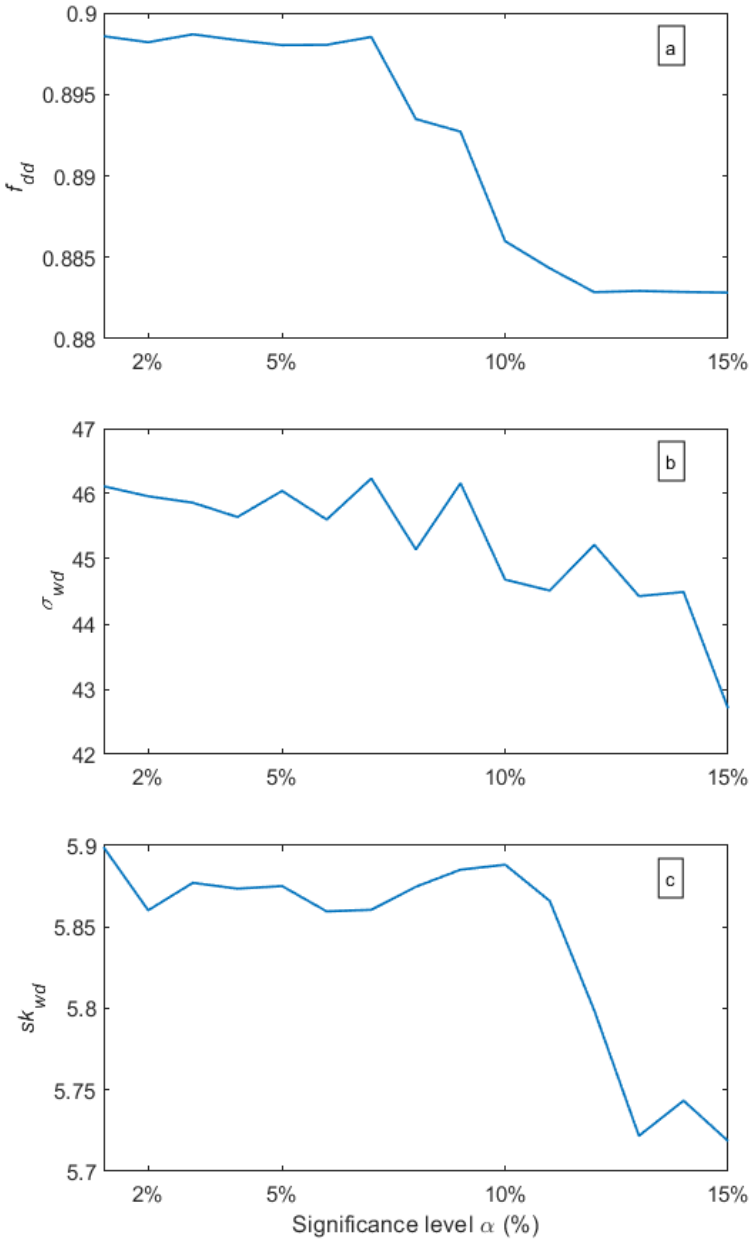

Figure A. 1. Dependence of the optimal thresholds of the fraction of dry days f_{dd} (a), and the standard deviation σ_{wd} (b) and skewness coefficient sk_{wd} (c) of rainfall in wet days, on the level of significance α of the Anderson-Darling (AD) test, for the 3007 NOAA-NCDC daily rainfall timeseries analysed.

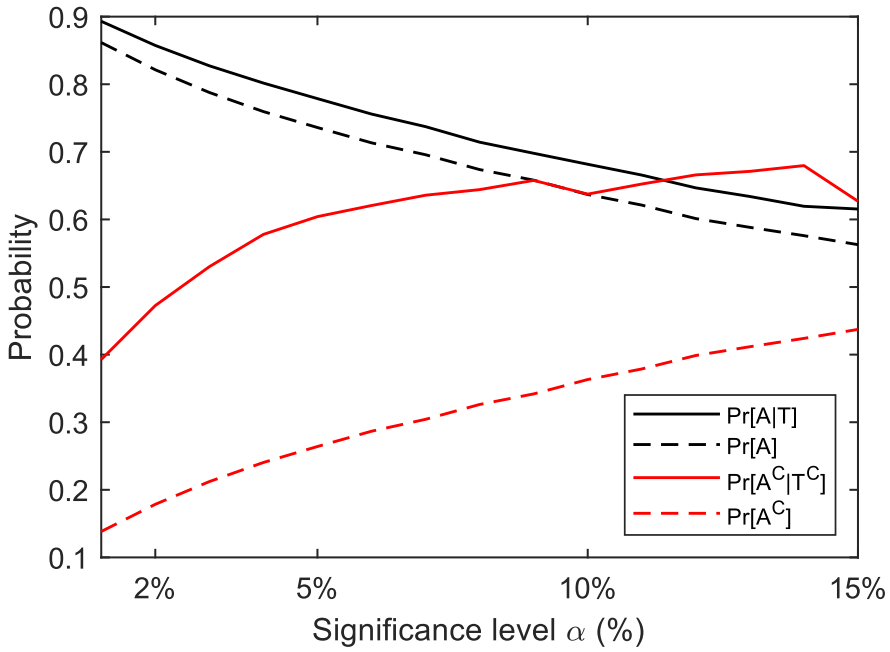

Figure A. 2. Comparison of the conditional probabilities $Pr(A|T)$ *and* $Pr(A^c|T^c)$*, with the marginal probabilities* $Pr(A)$ *and* $Pr(A^c)$ *= 1-*$Pr(A)$*, as a function of the level of significance α used for the Anderson-Darling (AD) test, for the case when three influential predictor variables (i.e. Set II:* f_{dd}*,* σ_{wd}*,* sk_{wd}*) are used to constraint classification to G and NG groups; see main text for details.*

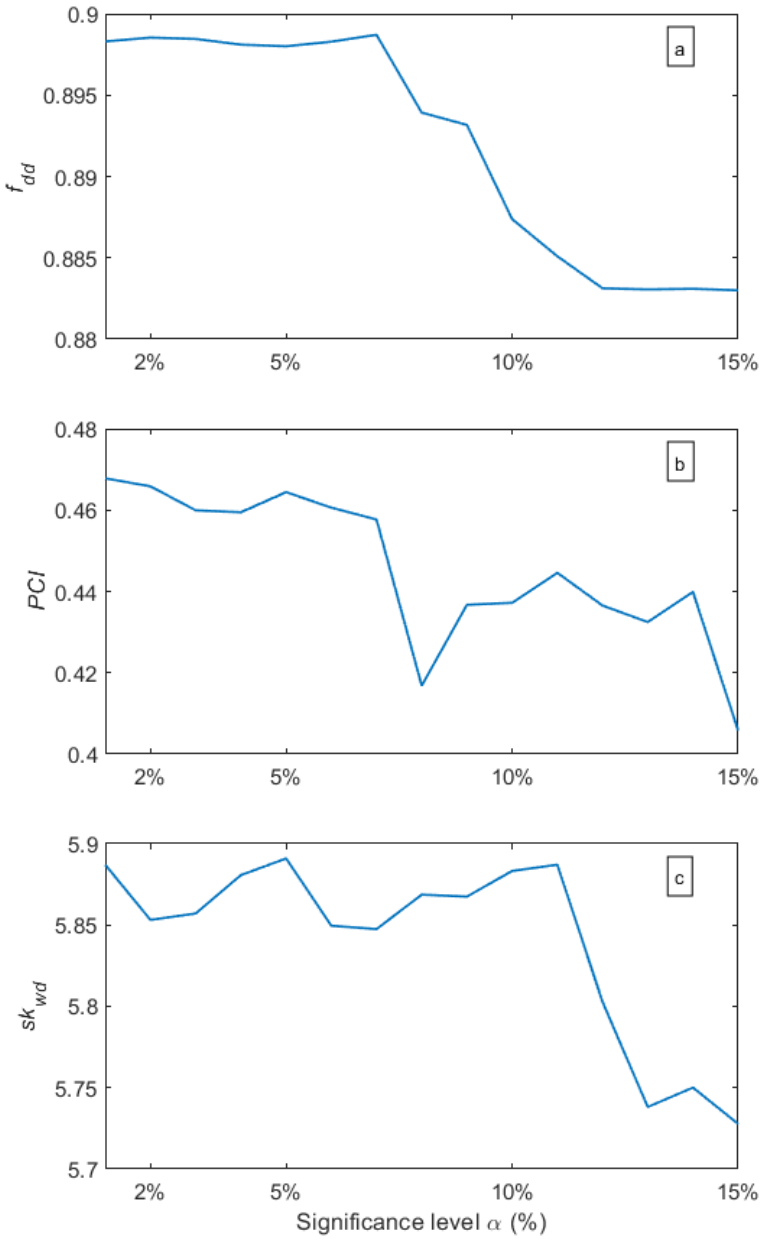

Figure A. 3. Dependence of the optimal thresholds of the fraction of dry days f_{dd} (a), precipitation concentration index PCI (b), and skewness coefficient sk_{wd} of rainfall in wet days (c), on the level of significance α of the Anderson-Darling (AD) test, for the 3007 NOAA-NCDC daily rainfall timeseries analyzed.

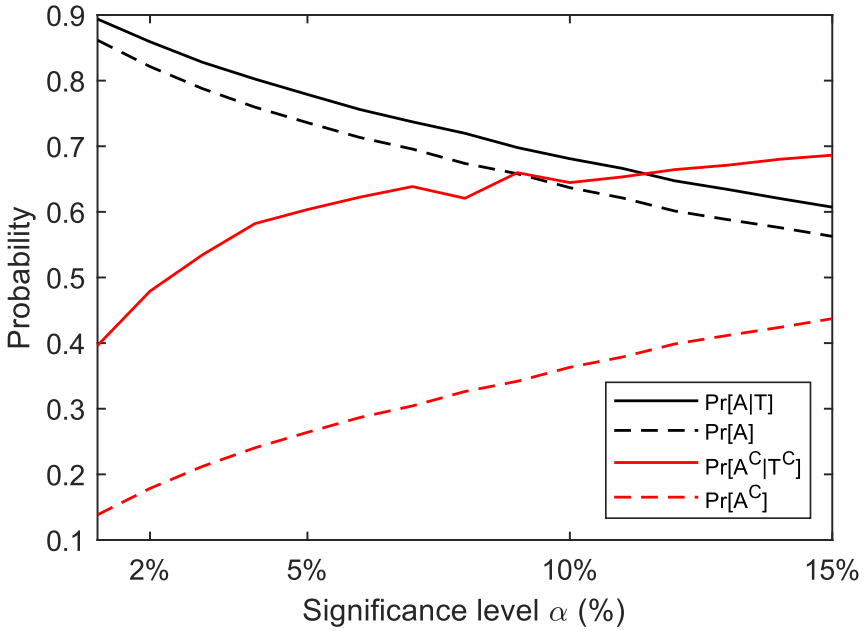

Figure A. 4. Comparison of the conditional probabilities $Pr(A|T)$ *and* $Pr(A^c|T^c)$*, with the marginal probabilities* $Pr(A)$ *and* $Pr(A^c)$ *= 1-*$Pr(A)$*, as a function of the level of significance α used for the Anderson-Darling (AD) test, for the case when three influential predictor variables (i.e. Set III:* f_{dd}*, PCI,* sk_{wd}*) are used to constraint classification to G and NG groups; see main text for details.*

References

Abatzoglou, J.T., Ficklin, D.L., 2017. Climatic and physiographic controls of spatial variability in surface water balance over the contiguous United States using the Budyko relationship. Water Resources Research, 53(9): 7630-7643. DOI:10.1002/2017wr020843

Abdullah, M.A., Al-Mazroui, M.A., 1998. Climatological study of the southwestern region of Saudi Arabia. I. Rainfall analysis. Climate Research, 9(3): 213-223.

Abera, W., Tamene, L., Abegaz, A., Solomon, D., 2019. Understanding climate and land surface changes impact on water resources using Budyko framework and remote sensing data in Ethiopia. Journal of Arid Environments, 167: 56-64. DOI:https://doi.org/10.1016/j.jaridenv.2019.04.017

Alexander, L.V. et al., 2006. Global observed changes in daily climate extremes of temperature and precipitation. Journal of Geophysical Research Atmospheres, 111(5). DOI:10.1029/2005JD006290

Anderson, T.W., Darling, D.A., 1952. Asymptotic theory of certain" goodness of fit" criteria based on stochastic processes. The annals of mathematical statistics, 23(2): 193-212.

Augustin, N.H., Beevers, L., Sloan, W.T., 2008. Predicting river flows for future climates using an autoregressive multinomial logit model. Water Resources Research, 44(7). DOI:10.1029/2006wr005127

Beck, H.E. et al., 2013. Global patterns in base flow index and recession based on streamflow observations from 3394 catchments. Water Resources Research, 49(12):

7843-7863. DOI:10.1002/2013wr013918

Ben-Gai, T., Bitan, A., Manes, A., Alpert, P., Rubin, S., 1998. Spatial and temporal changes in rainfall frequency distribution patterns in Israel. Theoretical and Applied Climatology, 61(3-4): 177-190. DOI:10.1007/s007040050062

Benjamin, J.R., Cornell, C.A., 1970. Probability, Statistics, and Decision for Civil Engineers. McGraw-Hill.

Berkson, J., 1944. Application of the logistic function to bio-assay. Journal of the American Statistical Association, 39(227): 357-365.

Beven, K., 1989. Changing ideas in hydrology — The case of physically-based models. Journal of Hydrology, 105(1): 157-172. DOI:https://doi.org/10.1016/0022-1694(89)90101-7

Bliss, C.I., 1934. The method of probits. Science.

Boé, J., Terray, L., Habets, F., Martin, E., 2007. Statistical and dynamical downscaling of the Seine basin climate for hydro-meteorological studies. International Journal of Climatology, 27(12): 1643-1655. DOI:10.1002/joc.1602

Bonan, G.B., 2008. Forests and climate change: Forcings, feedbacks, and the climate benefits of forests. Science, 320(5882): 1444-1449. DOI:10.1126/science.1155121

Boyer, C., Chaumont, D., Chartier, I., Roy, A.G., 2010. Impact of climate change on the hydrology of St. Lawrence tributaries. Journal of Hydrology, 384(1-2): 65-83. DOI:10.1016/j.jhydrol.2010.01.011

Breuer, L. et al., 2009. Assessing the impact of land use change on hydrology by ensemble modeling (LUCHEM). I: Model intercomparison with current land use.

Advances in Water Resources, 32(2): 129-146. DOI:https://doi.org/10.1016/j.advwatres.2008.10.003

Brohan, P., Kennedy, J.J., Harris, I., Tett, S.F.B., Jones, P.D., 2006. Uncertainty estimates in regional and global observed temperature changes: A new data set from 1850. Journal of Geophysical Research Atmospheres, 111(12). DOI:10.1029/2005JD006548

Brown, A.E., Western, A.W., McMahon, T.A., Zhang, L., 2013. Impact of forest cover changes on annual streamflow and flow duration curves. Journal of Hydrology, 483: 39-50. DOI:https://doi.org/10.1016/j.jhydrol.2012.12.031

Budyko, M., 1974. Climate and Life, 508 pp. Academic Press, New York.

Cannarozzo, M., Noto, L.V., Viola, F., 2006. Spatial distribution of rainfall trends in Sicily (1921–2000). Physics and Chemistry of the Earth, Parts A/B/C, 31(18): 1201-1211. DOI:https://doi.org/10.1016/j.pce.2006.03.022

Caracciolo, D., Deidda, R., Viola, F., 2017. Analytical estimation of annual runoff distribution in ungauged seasonally dry basins based on a first order Taylor expansion of the Fu's equation. Advances in Water Resources, 109: 320-332. DOI:https://doi.org/10.1016/j.advwatres.2017.09.019

Chatterjee, S., Price, B., 1991. Regression diagnostics. New York.

Choudhury, B., 1999. Evaluation of an empirical equation for annual evaporation using field observations and results from a biophysical model. Journal of Hydrology, 216(1-2): 99-110.

Christensen, J.H., Carter, T.R., Rummukainen, M., Amanatidis, G., 2007. Evaluating the performance and utility of regional climate models: The PRUDENCE project.

Climatic Change, 81(SUPPL. 1): 1-6. DOI:10.1007/s10584-006-9211-6

Christensen, N.S., Wood, A.W., Voisin, N., Lettenmaier, D.P., Palmer, R.N., 2004. The effects of climate change on the hydrology and water resources of the Colorado River basin. Climatic Change, 62(1-3): 337-363. DOI:10.1023/B:CLIM.0000013684.13621.1f

Cihlar, J., 2000. Land cover mapping of large areas from satellites: Status and research priorities. International Journal of Remote Sensing, 21(6-7): 1093-1114. DOI:10.1080/014311600210092

Costa, M.H., Botta, A., Cardille, J.A., 2003. Effects of large-scale changes in land cover on the discharge of the Tocantins River, Southeastern Amazonia. Journal of Hydrology, 283(1-4): 206-217. DOI:10.1016/s0022-1694(03)00267-1

Cox, P.M., Betts, R.A., Jones, C.D., Spall, S.A., Totterdell, I.J., 2000. Acceleration of global warming due to carbon-cycle feedbacks in a coupled climate model. Nature, 408(6809): 184-187. DOI:10.1038/35041539

Cramér, H., 1928. On the composition of elementary errors. Scandinavian Actuarial Journal, 1928(1): 13-74. DOI:10.1080/03461238.1928.10416862

Cuo, L., Zhang, Y., Gao, Y., Hao, Z., Cairang, L., 2013. The impacts of climate change and land cover/use transition on the hydrology in the upper Yellow River Basin, China. Journal of Hydrology, 502: 37-52. DOI:10.1016/j.jhydrol.2013.08.003

Dahamsheh, A., Aksoy, H., 2007. Structural characteristics of annual precipitation data in Jordan. Theoretical and Applied Climatology, 88(3-4): 201-212. DOI:10.1007/s00704-006-0247-3

De Lima, M.I.P., Carvalho, S.C.P., P. De Lima, J.L.M., 2010. Investigating annual and

monthly trends in precipitation structure: An overview across Portugal. Natural Hazards and Earth System Science, 10(11): 2429-2440. DOI:10.5194/nhess-10-2429-2010

De Luis, M., González-Hidalgo, J.C., Raventós, J., Sánchez, J.R., Cortina, J., 1997. Distribucion espacial de la concentracion y agresividad de la lluvia en el territorio de la Comunidad Valenciana. Cuaternario y Geomorfologia, 11(3-4): 33-44.

DeFries, R.S., Hansen, M., Townshend, J.R.G., Sohlberg, R., 1998. Global land cover classifications at 8 km spatial resolution: The use of training data derived from Landsat imagery in decision tree classifiers. International Journal of Remote Sensing, 19(16): 3141-3168. DOI:10.1080/014311698214235

Deidda, R. et al., 2013. Regional climate models' performance in representing precipitation and temperature over selected Mediterranean areas. Hydrology and Earth System Sciences, 17(12): 5041-5059. DOI:10.5194/hess-17-5041-2013

Deidda, R., Puliga, M., 2006. Sensitivity of goodness-of-fit statistics to rainfall data rounding off. Physics and Chemistry of the Earth, 31(18): 1240-1251. DOI:10.1016/j.pce.2006.04.041

Deng, W. et al., 2018. Analyzing the impacts of climate variability and land surface changes on the annual water-energy balance in the Weihe River Basin of China. Water (Switzerland), 10(12). DOI:10.3390/w10121792

Deng, Z., Cao, J., Hu, Y., 2020. Spatial and temporal evolution of landscape pattern in downtown area of Jixi City, China. European Journal of Remote Sensing, 53(sup1): 104-113. DOI:10.1080/22797254.2020.1713024

Dewan, A.M., Yamaguchi, Y., 2009. Land use and land cover change in Greater Dhaka,

Bangladesh: Using remote sensing to promote sustainable urbanization. Applied Geography, 29(3): 390-401. DOI:10.1016/j.apgeog.2008.12.005

Donohue, R.J., Roderick, M.L., McVicar, T.R., 2007a. On the importance of including vegetation dynamics in Budyko's hydrological model. Hydrol. Earth Syst. Sci., 11(2): 983-995. DOI:10.5194/hess-11-983-2007

Donohue, R.J., Roderick, M.L., McVicar, T.R., 2007b. On the importance of including vegetation dynamics in Budyko's hydrological model. Hydrology and Earth System Sciences, 11(2): 983-995. DOI:10.5194/hess-11-983-2007

Donohue, R.J., Roderick, M.L., McVicar, T.R., 2011. Assessing the differences in sensitivities of runoff to changes in climatic conditions across a large basin. Journal of Hydrology, 406(3-4): 234-244. DOI:10.1016/j.jhydrol.2011.07.003

Duan, Q. et al., 2006. Model Parameter Estimation Experiment (MOPEX): An overview of science strategy and major results from the second and third workshops. Journal of Hydrology, 320(1): 3-17. DOI:https://doi.org/10.1016/j.jhydrol.2005.07.031

Easterling, D.R. et al., 1997. Maximum and minimum temperature trends for the globe. Science, 277(5324): 364-367. DOI:10.1126/science.277.5324.364

Elsner, M.M. et al., 2010. Implications of 21st century climate change for the hydrology of Washington State. Climatic Change, 102(1-2): 225-260. DOI:10.1007/s10584-010-9855-0

Fan, Y. et al., 2013. An assembled extreme value statistical model of karst spring discharge. Journal of Hydrology, 504: 57-68. DOI:10.1016/j.jhydrol.2013.09.023

Farrell, P.J., Rogers-Stewart, K., 2006. Comprehensive study of tests for normality and

symmetry: extending the Spiegelhalter test. Journal of Statistical Computation and Simulation, 76(9): 803-816. DOI:10.1080/10629360500109023

Feller, W., 1968. An Introduction to Probability Theory and Its Applications: Volume I. Wiley India Pvt. Limited.

Feng, X., Porporato, A., Rodriguez-Iturbe, I., 2015. Stochastic soil water balance under seasonal climates. Proceedings of the Royal Society A: Mathematical, Physical and Engineering Sciences, 471(2174). DOI:10.1098/rspa.2014.0623

Fisher, R.A., 1925. Statistical methods for research workers Oliver and Boyd. Edinburgh, Scotland, 6.

Fisz, M., 1963. Probability theory and mathematical statistics. Polish Scientifique.

Foufoula-Georgiou, E., Lettenmaier, D.P., 1986. Continuous-Time Versus Discrete-Time Point Process Models for Rainfall Occurrence Series. Water Resources Research, 22(4): 531-542. DOI:10.1029/WR022i004p00531

Fowler, H.J., Blenkinsop, S., Tebaldi, C., 2007. Linking climate change modelling to impacts studies: Recent advances in downscaling techniques for hydrological modelling. International Journal of Climatology, 27(12): 1547-1578. DOI:10.1002/joc.1556

Frich, P. et al., 2002. Observed coherent changes in climatic extremes during the second half of the twentieth century. Climate Research, 19(3): 193-212. DOI:10.3354/cr019193

Fu, B., 1981. On the calculation of the evaporation from land surface. Sci. Atmos. Sin, 5(1): 23-31.

Gao, Z. et al., 2016. Long-term streamflow trends in the middle reaches of the Yellow

River Basin: Detecting drivers of change. Hydrological Processes, 30(9): 1315-1329. DOI:10.1002/hyp.10704

Giorgi, F., 1990. Simulation of Regional Climate Using a Limited Area Model Nested in a General Circulation Model. Journal of Climate, 3(9): 941-963. DOI:10.1175/1520-0442(1990)003<0941:Sorcua>2.0.Co;2

Giorgi, F., Jones, C., Asrar, G.R., 2009. Addressing climate information needs at the regional level: the CORDEX framework. World Meteorological Organization (WMO) Bulletin, 58(3): 175.

Gordon, L.J. et al., 2005. Human modification of global water vapor flows from the land surface. Proceedings of the National Academy of Sciences of the United States of America, 102(21): 7612-7617. DOI:10.1073/pnas.0500208102

Green, T.R. et al., 2011. Beneath the surface of global change: Impacts of climate change on groundwater. Journal of Hydrology, 405(3-4): 532-560. DOI:10.1016/j.jhydrol.2011.05.002

Grotch, S.L., MacCracken, M.C., 1991. The Use of General Circulation Models to Predict Regional Climatic Change. Journal of Climate, 4(3): 286-303. DOI:10.1175/1520-0442(1991)004<0286:tuogcm>2.0.co;2

Haddeland, I., Skaugen, T., Lettenmaier, D.P., 2007. Hydrologic effects of land and water management in North America and Asia: 1700-1992. Hydrology and Earth System Sciences, 11(2): 1035-1045. DOI:10.5194/hess-11-1035-2007

Hagemann, S. et al., 2013. Climate change impact on available water resources obtained using multiple global climate and hydrology models. Earth System Dynamics,

4(1): 129-144. DOI:10.5194/esd-4-129-2013

Hansen, J. et al., 2001. A closer look at United States and global surface temperature change. Journal of Geophysical Research Atmospheres, 106(20): 23947-23963.

Hansen, M.C., Sohlberg, R., Defries, R.S., Townshend, J.R.G., 2000. Global land cover classification at 1 km spatial resolution using a classification tree approach. International Journal of Remote Sensing, 21(6-7): 1331-1364. DOI:10.1080/014311600210209

Harris, I., Jones, P.D., Osborn, T.J., Lister, D.H., 2014. Updated high-resolution grids of monthly climatic observations – the CRU TS3.10 Dataset. International Journal of Climatology, 34(3): 623-642. DOI:10.1002/joc.3711

Heo, J.H., Kho, Y.W., Shin, H., Kim, S., Kim, T., 2008. Regression equations of probability plot correlation coefficient test statistics from several probability distributions. Journal of Hydrology, 355(1-4): 1-15. DOI:10.1016/j.jhydrol.2008.01.027

Hewitt, C.D., Griggs, D.J., 2004. Ensembles-based predictions of climate changes and their impacts. Eos, 85(52): 566. DOI:10.1029/2004EO520005

Huang, T., Yu, D., Cao, Q., Qiao, J., 2019. Impacts of meteorological factors and land use pattern on hydrological elements in a semi-arid basin. Science of the Total Environment, 690: 932-943. DOI:https://doi.org/10.1016/j.scitotenv.2019.07.068

Hurst, H.E., 1951. Long-term storage capacity of reservoirs. Trans. Amer. Soc. Civil Eng., 116: 770-799.

IPCC, 2014. Synthesis report. Contribution of working groups I, II and III to the fifth assessment report of the intergovernmental panel on climate change. Geneva Switzerland,

2014: 151.

Jacob, D. et al., 2014. EURO-CORDEX: New high-resolution climate change projections for European impact research. Regional Environmental Change, 14(2): 563-578. DOI:10.1007/s10113-013-0499-2

Jiang, C. et al., 2015. Separating the impacts of climate change and human activities on runoff using the Budyko-type equations with time-varying parameters. Journal of Hydrology, 522: 326-338. DOI:https://doi.org/10.1016/j.jhydrol.2014.12.060

Johnson, F., Sharma, A., 2012. A nesting model for bias correction of variability at multiple time scales in general circulation model precipitation simulations. Water Resources Research, 48(1). DOI:10.1029/2011WR010464

Jovanovic, T., Mejía, A., Gall, H., Gironás, J., 2016. Effect of urbanization on the long-term persistence of streamflow records. Physica A: Statistical Mechanics and its Applications, 447: 208-221. DOI:10.1016/j.physa.2015.12.024

Kalnay, E., Cai, M., 2003. Impact of urbanization and land-use change on climate. Nature, 423(6939): 528-531. DOI:10.1038/nature01675

Katz, R.W., 1993. Towards a statistical paradigm for climate change. Climate Research, 2(3): 167-175. DOI:10.3354/cr002167

Kendall, M.G., Gibbons, J.D., 1990. Rank correlation methods. Ed. Edward Arnold.

Koster, R.D., Suarez, M.J., 1999. A simple framework for examining the interannual variability of land surface moisture fluxes. Journal of Climate, 12(7): 1911-1917.

Kottek, M., Grieser, J., Beck, C., Rudolf, B., Rubel, F., 2006. World map of the Köppen-Geiger climate classification updated. Meteorologische Zeitschrift, 15(3): 259-

263. DOI:10.1127/0941-2948/2006/0130

Koutsoyiannis, D., 2003. Climate change, the Hurst phenomenon, and hydrological statistics. Hydrological Sciences Journal, 48(1): 3-24. DOI:10.1623/hysj.48.1.3.43481

Koutsoyiannis, D., Langousis, A., 2011. 2.02 - Precipitation. In: Wilderer, P. (Ed.), Treatise on Water Science. Elsevier, Oxford, pp. 27-77. DOI:https://doi.org/10.1016/B978-0-444-53199-5.00027-0

Lafon, T., Dadson, S., Buys, G., Prudhomme, C., 2013. Bias correction of daily precipitation simulated by a regional climate model: A comparison of methods. International Journal of Climatology, 33(6): 1367-1381. DOI:10.1002/joc.3518

Laio, F., 2004. Cramer–von Mises and Anderson-Darling goodness of fit tests for extreme value distributions with unknown parameters. Water Resources Research, 40(9). DOI:10.1029/2004wr003204

Langousis, A., Koutsoyiannis, D., 2006. A stochastic methodology for generation of seasonal time series reproducing overyear scaling behaviour. Journal of Hydrology, 322(1-4): 138-154. DOI:10.1016/j.jhydrol.2005.02.037

Langousis, A., Mamalakis, A., Puliga, M., Deidda, R., 2016. Threshold detection for the generalized Pareto distribution: Review of representative methods and application to the NOAA NCDC daily rainfall database. Water Resources Research, 52(4): 2659-2681. DOI:10.1002/2015WR018502

Le Cam, L., 1961. A stochastic description of precipitation, Proceedings of the fourth Berkeley symposium on mathematical statistics and probability. University of California Press Berkeley, pp. 165-186.

Lee, C.H., Yeh, H.F., 2019. Impact of climate change and human activities on streamflow variations based on the budyko framework. Water (Switzerland), 11(10). DOI:10.3390/w11102001

Legesse, D., Vallet-Coulomb, C., Gasse, F., 2003. Hydrological response of a catchment to climate and land use changes in Tropical Africa: Case study south central Ethiopia. Journal of Hydrology, 275(1-2): 67-85. DOI:10.1016/s0022-1694(03)00019-2

Lettenmaier, D.P., Burges, S.J., 1977. An operational approach to preserving skew in hydrologic models of long-term persistence. Water Resources Research, 13(2): 281-290. DOI:10.1029/WR013i002p00281

Li, D., Pan, M., Cong, Z., Zhang, L., Wood, E., 2013. Vegetation control on water and energy balance within the Budyko framework. Water Resources Research, 49(2): 969-976. DOI:10.1002/wrcr.20107

Li, H., Sheffield, J., Wood, E.F., 2010. Bias correction of monthly precipitation and temperature fields from Intergovernmental Panel on Climate Change AR4 models using equidistant quantile matching. Journal of Geophysical Research Atmospheres, 115(10). DOI:10.1029/2009JD012882

Li, H., Zhang, Y., Vaze, J., Wang, B., 2012. Separating effects of vegetation change and climate variability using hydrological modelling and sensitivity-based approaches. Journal of Hydrology, 420-421: 403-418. DOI:10.1016/j.jhydrol.2011.12.033

Li, Z., Liu, W.z., Zhang, X.c., Zheng, F.l., 2009. Impacts of land use change and climate variability on hydrology in an agricultural catchment on the Loess Plateau of China. Journal of Hydrology, 377(1-2): 35-42. DOI:10.1016/j.jhydrol.2009.08.007

Liang, X., Lettenmaier, D.P., Wood, E.F., Burges, S.J., 1994. A simple hydrologically based model of land surface water and energy fluxes for general circulation models. Journal of Geophysical Research, 99(D7): 14,415-14,428.

Lilliefors, H.W., 1967. On the Kolmogorov-Smirnov Test for Normality with Mean and Variance Unknown. Journal of the American Statistical Association, 62(318): 399-402. DOI:10.1080/01621459.1967.10482916

Lindquist, E.F., 1940. Statistical analysis in educational research.

Liu, X. et al., 2018. High-resolution multi-temporal mapping of global urban land using Landsat images based on the Google Earth Engine Platform. Remote Sensing of Environment, 209: 227-239. DOI:10.1016/j.rse.2018.02.055

López-Rodríguez, F., García-Sanz-Calcedo, J., Moral-García, F.J., García-Conde, A.J., 2019. Statistical study of rainfall control: The Dagum distribution and applicability to the Southwest of Spain. Water (Switzerland), 11(3). DOI:10.3390/w11030453

Lu, D., Weng, Q., 2007. A survey of image classification methods and techniques for improving classification performance. International Journal of Remote Sensing, 28(5): 823-870. DOI:10.1080/01431160600746456

Lu, J., Sun, G., McNulty, S.G., Amatya, D.M., 2005. A comparison of six potential evapotranspiration methods for regional use in the southeastern United States. Journal of the American Water Resources Association, 41(3): 621-633. DOI:10.1111/j.1752-1688.2005.tb03759.x

Mamalakis, A., Langousis, A., Deidda, R., Marrocu, M., 2017. A parametric approach for simultaneous bias correction and high-resolution downscaling of climate model

rainfall. Water Resources Research, 53(3): 2149-2170. DOI:10.1002/2016wr019578

Mandelbrot, B.B., Wallis, J.R., 1969. Some long-run properties of geophysical records. Water Resources Research, 5(2): 321-340. DOI:10.1029/WR005i002p00321

Mango, L.M., Melesse, A.M., McClain, M.E., Gann, D., Setegn, S.G., 2011. Land use and climate change impacts on the hydrology of the upper Mara River Basin, Kenya: Results of a modeling study to support better resource management. Hydrology and Earth System Sciences, 15(7): 2245-2258. DOI:10.5194/hess-15-2245-2011

Markovic, R.D., 1965. Probability functions of best fit to distributions of annual precipitation and runoff. Hydrology papers (Colorado State University); no. 8.

Mascaro, G., Viola, F., Deidda, R., 2018. Evaluation of Precipitation From EURO-CORDEX Regional Climate Simulations in a Small-Scale Mediterranean Site. Journal of Geophysical Research: Atmospheres, 123(3): 1604-1625. DOI:10.1002/2017jd027463

Massey, F.J., Jr., 1951. The Kolmogorov-Smirnov Test for Goodness of Fit. Journal of the American Statistical Association, 46(253): 68-78. DOI:10.1080/01621459.1951.10500769

Mearns, L.O., Bogardi, I., Giorgi, F., Matyasovszky, I., Palecki, M., 1999. Comparison of climate change scenarios generated from regional climate model experiments and statistical downscaling. Journal of Geophysical Research Atmospheres, 104(D6): 6603-6621. DOI:10.1029/1998JD200042

Mechoso, C.R., Arakawa, A., 2015. NUMERICAL MODELS | General Circulation Models. In: North, G.R., Pyle, J., Zhang, F. (Eds.), Encyclopedia of Atmospheric Sciences (Second Edition). Academic Press, Oxford, pp. 153-160.

DOI:https://doi.org/10.1016/B978-0-12-382225-3.00157-2

Mehrotra, R., Sharma, A., 2016. A multivariate quantile-matching bias correction approach with auto- and cross-dependence across multiple time scales: implications for downscaling. Journal of Climate, 29(10): 3519-3539. DOI:10.1175/JCLI-D-15-0356.1

Mehrotra, R., Sharma, A., 2019. A Resampling Approach for Correcting Systematic Spatiotemporal Biases for Multiple Variables in a Changing Climate. Water Resources Research, 55(1): 754-770. DOI:10.1029/2018WR023270

Mekonnen, D.F., Duan, Z., Rientjes, T., Disse, M., 2018. Analysis of combined and isolated effects of land-use and land-cover changes and climate change on the upper Blue Nile River basin's streamflow. Hydrol. Earth Syst. Sci., 22(12): 6187-6207. DOI:10.5194/hess-22-6187-2018

Melo, D.D.C.D., Scanlon, B.R., Zhang, Z., Wendland, E., Yin, L., 2016. Reservoir storage and hydrologic responses to droughts in the Paraná River basin, south-eastern Brazil. Hydrology and Earth System Sciences, 20(11): 4673-4688. DOI:10.5194/hess-20-4673-2016

Menne, M.J., Durre, I., Vose, R.S., Gleason, B.E., Houston, T.G., 2012. An overview of the global historical climatology network-daily database. Journal of Atmospheric and Oceanic Technology, 29(7): 897-910. DOI:10.1175/jtech-d-11-00103.1

Michiels, P., Gabriels, D., Hartmann, R., 1992. Using the seasonal and temporal Precipitation concentration index for characterizing the monthly rainfall distribution in Spain. Catena, 19(1): 43-58. DOI:10.1016/0341-8162(92)90016-5

Middelkoop, H. et al., 2001. Impact of climate change on hydrological regimes and

water resources management in the Rhine basin. Climatic Change, 49(1-2): 105-128. DOI:10.1023/A:1010784727448

Milly, P.C.D. et al., 2008. Climate change: Stationarity is dead: Whither water management? Science, 319(5863): 573-574. DOI:10.1126/science.1151915

Milly, P.C.D., Dunne, K.A., Vecchia, A.V., 2005. Global pattern of trends in streamflow and water availability in a changing climate. Nature, 438(7066): 347-350. DOI:10.1038/nature04312

Moberg, A. et al., 2006. Indices for daily temperature and precipitation extremes in Europe analyzed for the period 1901-2000. Journal of Geophysical Research Atmospheres, 111(22). DOI:10.1029/2006JD007103

Montanari, A., Rosso, R., Taqqu, M.S., 1997. Fractionally differenced ARIMA models applied to hydrologic time series: Identification, estimation, and simulation. Water Resources Research, 33(5): 1035-1044. DOI:10.1029/97wr00043

Montzka, S.A., Dlugokencky, E.J., Butler, J.H., 2011. Non-CO 2 greenhouse gases and climate change. Nature, 476(7358): 43-50.

Mooley, D.A., Parthasarathy, B., Sontakke, N.A., Munot, A.A., 1981. Annual rain-water over India, its variability and impact on the economy. Journal of Climatology, 1(2): 167-186. DOI:10.1002/joc.3370010206

Murphy, J., 1999. An evaluation of statistical and dynamical techniques for downscaling local climate. Journal of Climate, 12(8 PART 1): 2256-2284. DOI:10.1175/1520-0442(1999)012<2256:aeosad>2.0.co;2

Navas, R., Alonso, J., Gorgoglione, A., Vervoort, R.W., 2019. Identifying climate and

human impact trends in streamflow: A case study in Uruguay. Water (Switzerland), 11(7). DOI:10.3390/w11071433

Nerantzaki, S.D., Nikolaidis, N.P., 2020. The response of three Mediterranean karst springs to drought and the impact of climate change. Journal of Hydrology, 591. DOI:10.1016/j.jhydrol.2020.125296

Neyman, J., Pearson, E.S., 1933. IX. On the problem of the most efficient tests of statistical hypotheses. Philosophical Transactions of the Royal Society of London. Series A, Containing Papers of a Mathematical or Physical Character, 231(694-706): 289-337.

Nijssen, B., O'Donnell, G.M., Hamlet, A.F., Lettenmaier, D.P., 2001. Hydrologic sensitivity of global rivers to climate change. Climatic Change, 50(1-2): 143-175. DOI:10.1023/a:1010616428763

O'Brien, R.M., 2007. A caution regarding rules of thumb for variance inflation factors. Quality and Quantity, 41(5): 673-690. DOI:10.1007/s11135-006-9018-6

Ogungbenro, S.B., Morakinyo, T.E., 2014. Rainfall distribution and change detection across climatic zones in Nigeria. Weather and Climate Extremes, 5(1): 1-6. DOI:10.1016/j.wace.2014.10.002

Ol'Dekop, E., 1911. Ob isparenii s poverknosti rechnykh basseinov (On evaporation from the surface of river basins). Transactions on Meteorological Observations, University of Tartu, 4.

Oliver, J.E., 1980. Monthly precipitation distribution: A comparative index. Professional Geographer, 32(3): 300-309. DOI:10.1111/j.0033-0124.1980.00300.x

Öner, M., Kocakoç, I.D., 2017. JMASM 49: A compilation of some popular goodness

of fit tests for normal distribution: Their algorithms and MATLAB codes (MATLAB). Journal of Modern Applied Statistical Methods, 16(2): 547-575. DOI:10.22237/jmasm/1509496200

Onof, C. et al., 2000. Rainfall modelling using Poisson-cluster processes: a review of developments. Stochastic Environmental Research and Risk Assessment, 14(6): 384-411.

Osei, M.A. et al., 2019. The impact of climate and land-use changes on the hydrological processes of Owabi catchment from SWAT analysis. Journal of Hydrology: Regional Studies, 25: 100620. DOI:https://doi.org/10.1016/j.ejrh.2019.100620

Pan, S. et al., 2017. Runoff responses to climate and land use/cover changes under future scenarios. Water, 9(7): 475.

Papalexiou, S.M., AghaKouchak, A., Trenberth, K.E., Foufoula-Georgiou, E., 2018. Global, Regional, and Megacity Trends in the Highest Temperature of the Year: Diagnostics and Evidence for Accelerating Trends. Earth's Future, 6(1): 71-79. DOI:10.1002/2017ef000709

Papalexiou, S.M., Montanari, A., 2019. Global and Regional Increase of Precipitation Extremes Under Global Warming. Water Resources Research, 0(0). DOI:10.1029/2018wr024067

Papoulis, A., 1990. Probability & statistics, 2. Prentice-Hall Englewood Cliffs.

Parzen, E., 1960. Modern probability theory and its applications. John Wiley & Sons, Incorporated.

Pettitt, A.N., 1979. A non-parametric approach to the change-point problem. Journal of the Royal Statistical Society: Series C (Applied Statistics), 28(2): 126-135.

Piani, C., Haerter, J.O., Coppola, E., 2010. Statistical bias correction for daily precipitation in regional climate models over Europe. Theoretical and Applied Climatology, 99(1): 187-192. DOI:10.1007/s00704-009-0134-9

Piao, S. et al., 2007. Changes in climate and land use have a larger direct impact than rising CO2 on global river runoff trends. Proceedings of the National Academy of Sciences of the United States of America, 104(39): 15242-15247. DOI:10.1073/pnas.0707213104

Pike, J., 1964. The estimation of annual run-off from meteorological data in a tropical climate. Journal of Hydrology, 2(2): 116-123.

Porporato, A., Daly, E., Rodriguez-Iturbe, I., 2004. Soil water balance and ecosystem response to climate change. American Naturalist, 164(5): 625-632. DOI:10.1086/424970

Potter, N., Zhang, L., Milly, P., McMahon, T.A., Jakeman, A., 2005. Effects of rainfall seasonality and soil moisture capacity on mean annual water balance for Australian catchments. Water Resources Research, 41(6).

Ramanathan, V., Carmichael, G., 2008. Global and regional climate changes due to black carbon. Nature Geoscience, 1(4): 221-227. DOI:10.1038/ngeo156

Ramanathan, V., Feng, Y., 2009. Air pollution, greenhouse gases and climate change: Global and regional perspectives. Atmospheric Environment, 43(1): 37-50. DOI:10.1016/j.atmosenv.2008.09.063

Razavi, S., Vogel, R., 2018. Prewhitening of hydroclimatic time series? Implications for inferred change and variability across time scales. Journal of Hydrology, 557: 109-115. DOI:10.1016/j.jhydrol.2017.11.053

Rodell, M., Velicogna, I., Famiglietti, J.S., 2009. Satellite-based estimates of groundwater depletion in India. Nature, 460(7258): 999-U80. DOI:10.1038/nature08238

Rosso, R., Peano, A., Becchi, I., Bemporad, G., 1994. An introduction to spatially distributed modelling of basin response. Advances in distributed hydrology, 3: 30.

Roudier, P. et al., 2016. Projections of future floods and hydrological droughts in Europe under a +2°C global warming. Climatic Change, 135(2): 341-355. DOI:10.1007/s10584-015-1570-4

Salas, J.D., Boes, D.C., Yevjevich, V., Pegram, G.G.S., 1979. Hurst phenomenon as a pre-asymptotic behavior. Journal of Hydrology, 44(1-2): 1-15. DOI:10.1016/0022-1694(79)90143-4

Schmidli, J., Frei, C., Vidale, P.L., 2006. Downscaling from GCM precipitation: A benchmark for dynamical and statistical downscaling methods. International Journal of Climatology, 26(5): 679-689. DOI:10.1002/joc.1287

Schmidli, J. et al., 2007. Statistical and dynamical downscaling of precipitation: An evaluation and comparison of scenarios for the European Alps. Journal of Geophysical Research Atmospheres, 112(4). DOI:10.1029/2005JD007026

Schreiber, P., 1904. Über die Beziehungen zwischen dem Niederschlag und der Wasserführung der Flüsse in Mitteleuropa. Z. Meteorol, 21(10): 441-452.

Sculley, S.P., 1986. Frequency analysis of SFWMD rainfall. Water Resources Division, Resource Planning Department, South Florida Water ….

Serpa, D. et al., 2015. Impacts of climate and land use changes on the hydrological and erosion processes of two contrasting Mediterranean catchments. Science of the Total

Environment, 538: 64-77. DOI:10.1016/j.scitotenv.2015.08.033

Shalaby, A., Tateishi, R., 2007. Remote sensing and GIS for mapping and monitoring land cover and land-use changes in the Northwestern coastal zone of Egypt. Applied Geography, 27(1): 28-41. DOI:10.1016/j.apgeog.2006.09.004

Shao, Q., Traylen, A., Zhang, L., 2012. Nonparametric method for estimating the effects of climatic and catchment characteristics on mean annual evapotranspiration. Water Resources Research, 48(3). DOI:10.1029/2010wr009610

Shrestha, S., Bhatta, B., Shrestha, M., Shrestha, P.K., 2018. Integrated assessment of the climate and landuse change impact on hydrology and water quality in the Songkhram River Basin, Thailand. Science of the Total Environment, 643: 1610-1622. DOI:10.1016/j.scitotenv.2018.06.306

Siriwardena, L., Finlayson, B.L., McMahon, T.A., 2006. The impact of land use change on catchment hydrology in large catchments: The Comet River, Central Queensland, Australia. Journal of Hydrology, 326(1-4): 199-214. DOI:10.1016/j.jhydrol.2005.10.030

Smith, T.M., Reynolds, R.W., 2005. A global merged land-air-sea surface temperature reconstruction based on historical observations (1880-1997). Journal of Climate, 18(12): 2021-2036. DOI:10.1175/JCLI3362.1

Solomon, S., Plattner, G.K., Knutti, R., Friedlingstein, P., 2009. Irreversible climate change due to carbon dioxide emissions. Proceedings of the National Academy of Sciences of the United States of America, 106(6): 1704-1709. DOI:10.1073/pnas.0812721106

Song, P., Kroll, C., 2011. The impact of multicollinearity on small sample hydrologic regional regression, World Environmental and Water Resources Congress 2011: Bearing Knowledge for Sustainability - Proceedings of the 2011 World Environmental and Water Resources Congress, pp. 3713-3722. DOI:10.1061/41173(414)389

Stednick, J.D., 1996. Monitoring the effects of timber harvest on annual water yield. Journal of Hydrology, 176(1): 79-95. DOI:https://doi.org/10.1016/0022-1694(95)02780-7

Stephens, M.A., 1986. Tests Based on EDF Statistics. In 'Goodness-of-Fit Techniques'.(Eds RB D'Agostino and MA Stephens.) pp. 97–194. Marcel Dekker: New York.

Stevens, B., Bony, S., 2013. What are climate models missing? Science, 340(6136): 1053-1054. DOI:10.1126/science.1237554

Tang, J. et al., 2016. Statistical downscaling and dynamical downscaling of regional climate in China: Present climate evaluations and future climate projections. Journal of Geophysical Research, 121(5): 2110-2129. DOI:10.1002/2015JD023977

Taylor, K.E., Stouffer, R.J., Meehl, G.A., 2012. An Overview of CMIP5 and the Experiment Design. Bulletin of the American Meteorological Society, 93(4): 485-498. DOI:10.1175/bams-d-11-00094.1

Teutschbein, C., Seibert, J., 2012. Bias correction of regional climate model simulations for hydrological climate-change impact studies: Review and evaluation of different methods. Journal of Hydrology, 456-457: 12-29. DOI:https://doi.org/10.1016/j.jhydrol.2012.05.052

Thornthwaite, C.W., 1948. An Approach toward a Rational Classification of Climate. Geographical Review, 38(1): 55-94. DOI:10.2307/210739

Tomer, M.D., Schilling, K.E., 2009. A simple approach to distinguish land-use and climate-change effects on watershed hydrology. Journal of Hydrology, 376(1-2): 24-33. DOI:10.1016/j.jhydrol.2009.07.029

Townshend, J.R. et al., 1994. The 1 km resolution global data set: Needs of the international geosphere biosphere programme! International Journal of Remote Sensing, 15(17): 3417-3441. DOI:10.1080/01431169408954338

Trabucco, A., Zomer, R.J., Bossio, D.A., van Straaten, O., Verchot, L.V., 2008. Climate change mitigation through afforestation/reforestation: A global analysis of hydrologic impacts with four case studies. Agriculture, Ecosystems & Environment, 126(1): 81-97. DOI:https://doi.org/10.1016/j.agee.2008.01.015

Trenberth, K. et al., 2007. Observations: surface and atmospheric climate change. Chapter 3. Climate change: 235-336.

Turc, L., 1953. Le bilan d'eau des sols: relations entre les précipitations, l'évaporation et l'écoulement.

Vaheddoost, B., Aksoy, H., 2017. Structural characteristics of annual precipitation in Lake Urmia basin. Theoretical and Applied Climatology, 128(3-4): 919-932. DOI:10.1007/s00704-016-1748-3

Van Steenbergen, N., Willems, P., 2013. Increasing river flood preparedness by real-time warning based on wetness state conditions. Journal of Hydrology, 489: 227-237. DOI:10.1016/j.jhydrol.2013.03.015

Veneziano, D., Langousis, A., 2010. Scaling and fractals in hydrology, Advances in data-based approaches for hydrologic modeling and forecasting. World Scientific, pp. 107-243.

Viola, F., Feng, X., Caracciolo, D., 2019. Impacts of Hydrological Changes on Annual Runoff Distribution in Seasonally Dry Basins. Water Resources Management, 33(7): 2319-2333. DOI:10.1007/s11269-019-02250-7

Viola, F. et al., 2016. Co-evolution of hydrological components under climate change scenarios in the Mediterranean area. Science of the Total Environment, 544: 515-524. DOI:10.1016/j.scitotenv.2015.12.004

Viola, F., Hellies, M., Deidda, R., 2017. Retention performance of green roofs in representative climates worldwide. Journal of Hydrology, 553: 763-772. DOI:https://doi.org/10.1016/j.jhydrol.2017.08.033

Viola, F., Pumo, D., Noto, L.V., 2014. EHSM: A conceptual ecohydrological model for daily streamflow simulation. Hydrological Processes, 28(9): 3361-3372.

Von Mises, R., 1928. Statistik und wahrheit. Julius Springer, 20.

Wang, D., Hejazi, M., 2011. Quantifying the relative contribution of the climate and direct human impacts on mean annual streamflow in the contiguous United States. Water Resources Research, 47(9). DOI:10.1029/2010WR010283

Waylen, P.R., Quesada, M.E., Caviedes, C.N., 1996. Temporal and spatial variability of annual precipitation in Costa Rica and the Southern Oscillation. International Journal of Climatology, 16(2): 173-193.

Waymire, E., Gupta, V.K., 1981a. The mathematical structure of rainfall

representations: 1. A review of the stochastic rainfall models. Water resources research, 17(5): 1261-1272.

Waymire, E., Gupta, V.K., 1981b. The mathematical structure of rainfall representations: 2. A review of the theory of point processes. Water Resources Research, 17(5): 1273-1285.

Waymire, E., Gupta, V.K., 1981c. The mathematical structure of rainfall representations: 3. Some applications of the point process theory to rainfall processes. Water Resources Research, 17(5): 1287-1294.

Weng, Q., 2002. Land use change analysis in the Zhujiang Delta of China using satellite remote sensing, GIS and stochastic modelling. Journal of environmental management, 64(3): 273-284. DOI:10.1006/jema.2001.0509

Wigmosta, M.S., Vail, L.W., Lettenmaier, D.P., 1994. A distributed hydrology-vegetation model for complex terrain. Water Resources Research, 30(6): 1665-1679. DOI:10.1029/94wr00436

Wilby, R.L. et al., 1998. Statistical downscaling of general circulation model output: A comparison of methods. Water Resources Research, 34(11): 2995-3008. DOI:10.1029/98WR02577

Wilks, D.S., 1990. Maximum likelihood estimation for the gamma distribution using data containing zeros. Journal of Climate, 3(12): 1495-1501.

Wilks, D.S., 1998. Multisite generalization of a daily stochastic precipitation generation model. Journal of Hydrology, 210(1-4): 178-191. DOI:10.1016/S0022-1694(98)00186-3

Williams, C.A. et al., 2012. Climate and vegetation controls on the surface water balance: Synthesis of evapotranspiration measured across a global network of flux towers. Water Resources Research, 48(6). DOI:10.1029/2011wr011586

Wood, A.W., Leung, L.R., Sridhar, V., Lettenmaier, D.P., 2004. Hydrologic implications of dynamical and statistical approaches to downscaling climate model outputs. Climatic Change, 62(1-3): 189-216. DOI:10.1023/B:CLIM.0000013685.99609.9e

Xiao, J. et al., 2006. Evaluating urban expansion and land use change in Shijiazhuang, China, by using GIS and remote sensing. Landscape and Urban Planning, 75(1-2): 69-80. DOI:10.1016/j.landurbplan.2004.12.005

Xiong, J. et al., 2017. Nominal 30-m cropland extent map of continental Africa by integrating pixel-based and object-based algorithms using Sentinel-2 and Landsat-8 data on google earth engine. Remote Sensing, 9(10). DOI:10.3390/rs9101065

Xu, X., Liu, W., Scanlon, B.R., Zhang, L., Pan, M., 2013. Local and global factors controlling water-energy balances within the Budyko framework. Geophysical Research Letters, 40(23): 6123-6129. DOI:10.1002/2013gl058324

Xu, X., Yang, D., Yang, H., Lei, H., 2014. Attribution analysis based on the Budyko hypothesis for detecting the dominant cause of runoff decline in Haihe basin. Journal of Hydrology, 510: 530-540. DOI:10.1016/j.jhydrol.2013.12.052

Yang, D. et al., 2007. Analyzing spatial and temporal variability of annual water-energy balance in nonhumid regions of China using the Budyko hypothesis. Water Resources Research, 43(4): 12-16. DOI:10.1029/2006wr005224

Yang, L. et al., 2017. Identifying separate impacts of climate and land use/cover change on hydrological processes in upper stream of Heihe River, Northwest China. Hydrological Processes, 31(5): 1100-1112. DOI:10.1002/hyp.11098

Yang, W. et al., 2010. Distribution-based scaling to improve usability of regional climate model projections for hydrological climate change impacts studies. Hydrology Research, 41(3-4): 211-229. DOI:10.2166/nh.2010.004

Yang, Y., Donohue, R.J., McVicar, T.R., 2016. Global estimation of effective plant rooting depth: Implications for hydrological modeling. Water Resources Research, 52(10): 8260-8276. DOI:10.1002/2016wr019392

Ye, L., Hanson, L.S., Ding, P., Wang, D., Vogel, R.M., 2018. The probability distribution of daily precipitation at the point and catchment scales in the United States. Hydrol. Earth Syst. Sci., 22(12): 6519-6531. DOI:10.5194/hess-22-6519-2018

Ye, X., Zhang, Q., Liu, J., Li, X., Xu, C.Y., 2013. Distinguishing the relative impacts of climate change and human activities on variation of streamflow in the poyang lake catchment, china. Journal of Hydrology, 494: 83-95. DOI:10.1016/j.jhydrol.2013.04.036

Yokoo, Y., Sivapalan, M., Oki, T., 2008. Investigating the roles of climate seasonality and landscape characteristics on mean annual and monthly water balances. Journal of Hydrology, 357(3-4): 255-269. DOI:10.1016/j.jhydrol.2008.05.010

Yoo, C., Ha, E., 2007. Effect of zero measurements on the spatial correlation structure of rainfall. Stochastic Environmental Research and Risk Assessment, 21(3): 287-297. DOI:10.1007/s00477-006-0064-3

Zhang, L. et al., 2004. A rational function approach for estimating mean annual

evapotranspiration. Water Resources Research, 40(2): W025021-W02502114. DOI:10.1029/2003wr002710

Zhang, L., Nan, Z., Xu, Y., Li, S., 2016a. Hydrological impacts of land use change and climate variability in the headwater region of the Heihe River Basin, northwest China. PLoS ONE, 11(6). DOI:10.1371/journal.pone.0158394

Zhang, L., Zhao, F., Chen, Y., Dixon, R.N.M., 2011. Estimating effects of plantation expansion and climate variability on streamflow for catchments in Australia. Water Resources Research, 47(12). DOI:10.1029/2011wr010711

Zhang, S., Li, Z., Lin, X., Zhang, C., 2019. Assessment of Climate Change and Associated Vegetation Cover Change on Watershed-Scale Runoff and Sediment Yield. Water, 11(7): 1373.

Zhang, S., Yang, H., Yang, D., Jayawardena, A.W., 2016b. Quantifying the effect of vegetation change on the regional water balance within the Budyko framework. Geophysical Research Letters, 43(3): 1140-1148. DOI:10.1002/2015gl066952

Zhang, Y.K., Schilling, K.E., 2006. Increasing streamflow and baseflow in Mississippi River since the 1940 s: Effect of land use change. Journal of Hydrology, 324(1-4): 412-422. DOI:10.1016/j.jhydrol.2005.09.033

Zhao, Q. et al., 2019. Projecting climate change impacts on hydrological processes on the Tibetan Plateau with model calibration against the glacier inventory data and observed streamflow. Journal of Hydrology, 573: 60-81. DOI:10.1016/j.jhydrol.2019.03.043

Zhou, G. et al., 2015. Global pattern for the effect of climate and land cover on water yield. Nature Communications, 6. DOI:10.1038/ncomms6918

Zhou, J. et al., 2020. Choice of potential evapotranspiration formulas influences drought assessment: A case study in China. Atmospheric Research, 242. DOI:10.1016/j.atmosres.2020.104979

Zomer, R.J., Trabucco, A., Bossio, D.A., Verchot, L.V., 2008. Climate change mitigation: A spatial analysis of global land suitability for clean development mechanism afforestation and reforestation. Agriculture, Ecosystems & Environment, 126(1): 67-80. DOI:https://doi.org/10.1016/j.agee.2008.01.014